EPFL

Thèse n° 10 123

High-throughput microfluidic platforms for characterizing and engineering cell-free gene regulatory circuits

Présentée le 27 août 2020

à la Faculté des sciences et techniques de l'ingénieur
Laboratoire de caractérisation du réseau biologique
Programme doctoral en biotechnologie et génie biologique

pour l'obtention du grade de Docteur ès Sciences

par

Zoe Newell SWANK

Acceptée sur proposition du jury

Prof. A. Radenovic, présidente du jury
Prof. S. Maerkl, directeur de thèse
Prof. A. deMello, rapporteur
Prof. P. Freemont, rapporteur
Prof. B. Correia, rapporteur

École
polytechnique
fédérale
de Lausanne

2020

Acknowledgements

First I would like to thank Sebastian for giving me the opportunity to work in his lab and for mentoring me throughout my PhD. I greatly appreciate the time that he devoted to helping me with my project and I feel that I have benefited immensely from our scientific discussions. Secondly, thank you Aleksandra Radenovic, Bruno Correia, Paul Freemont and Andrew deMello for taking the time to evaluate my thesis and to serve as jury members for my defense. With respect to the work presented in my thesis, I would like to thank Nadanai for an enjoyable collaboration filled with interesting conversations. Thank you Esther and Jia-Chia for another fruitful collaboration and for introducing me to the world of droplets.

I was not only lucky to have had the opportunity to collaborate with other students, post-docs and professors, but I was doubly lucky to have been part of an amazing lab. When I first joined LBNC, I was warmly welcomed by Francesca, Francesco, Matt, Henrike, Ekaterina, Amanda, Zuzana, Kristina, Lea and Charlotte. I am happy to have met everyone and could not have chosen a better group to have passed the time together, both in and out of the lab. In particular, I would like to thank Henrike and Lea for your help introducing me to cell-free systems and micro-chemostats, Ekaterina for your constant enthusiasm, molecular biology tips and windsurfing adventures and Matt for your constant positive disposition and a lasting friendship. Although I already have a soft spot for Italians, I would have never expected to meet two great friends, Francesca and Francesco, who were always supporting and helpful in lab and a pleasure to be around outside the lab.

Next to join the lab was Ivan and Nadanai, to whom I am grateful for their friendship and numerous interesting discussions about life. The lab then expanded to include Barbora, Greg, Simone and Fabien. I would like to thank Barbora for her constant support and for always taking care of others, Greg for his calmness and openness to discuss anything, Simone for his strange humor, enthusiasm and Italian practice, and Fabien for his continuously positive and funny attitude. In the

past couple years the lab has continued to grow and I am thankful for the support from all of the remaining past and current members, including Ming, Evan, Michael, Julia, Shiyu, Josh, Laura, Amir, Praneeth, Asterios, Julie, Caro, Eugenia, Malek and Craig. I am especially happy to have started working together with Julia, whose constant encouragement is always uplifting. Outside LBNC, but on the same floor, I am thankful for all the friends from the neighbouring labs, LBEN, LANES and CLSE, with an extra thank you to Martina for her camaraderie in the final months leading up to our defenses. If I mention others connected with our lab, I must also express my gratitude to the iGEM 2017 team for an incredible experience and continuing friendships, mainly thanks to Lena, Elia and Tim, who keep bringing us together.

Lastly, I would like to thank my parents and my family for their constant love and support although it has not always been easy to live so far apart. Adapting to life away from home proved to be a relatively smooth transition thanks to the loving support of Adriano and his family. Any struggles encountered during the PhD life were always manageable when they could be shared with a fellow PhD student and partner, especially when that partner has an awesome melodramatic humor.

Abstract

Cell-free systems have emerged as a versatile platform for constructing complex biological systems from the bottom-up. In particular, they enable the rapid engineering and characterization of gene regulatory networks, a critical cellular subsystem that allows a cell to sense and respond to a myriad of signals with a computational-like logic. Building synthetic gene circuits provides the means to both program new functionalities and augment our understanding of natural networks. Genetic circuits are composed of elements that control transcription, translation and post-translational processes through biomolecular interactions involving DNA, RNA, proteins and small molecules. Even the design space of simple gene circuits can be sizeable, necessitating high-throughput methods capable of characterizing large libraries of regulatory components in a comprehensive manner that can guide the engineering of functional circuits. Therefore, we have developed microfluidic platforms that can be coupled with cell-free systems to facilitate the high-throughput screening of gene regulatory elements. In this work, we begin by presenting a microfluidic device capable of performing hundreds of independent cell-free transcription-translation reactions in parallel, using different combinations of surface immobilised DNA as the reaction templates. We employ this device to study different mechanisms for tuning transcriptional repression using synthetic zinc-fingers, whose affinity, specificity and coopertivity can be rationally engineered. Functional repression assays were combined with quantitative affinity measurements and thermodynamic modeling to generate a library of well-characterized synthetic transcription factors and corresponding promoters, with which we were able to build gene regulatory circuits *de novo*. As the first platform was limited to carrying out reactions in batch-mode, we then adapted the microfluidic device to enable the implementation of cell-free transcription-translation reactions at steady state, while maintaining high-throughput screening capabilities. The modified device consisted of individual reaction compartments that could be periodically supplied with cell-free reagents mixed on-chip to create programmable con-

centration gradients. For a proof of concept we measured the steady state repression levels for a subset of the synthetic components we had previously characterized in batch and demonstrated that we could implement a genetic toggle switch. Lastly, we developed a microfluidic device for generating double emulsion droplets to encapsulate cell-free gene expression reactions. The flow focusing device integrates pneumatic valves that enable on-chip mixing with minimal reagent volumes and drop sorting. Utilizing this device we were able to precisely titrate DNA template concentrations and monitor *in vitro* protein synthesis profiles in the droplets.

Zusammenfassung

‘Zell-freie’ Systeme etablierten sich als eine vielseitige Plattform für den Bau komplexer biologischer Systeme vom Grundbaustein zum Gesamtsystem (‘bottom-up’). Insbesondere ermöglichen sie das rasche Bauen und die Charakterisierung von genetischen Regulations-Netzwerken, die ein wichtiges zelluläres Teilsystem bilden. Genetische Regulations-Netzwerke ermöglichen es einer Zelle, eine Vielzahl an Signalen wahr zu nehmen, und auf diese mit einer Computer-ähnlichen Logik zu reagieren. Die Konstruktion synthetischer Gen-Schaltkreise ermöglicht es, sowohl neue Funktionalitäten zu programmieren, als auch unser Verstehen natürlicher Netzwerke zu erweitern. Gen-Schaltkreise bestehen aus Elementen, die durch Interaktionen zwischen DNA, RNA, Proteinen, und kleinen Molekülen die molekularbiologischen Programme der Transkription und Translation, sowie post-translationale Prozesse kontrollieren. Selbst die Möglichkeiten, einfache Gen-Schaltkreise zu konstruieren sind beträchtlich, so daß es neuer Methoden bedarf, um große Kollektionen regulatorischer Komponenten umfassend zu charakterisieren, und daraus funktionelle Gen-Schaltkreise zu bauen. Aus diesem Grund entwickelten wir ein System, basierend auf mikrofluidischer Technologie, welches mit Zell-freien Systemen kombiniert werden kann, um die Funktionalität einer Vielzahl von genetisch-regulatorischen Elementen zu testen. In dieser Arbeit präsentieren wir zuallererst ein mikrofluidisches System, welches verschiedene Kombinationen immobilisierter DNA verwendet, um Hunderte selbständige Zell-freie Transkriptions-Translations Reaktionen durchzuführen. Wir wandten diese Technologie an, um verschiedene Mechanismen für das Adjustieren transkriptioneller Repression mittels synthetischer Zink-Finger, deren Affinität, Spezifität und Kooperativität rational konstruiert werden können, zu erforschen. Wir kombinierten funktionelle Repressions-Analysen, quantitative Affinitätmessungen, und das Erstellen thermodynamischer Modelle, um eine Kollektion gut charakterisierter synthetischer Transkriptionsfaktoren und entsprechender Promoteren zu erstellen, womit wir neue genetisch regulatorische Schaltkreise konstruieren konnten. Da dieses erste

System auf die Durchführung von Reaktionen im Batch begrenzt war, passten wir die Mikrofluidik-Vorrichtung an, um Zell-freie Transkriptions-Translations Reaktionen unter kontinuierlichen Bedingungen zu ermöglichen, unter Beibehalten einer hohen Test-Kapazität. Die veränderte Vorrichtung besteht aus individuellen Reaktionskammern, die periodisch mit Zell-freien Reagenzien versorgt werden, um programmierbare Konzentrations-Gradienten zu erstellen; die Reagenzien mischen sich direkt in der Vorrichtung. Als Konzeptnachweis maßen wir die Stärke der Repression unter kontinuierlichen Bedingungen für einige synthetische Komponenten, die wir zuvor unter Batch-Bedingungen charakterisiert hatten. Weiters konnten wir einen genetischen Kippschalter implementieren. Zuletzt entwickelten wir eine Mikrofluidik-Vorrichtung zur Generierung von Doppel-Emulsions Tröpfchen, um Zell-freie Genexpressions-Reaktionen abzukapseln. Die Flussfokussierende Vorrichtung integriert Pneumatikventile für das direkte Mischen minimaler Reagenz-Volumen, und dem Sortieren der Tröpfchen direkt auf der Vorrichtung. Wir benutzten dieses System, um DNA-Konzentrationen präzise zu titrieren, und *in vitro* Protein-Synthese in den Tröpfchen zu beobachten.

Contents

List of Figures

List of Tables

1

Introduction

Parts of section 1.2 and 1.3 have been adapted from a recent review.

Reference: Laohakunakorn, N., Grasemann, L., Lavickova, B., Michielin, G., Shahein, A., Swank, Z. and Maerkl, S.J. (2019). Bottom-up construction of complex biological systems with cell-free synthetic biology. DOI: 10.5281/zenodo.3591964

1.1 Synthetic biology

Synthetic biology integrates engineering and biology with the aim of designing and assembling novel biomolecular components, networks and pathways with programmable outputs. Rewiring organisms with synthetic constructs has already proven to be a powerful tool with applications in biosensing, therapeutics and the synthesis of biofuels, pharmaceuticals and novel biomaterials [1]. At the same time, engineering complex artificial biological systems provides another route to understanding natural biological phenomena [2].

Owing to their study of the *lac* operon in *E. coli* [3] at the beginning of the 1960s, Jacob and Monod inspired the field of synthetic biology by postulating that a cell could respond to environmental cues due to underlying gene regulatory circuits. A computational logic was associated with gene regulation, making it possible to imagine that new regulatory networks could be built from molecular components [4]. The next two decades saw the development of molecular cloning [5] and polymerase chain reaction (PCR) [6, 7], laying the technical groundwork for genetic manipulation that would later be used to engineer artificial gene networks. During the 1990s, automated DNA

sequencing [8, 9] and improved computational tools facilitated the complete sequencing of microbial genomes [10, 11], and high-throughput techniques for measuring RNA, proteins and metabolites enabled the screening of a wide array of cellular components and their interactions [12, 13, 14, 15, 16, 17, 18, 19]. Together these technical advancements began to equip scientists with the necessary knowledge and methods for constructing biological systems that began to resemble the complex regulatory behavior found in microorganisms [20]. As research was scaled-up to the level of systems biology, cellular networks emerged as immense and intricate entities that could be broken down into a hierarchy of functional modules, analogous to many engineered machines [21].

Consequently, it was proposed that engineering principles, such as standardization, functional decoupling and abstraction, could be applied to design and build synthetic biological systems [22]. In particular, abstraction hierarchies can serve to manage complexity by separating the constituent parts of a system into varying levels, where work at any level can be carried out independently with a systematic exchange of information between levels. The design of new systems with given functionalities occurs from the bottom-up, while taking into account the overall context given by the top of the hierarchy. Just as we can visualize the hierarchy of computer engineering, we can similarly break down the components of synthetic biological systems, starting with DNA, RNA and proteins at the bottom, then moving to biochemical reactions, pathways and finally cells at the top (Figure 1.1) [23]. Furthermore, establishing standards to guide the quantitative characterization of discrete biological parts and their interactions would ensure that the overall system could be built through predictive design [24, 25]. Although a framework for synthetic biology was conceived according to the structured practices from other engineering fields, in reality, managing biological complexity reliably continues to pose a challenge [26].

Nonetheless, by combining model-based design with iterations of trial-and-error, the first gene regulatory circuits were constructed to carry out explicit functions. Specifically, Gardener *et al.* engineered a genetic toggle switch from two mutually inhibitory transcriptional repressors that could change from one stable expression state to another in reaction to external signals [27]. Concurrently, Elowitz and Leibler built an oscillatory gene circuit, termed the repressilator, which was composed of a triple negative-feedback loop formed from a succession of repressor-promoter pairs [28]. Both circuits contained a similar set of parts that each had to be tuned to varying degrees until the desired experimental output was reached, establishing a practical workflow that combined mathematical modeling with experimental measurements and hypothesis-driven debugging [29]. Subsequently,

synthetic biologists continued to investigate the link between network design and quantitative behavior, leading to the construction of autoregulatory negative- and positive-feedback modules [30, 31]. In addition, the combinatorial method was used to build a library of networks with varying connectivity, exhibiting a range of phenotypes corresponding to binary logic gates [32]. As gene regulatory network engineering was underway, the practice of implementing synthetic circuits proved to augment our basic understanding of biological systems, starting with studies that addressed the relationship between gene expression and molecular noise [33, 34].

Early obstacles faced by synthetic biologists included long circuit manufacturing times and a lack of thoroughly characterized genetic parts [26]. The decreasing cost of gene synthesis and the advent of high-throughput DNA assembly strategies served to expedite the building process [35, 36, 37, 38]. An increase in the number and characterization of genetic parts was accompanied by the construction of genetic circuits that could carry out more and more complex functions. For example, recombinase-based logic circuits were used to count events by creating permanent memories [39] and a logic gate cascade was built to respond to multiple inputs [40]. Though the overall number of circuits continued to rise, the number of regulatory parts they employed reached a plateau [41]. The scarcity of highly specific gene regulators motivated the creation of orthogonal libraries of components that could regulate transcription or translation within the same circuit in the absence of cross-reactivity [42, 43].

Despite tremendous progress, the reliable and predictable engineering of biomolecular circuits is often hindered by the inherent variability of complex biological systems and a lack of mechanistic understanding. Confronted with potentially unknown complexity, one strategy is to make use of automated high-throughput experimental techniques to generate functional circuit designs by screening large libraries of alternative constructs [44]. To effectively explore the parameter space, these screens can be conducted by rational design or directed evolution [45]. A cornerstone of synthetic biology, rational design approaches strive to assemble circuits in a modular manner from an array of well-characterized parts. What remains unknown can sometimes be mitigated by adopting methods from control theory to design network architectures that are robust to specific uncertainties [46, 47, 48]. On the other hand, directed evolution introduces random genetic mutations of unknown impact to refine an imperfect network design or to optimize a given component [49, 50, 51].

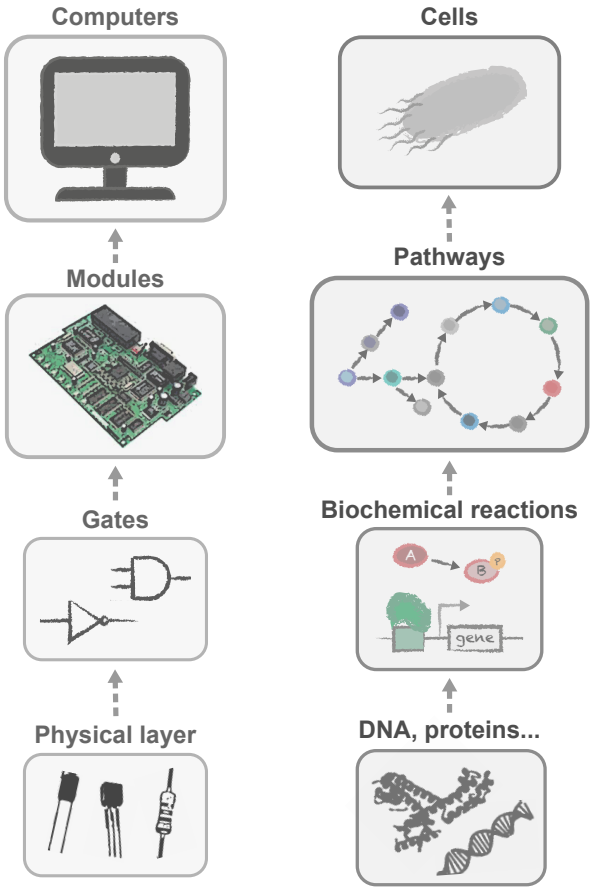

Figure 1.1: **Abstraction hierarchy for synthetic biology inspired by computer engineering.** Figure adapted from Andrianantoandro *et al.* [23].

1.2 Bioengineering in cell-free systems

The previous section has introduced gene regulatory circuit engineering within the context of cell-based systems, however cell-free systems have recently evolved into key bioengineering platforms [52, 53, 54]. Cell-based synthetic biology relies on laborious molecular cloning methods to insert artificial networks into living cells, leading to time-consuming design-build-test cycles. Additionally, the synthetic circuit components may exhibit unknown interactions with endogenous molecular machinery or present a metabolic burden for the host cell, requiring iterative testing to arrive at a functional design. Cell-free systems provide a means to circumvent these limitations and form the basis for a fully bottom-up approach to rationally construct complex biological networks

[55, 56, 57, 58, 59, 60]. In principle, we can define and quantify the major interactions within a cell-free system, leading to well-informed models of increasingly complex biological systems with the potential to guide entirely predictive design in the future [61]. Though the ultimate goal of reliably engineering artificial biological systems will likely depend on the combination of many different approaches, cell-free synthetic biology has already demonstrated that it can play a key role [62].

Cell-free systems combine cellular enzymes with a DNA template, amino acids, an adenosine triphosphate (ATP)-regeneration system, salts and other buffers to carry out transcription and translation (TX-TL) *in vitro*. Isolating only the necessary machinery from cells, strips away the complexity associated with cellular regulation, homeostasis and growth, yielding a simplified and open environment for reconstituting biochemical reactions. Beginning in the 1960s, scientists used *E. coli* based cell-free systems to experimentally validate the central dogma of biology, showing that peptides could be synthesized from amino acids [63], RNA [64] and finally DNA through the coupled process of transcription and translation [65, 66, 67]. During that same period, another notable set of cell-free experiments entailed the study of translation from synthetic polyribonucleotides, which led to the breaking of the genetic code [68]. Over the following decades, *in vitro* systems were often adopted to eulcidate biomolecular mechanisms, including RNA replication [69], splicing [70] and Golgi trafficking [71]. In parallel, an interest in *in vitro* protein synthesis prompted work to produce more efficient cell-free extracts by adjusting the composition of the reaction mixture and improving the energy regeneration system [72]. The integration of extract engineering and synthetic biology then gave way to the field of cell-free synthetic biology in the early 2000s [73].

Historically, the most efficient cell-free protein synthesis systems were derived from *E. coli*, rabbit reticulocytes or wheat germ [74], however recently cell-free extract has been produced from a growing number of different organisms. The repertoire of highly adopted cell-free protein synthesis platforms has expanded to include extracts prepared from insect, yeast, Chinese hamster ovary and HeLa cells [75]. Since their conception these platforms have steadily increased their user base thanks to a breadth of supporting literature and the commercial availability of many extracts. While only in the beginning stages of development, cell-free systems based on *B. subtilis* [76], V. natriegens [77] and *P. putida* [78] among others have emerged as promising candidates for new applications [79]. Despite the cell-type, the basic steps for generating a functional cell-free extract are analogous. In brief, a given cell-line is cultured, then the cells are lysed without impairing protein activity, and the generated lysate is combined with a DNA or RNA template and other reaction substrates

to carry out (TX)-TL *in vitro*. From platform to platform and within a single platform, these basic steps can vary substantially, and even subtle changes can result in variable performance. For example, there is known variability between different batch preparations of *E. coli* extracts [80], not to mention significant variability across laboratories [81]. Consequently, a tremendous effort has been underway to discover the sources of this variability. We are beginning to understand the importance of each preparation step with regards to lysate performance and which factors are responsible for reproducibility [82]. Additionally the quantitative analysis of lysate proteomes has revealed the link between extract composition and performance for different cell strains and preparation methods [62, 83, 84, 85]. Ongoing work to deconstruct cell-free extract may one day lead to standardized preparation methods that correlate with fully reliable performance, however currently we are constrained due to an incomplete understanding of the system.

In the meantime, another approach to reduce complexity was the bottom-up assembly of a completely recombinant cell-free system that was composed of precisely defined parts. Combining a small set of purified proteins necessary for TX-TL with a creatine-phosphate-based energy regeneration system, Shimizu *et al.* created the platform known as PURE (protein synthesis using recombinant elements). There are several commercially available versions of this system that are increasingly popular, but also more expensive than lysate systems [86]. Furthermore, although the commercial systems stem from the original PURE system, their exact composition is often undisclosed and functional inconsistencies are observed between the different systems with respect to batch variability, protein synthesis yield and translation rate [87]. A user-defined PURE system can be produced in-house at lower cost, but entails a labor-intensive protocol that involves the purification of ribosomes and over thirty His-tagged proteins [88]. As a result, simplified protocols have been developed, including a method that purifies all proteins apart from the ribosomes in a single step [89] and another that His-tags enzyme pathways *in vivo* [90]. In addition to increasing the accessibility of recombinant systems, considerable work has focused on increasing protein expression yield in the existing systems [91, 92, 93]. Though the modular nature of PURE makes it an ideal starting point for engineering biological systems, the scope of gene regulatory networks which can be implemented in PURE is limited by low protein expression levels and inefficient *E. coli* σ-factor based transcription [94].

Regardless of incomplete characterization and persistent variability, cell-free systems have nonetheless served as an ideal testbed for prototyping gene regulatory circuits. The first *in vitro* genetic

cascades were composed of only a few bacteriophage regulatory elements, but served to illustrate the importance of balancing cell extract resources [73]. Similar to advances made *in vivo*, an expanded library of characterized parts led to the construction of more complex circuit designs *in vitro*, including multiple stage cascades, AND gates and negative feed-back loops [95]. The ability to use linear DNA templates gave an added advantage to cell-free systems [96, 97], eliminating the need for molecular cloning and accelerating the pace for testing new genetic parts. Additionally, the process of engineering cell-free gene circuits was improved through a deeper understanding of resource constraints. In particular, the impact of changing promoter strength, DNA template concentration and nucleoside triphosphate concentration was probed through independent measurements of transcriptional and translational activities [98]. It was then possible to identify the specific limitations imposed by essential biomolecular resources with respect to the overall performance of a gene activation cascade. Building upon this work, a model was developed to describe resource competition between genes [99]. Using data from individually characterized DNA parts, they were able to successfully predict the protein expression profiles for multiple co-expressed DNA parts. These studies demonstrated that fundamental aspects of biocircuit operation could be studied quantitatively and with greater ease in a cell-free context compared to *in vivo* environments. Although cell-free systems offered many benefits, Noireaux *et al.* already recognized that protein lifetime was an intrinsic limitation of batch-mode cell-free expression, preventing the reconstitution of oscillatory networks [73]. This obstacle was later surpassed by the fabrication of microfluidic devices that enabled cell-free gene expression to be carried out at steady state, facilitating the implementation of genetic oscillator circuits [100, 101].

1.3 Microfluidic platforms applied to cell-free synthetic biology

While cell-free reactions can be carried out in a simple test tube, the complexity and sophistication of experiments can be dramatically augmented by coupling them to the appropriate technological platform. There have been numerous technological advancements with respect to cell-free gene expression over the past few decades; we will focus on recent platforms enabling increased control over batch and steady state reactions.

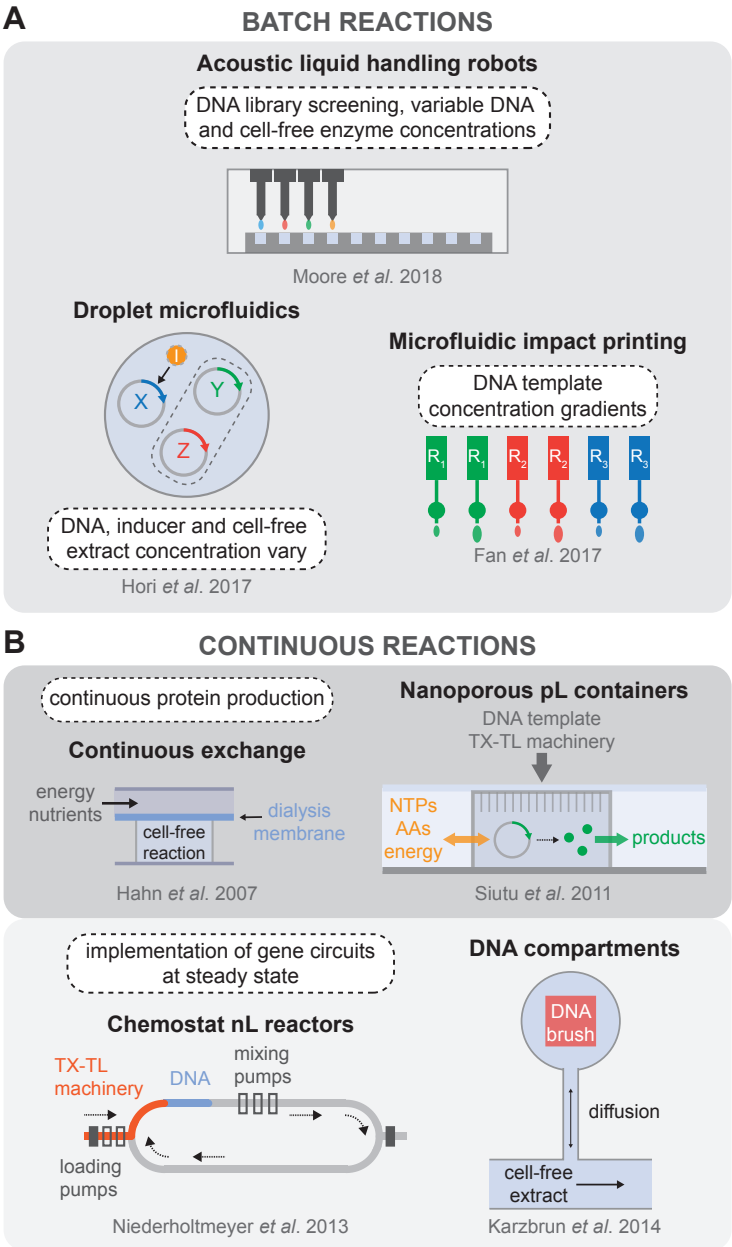

Figure 1.2: **Batch and continuous cell-free reaction platforms. (A)** Overview of the technologies used to carry out high-throughput batch reactions, including the possibilities to vary the concentration of many reaction components, in addition to exploring the sequence space of DNA templates. **(B)** Devices developed for continuous cell-free reactions, separated into two categories: continuous protein production and steady state reactors that enabled the implementation of genetic oscillatory circuits. Figure adapted from Laohakunakorn *et al.* [102].

1.3.1 Increased throughput and spatial control of batch reactions

Early high-throughput methods of spatially confined cell-free batch reactions were applied to the generation of protein arrays. In 2004, Ramachandran *et al.* showed that a plasmid array spotted on a glass slide could be transformed into a protein array by submersing the entire slide in a cell-free reaction. mRNA and proteins were being locally transcribed and translated from the spotted plasmid DNA and proximally captured by surface bound antibodies [103, 104]. The *in situ* generated protein array could then be interrogated with a protein of interest. A similar concept was later integrated into a microfluidic device for the automated mapping of protein-protein interactions [105]. Here linear expression DNA templates are spotted on a glass slide in pairs. The DNA array is then aligned to a MITOMI microfluidic device [106] so that each pair of linear templates is enclosed by a reaction chamber. Loading of the device with cell-free reaction solution synthesizes the bait and prey proteins, which are then assayed for interaction using the MITOMI method. A similar approach was used to generate large numbers of defined bHLH (basic helix-loop-helix) transcription factor mutants to assess the evolutionary accessible DNA binding specificity repertoire of these transcription factors [107]. Martin *et al.* used the method to generate a RNA array for protein-RNA interaction studies [108]. More recently, hundreds of full-length *Drosophila* transcription factors spanning a size range of 37–231 kDa were expressed on-chip using a wheat germ cell-free system [109]. Such approaches are becoming appealing for protein engineering, especially with the rapid decrease in synthetic DNA cost. In 2015, it was demonstrated that over 400 synthetic zinc-finger transcription factors could be synthesized and characterized *in vitro* using this approach [110].

As synthetic gene networks began to emerge, the advantages of cell-free protein expression were adopted to rapidly screen large libraries of functional DNA parts, avoiding *in vivo* cloning steps, and speeding up the design-build-test cycle ([80, 98]). The advent of acoustic liquid handling robots has enabled cell-free reactions to be carried out in standard microwell plate systems with increased throughput and precision, while simultaneously reducing reagent usage. This was recently demonstrated, coupled with a Bayesian modeling approach, which offered a fast route to characterizing regulatory elements from a non-model microbial host [111]. With their rapid and automated method the authors were able to infer previously unknown transcription factor binding affinities as well as quantify resource competition in cell-free reactions (Figure 1.2A). Automated

acoustic liquid handling was also used to test serine integrase recombination dynamics [112]. A Python package built to model and simulate biological circuits was then applied to the cell-free prototyping data to carry out parameter inference.

Microfluidic platforms applied to cell-free TX-TL have also enabled the exploration of larger design spaces at faster time scales. For example, droplet microfluidics was used to rapidly generate a library of distinct combinations of DNA templates, inducer molecules, and cell-free extract concentrations, with the possibility of generating millions of parameter combinations per hour [113]. Together with a dye labelling scheme, it was possible to create a detailed map of biocircuit expression versus parameter combination (Figure 1.2A). Another quantitative and multi-dimensional study of genetic promoters was carried out using parallel piezoelectric cantilever beams that were able to generate an array of droplets containing cell-free TX-TL reaction mixtures with highly accurate concentration gradients [114] (Figure 1.2A).

Setting aside high-throughput techniques, there still exist many other innovative technologies for cell-free gene expression, including methods that have sought to introduce spatial organization. In particular, a chip was developed to separate transcription and translation into different compartments [115]. Additionally multi-compartment vesicles were used to predefine regions in which different proteins would be synthesized *in vitro* [116]. Furthermore, Jiao *et al.* fabricated a microfluidic device for the encapsulation of plasmid integrated clay microgels [117]. The incorporation of magnetic beads in the microgels permitted their recovery and re-use in subsequent cell-free TX-TL reactions. A bead-based approach was also used to express and capture recombinant proteins in a hydrogel matrix [118]. Lastly, surface-bound DNA microarrays were aligned with a hydrogel matrix embedding protein synthesis machinery enabling localized protein synthesis [119].

1.3.2 Steady state cell-free reactions

While cell-free batch reactions provide a means to characterize gene circuits, parts, and devices, the complexity of biological networks that can be implemented is constrained as the systems quickly reach chemical equilibrium. This has motivated the development of *in vitro* systems that can exchange reagents over time, maintaining the reaction in a non-equilibrium steady state, and mimicking the dilution of cellular components during cell growth. Over 30 years ago there was an interest in prolonging cell-free TX-TL reactions by providing a continuous flow of amino acids and energy sources to a reaction chamber from which synthesized proteins and by-products could be

removed across an ultrafiltration membrane [120]. Successive work aimed to improve protein synthesis yield for cell-free TX-TL reactions by using a dialysis membrane to separate the reaction from the feeding solution of amino acids and energy sources, leading to a semi-continuous reaction [121, 122]. This idea was then extended to be compatible with standard micro-well plate systems that could be used for higher throughput applications [123, 124, 125, 126]. Following upon the same principles of continuous exchange cell-free reactions, a passive PDMS microreactor was built, which separated the feeding and reaction chambers with a dialysis membrane, enabling protein synthesis for up to 15 hours [127] (Figure 1.2B).

Recent improvements in implementing continuous cell-free TX-TL reactions came in the form of novel microfluidic devices. For instance, continuous protein synthesis was demonstrated in an array of cell-sized nanoporous silicon containers that could exchange energy and materials with the surrounding microfluidic environment [128]. In 2013, Niederholtmeyer *et al.* reported a two-layer PDMS device with 8 independent nano-reactors that could exchange reagents at dilution rates similar to those of growing bacteria. Steady state TX-TL reactions could be maintained for up to 30 hours, enabling the first *in vitro* implementation of genetic oscillator circuits [100] (Figure 1.2B). Using the same device, Yelleswerapu *et al.* recently demonstrated the construction of synthetic oscillating networks using sigma-factor-based regulation of native RNAP in *E. coli* lysate [129]. In 2014, Karzbrun *et al.* demonstrated two-dimensional DNA compartments capable of creating oscillating protein expression patterns and protein gradients. Each DNA compartment was linked to a supply channel through a small capillary, allowing the continuous diffusion of nutrients and products into and out of the compartment [101] (Figure 1.2B). The geometry of the compartments determined the dilution rate of the reaction, giving rise to different observed reaction kinetics. Using high frequency localized electric field gradients, the same group was able to push the TX-TL machinery away from the DNA brush, thereby arresting transcription and translation. They showed that different biomolecules can be manipulated efficiently depending on the applied voltage and obtained sustained oscillation of gene expression from controlled ON/OFF switching of the TX-TL reaction [130].

1.4 Overview and objectives of this work

As outlined in the previous sections, cell-free systems have evolved into an efficient platform for rapidly characterizing and engineering gene regulatory networks. Moreover, coupling cell-free systems with microfluidic platforms can significantly improve our experimental capabilities. Therefore, we set out to develop a microfluidic platform that would facilitate the in-depth study of gene regulatory elements with the aim of guiding rational circuit design. Often a similar set of transcriptional regulators are reused in synthetic networks, limiting the size and complexity of networks that can be built. In Chapter 2, we utilize an expandable library of synthetic transcription factors [110] to build gene regulatory networks based on transcriptional repression. Modulating transcriptional repression can be achieved at the level of DNA, protein, and cooperative protein-protein interactions, requiring high-throughput experimental approaches for a comprehensive characterization of the parameter space. For that reason, we developed a microfluidic platform that could carry out cell-free TX-TL in high-throughput, using different combinations of surface immobilized DNA as the reaction templates. With the capability to vary DNA sequence and concentration for up to 768 individual reactions, we could quickly screen a library of programmable zinc fingers for functional repression activity. We coupled cell-free TX-TL assays with binding affinity measurements [106] and thermodynamic modeling to gain a mechanistic understanding of synthetic gene regulators, which we then applied to engineering functional logic gates.

While the platform we describe in Chapter 2 demonstrated the vast potential of applying high-throughput and quantitative methods to engineering gene regulatory circuits, it is limited to testing circuits in batch-mode. As a result, we went on to adapt this platform to enable the implementation of steady state cell-free TX-TL reactions at high-throughput. In Chapter 3, we present a microfluidic device that is again based on surface immobilized DNA templates, which are housed in an array of unit cells that can be replenished with fresh cell-free reagents over time. We can tune DNA sequence and concentration as before, and differences in unit cell geometries give rise to a range of steady state protein expression profiles as well. Furthermore, we have integrated on-chip mixing with pulse width modulation, enabling us to program the concentration of different inputs over time. We anticipate that this platform could serve as a powerful tool for characterizing gene regulatory networks that necessitate a non-equilibrium reaction environment.

The microfluidic devices fabricated in Chapter 2 and 3 enclose nL-volume *in vitro* TX-TL

reactions in physical compartments created by pneumatic valves, however another strategy for separating individual reactions is to encapsulate them in droplets. In chapter 4, we describe a microfluidic flow focusing device to produce double emulsion droplets containing cell-free reagents. The device also incoporates pneumatic valves that enable the real-time formulation of different reagents using pulse width modulation, providing the means to precisely titrate the concentration of different reaction components. Additionally, the pneumatic valves can effectively control fluid flow into and out of the device, permitting drop production from reagent volumes as low as 10 μL with minimal sample loss. When using expensive cell-free reagents, such as commercial PURE and lysate reactions, this feature is especially convenient.

2

Cell-free gene regulatory network engineering with synthetic transcription factors

This work has been published in *PNAS*, 2019.

Authors: Zoe Swank*, Nadanai Laohakunakorn*, Sebastian J. Maerkl
*equal contributions

Reference: Swank, Z., Laohakunakorn, N., and Maerkl, S.J. (2019). Cell-free gene-regulatory network engineering with synthetic transcription factors. *Proceedings of the National Academy of Sciences*, 116(13):5892–5901.
DOI: 10.1073/pnas.1816591116

2.1 Abstract

Gene regulatory networks are ubiquitous in nature and critical for bottom-up engineering of synthetic networks. Transcriptional repression is a fundamental function that can be tuned at the level of DNA, protein, and cooperative protein – protein interactions, necessitating high-throughput experimental approaches for in-depth characterization. Here we used a cell-free system in combination with a high-throughput microfluidic device to comprehensively study the different tuning mechanisms of a synthetic zinc-finger repressor library, whose affinity, specificity, and cooperativity can be rationally engineered. The device is integrated into a comprehensive workflow that includes determination of transcription factor binding energy landscapes and mechanistic modeling, enabling us to generate a library of well-characterized synthetic transcription factors and corresponding promoters, which we then used to build gene regulatory networks *de novo*. The well-characterized synthetic parts and insights gained should be useful for rationally engineering gene regulatory networks and for studying the biophysics of transcriptional regulation.

2.2 Introduction

Cell-free systems have emerged as versatile and efficient platforms for rapid engineering, characterization, and implementation of genetic networks. It has been demonstrated that linear genetic cascades [73], logic gates [95], and oscillators [100, 101, 131] could be implemented and characterized in cell-free systems, and that networks engineered in cell-free systems function in cells with remarkably similar characteristics, indicating that cell-free systems accurately emulate the cellular environment [131, 132]. Besides these examples in molecular systems engineering and characterization of complex biological systems, cell-free systems provide a viable starting point for the bottom-up synthesis of artificial cells [56, 133]. Work is progressing in establishing critical cellular sub-systems including DNA replication [134], metabolism [135], ribosome synthesis [136], membrane synthesis [137], and protein structures [138]. Gene regulatory networks (GRNs) are one such critical sub-system, and here we demonstrate *de novo* bottom-up engineering and comprehensive characterization of synthetic GRNs in a cell-free system.

GRNs execute the genome and thus play a central role across all domains of life. Due to their importance and ubiquity, GRNs have been intensely studied and considerable progress is being

made in deciphering components, topologies, and general mechanisms of GRNs, although a complete mechanistic understanding is still lacking. Because GRNs perform many sophisticated cellular tasks, synthetic biologists use GRNs to engineer new systems [139] such as logic gates [140], toggle switches [27], band-pass filters [141], and oscillators [28]. Nonetheless, past and current efforts in engineering GRNs have shown that rational design is not yet possible, and that engineering GRNs still heavily relies on trial-and-error and high-throughput screening approaches [140]. The inability to rationally design GRNs is in part due to the aforementioned lack of complete mechanistic understanding, and because basic GRN components such as transcriptional regulators and promoters are often neither fully characterized nor standardized. A corollary of the lack of an in-depth mechanistic understanding of these systems is that individual components are not yet readily composable. Nature provides a plethora of potential transcriptional regulators, but the number that have been tested and characterized remains rather limited. Most engineered GRNs make use of naturally occurring transcription factors, making it difficult to robustly engineer GRNs with such a non-standard set of proteins [142]. A library of well-characterized, synthetic transcription factors could alleviate many of these problems by providing a set of standardized transcription factors that are based on the same basic structural framework, and whose function can be extended by generating fusion proteins in a plug-and-play format.

Native GRNs employ a wide range of transcription factors that can be categorized into several structural families. The family with the largest number of members is the zinc-finger (ZF) family, followed by homeodomain, basic helix-loop-helix, and basic-leucine zipper (LZ) families [143]. ZFs are of interest in biology as they represent the largest class of transcriptional regulators and are involved in diverse biological functions. ZFs are also appealing for bottom-up engineering as they consist of well-defined subunits that, in combination, determine DNA sequence specificity [144, 145]. Many resources are therefore available that provide sequence specificity information for a large number of native [146] and engineered [147] ZF transcription factors. An additional advantage is that ZFs are small (264 bp, 10.6 kDa (Zif268)) compared to other engineerable transcriptional regulators such as TALE (e.g. 1161–2397 bp, 39.9–82.6 kDa, DNA binding domain only [148]) or dCas9 (4107 bp, 158.3 kDa), so that the coding sequence for ZFs is easily obtainable and modifiable. Due to their small size and simple structure, ZFs can be readily expressed both *in vivo* and *in vitro*. Synthetic ZFs have already been successfully used as activators in *S. cerevisiae* [149] and human cells [150]. Here we engineer and explore the use of synthetic ZF transcriptional regulators as ideal

building blocks for bottom-up design and implementation of cell-free GRNs.

In this paper, we took advantage of an existing synthetic ZF library [110] to generate a well-characterized resource of transcriptional repressors and corresponding synthetic promoters that can be used for bottom-up design, implementation, and characterization of GRNs in cell-free systems. While the mechanism of action of the simplest prokaryotic repression is competitive inhibition [151], it has long been appreciated that both *cis* modifications to the promoter, such as operator position [152], basal promoter strength [153], as well as *trans* modifications to the transcription factor itself strongly affect repression [154, 155]. These inter-dependencies result in a large experimental space with many degrees of freedom. In order to tackle this complexity we developed a microfluidics based method capable of performing 768 cell-free transcription-translation (TX-TL) reactions on a single device. The ability to rapidly generate ZF repressor and promoter variants using fast PCR assembly and the use of our high-throughput microfluidic device allowed us to perform a comprehensive characterization of repressors and promoters. We investigated the effects of binding site position, binding site affinity, binding site combinations, and cooperative interactions between the repressors on transcriptional repression performance. We generated quantitative position weight matrices (PWMs) for four ZF repressors with MITOMI [106], which allowed us to rationally tune binding site affinity and promoter output. Finally, we used the parts library and insights acquired in this study to engineer logic gates, showing that *de novo* synthetic GRNs can be rationally engineered using a bottom-up approach. The transcription factor / promoter parts library, data, and methods described here provide a resource that should facilitate efforts to build synthetic GRNs, serve as a viable approach for building GRNs for use in artificial cells, and establish an experimental platform for studying the biophysics of transcriptional regulation.

2.3 Results

2.3.1 Design and characterization of a microfluidic device for high-throughput cell-free experiments

The design space of even a single TF – promoter pair is large, encompassing different binding site affinities, binding site positions, binding site sequences, and binding site combinations. This complexity necessitates high-throughput methods capable of the functional characterization of hundreds to thousands of engineered variants. Current approaches in cell-free synthetic biology primarily rely

on standard microtiter plates, which require a minimal reaction volume of 5 – 10 μL. Such relatively large volumes quickly become cost-limiting in terms of how much cell-free reaction solution and DNA is required to perform the assays. Researchers recently made use of an acoustic liquid handling robot that reduced reaction volumes to 2 μL in a 384 well plate format [111]. Here we repurposed the MITOMI platform, a microfluidic device originally developed for high-throughput molecular interaction analysis [106, 156], and applied it to the high-throughput characterization of cell-free genetic networks. The repurposed device performs 768 cell-free reactions, and reduces volumes by ∼4 orders of magnitude to ∼690 pL per reaction.

The process involves the synthesis of DNA parts, followed by microarraying and incorporation into microfluidic unit cells where they serve as templates in cell-free TX-TL reactions (Fig. 2.1A). To expedite the synthesis of large libraries of DNA parts we used an assembly PCR strategy to generate linear DNA templates with different promoter regions upstream of a deGFP gene. A microarray robot is used to spot the linear templates onto an epoxy-coated glass slide, on top of which the PDMS device is aligned. Immobilizing DNA within each reaction chamber first requires surface patterning in the assay section of each unit cell, resulting in a circular area of neutravidin to which biotinlyated DNA can bind. Once DNA is surface immobilized, cell-free extract is flowed into the device and the unit cells are isolated from one another while the TX-TL reactions occur. A detailed schematic of the experimental procedure is shown in Supplementary Figure 2.8A.

Controlling the precise amount of DNA in each unit cell is important for quantitative experiments. By simply varying the concentration of spotted biotinylated DNA templates we were unable to precisely control DNA concentration on-chip. We thus developed an approach based on spotting a mixture of single stranded biotinylated DNA oligos (ssDNA) and double stranded DNA templates (dsDNA). The amount of DNA immobilized on the surface reached saturation at a concentration of ∼100 nM spotted DNA (Supplementary Fig. 2.9). We therefore held the total concentration of spotted DNA above this saturation point. Changing the ratio of dsDNA:ssDNA gave rise to a linear correlation between the concentration of dsDNA free in solution (DNA_F) and dsDNA bound to the surface (DNA_B), and was insensitive to the total amount of DNA deposited during spotting (Fig. 2.1B, C). This approach allowed us to immobilize DNA over a wide concentration range, which gave rise to corresponding levels of expressed deGFP (Fig. 2.1D, E). The results obtained with the high-throughput microfluidic device are reproducible with a global normalized root-mean-square deviation of ∼14%, not only when a single dsDNA template is used, but also

for more complex experiments requiring multiple templates in each unit cell (Supplementary Fig. 2.10). Furthermore, a subset of on-chip measurements was carried out in standard micro-well plate reactions, showing good correlation (Supplementary Fig. 2.11).

To demonstrate the high-throughput capabilities of our microfluidic chip we created and characterized a library based on the *E. coli* σ_{70} λP_R promoter. We synthesized 124 promoter variants that covered all possible single base mutations within the -47 to -7 region of the λP_R promoter (Fig. 2.1F). Cell-free reactions for each promoter were run in 6 replicates on a single chip and yielded deGFP expression profiles revealing the impact of each mutation on protein expression (Fig. 2.1F, Supplementary Fig. 2.10A). As expected, mutations within the -10 and -35 boxes affected deGFP expression most strongly and the results are comparable to previous results obtained by an *in vivo* analysis of the lac promoter [157].

Protein synthesis eventually stops in cell-free batch reactions as seen in the saturation dynamics in time course measurements (Fig. 2.1E); this is fundamentally different from cellular steady state protein levels which result from balancing production with degradation and dilution rates. In this paper we report end-point batch reaction values and derived quantities such as fold repression. It is thus important that the end-point values correspond to protein production rates. While the relationship between the initial rate of deGFP production and its final saturated level may be complex, we observe a linear relationship between the two quantities under our experimental conditions (Supplementary Fig. 2.12). This is an important validation of our use of end-point protein levels and linearly derived quantities such as fold repression as proxies for synthesis rates and their ratios.

2.3.2 Zinc-finger repressor and promoter library design

Using the characterization of the λP_R promoter as a starting point, we applied our chip to the in depth characterization of synthetic ZFs for use as transcriptional repressors. We adopted a ZF design based on Zif268, a three-finger Cys2His2 protein. A large ZF repressor library can be generated by combinatorially shuffling a small number of individual ZF domains (Fig. 2.2A). We utilized ZF proteins drawn from a 64-member library that we previously synthesized and characterized [110] (Supplementary Fig. 2.13).

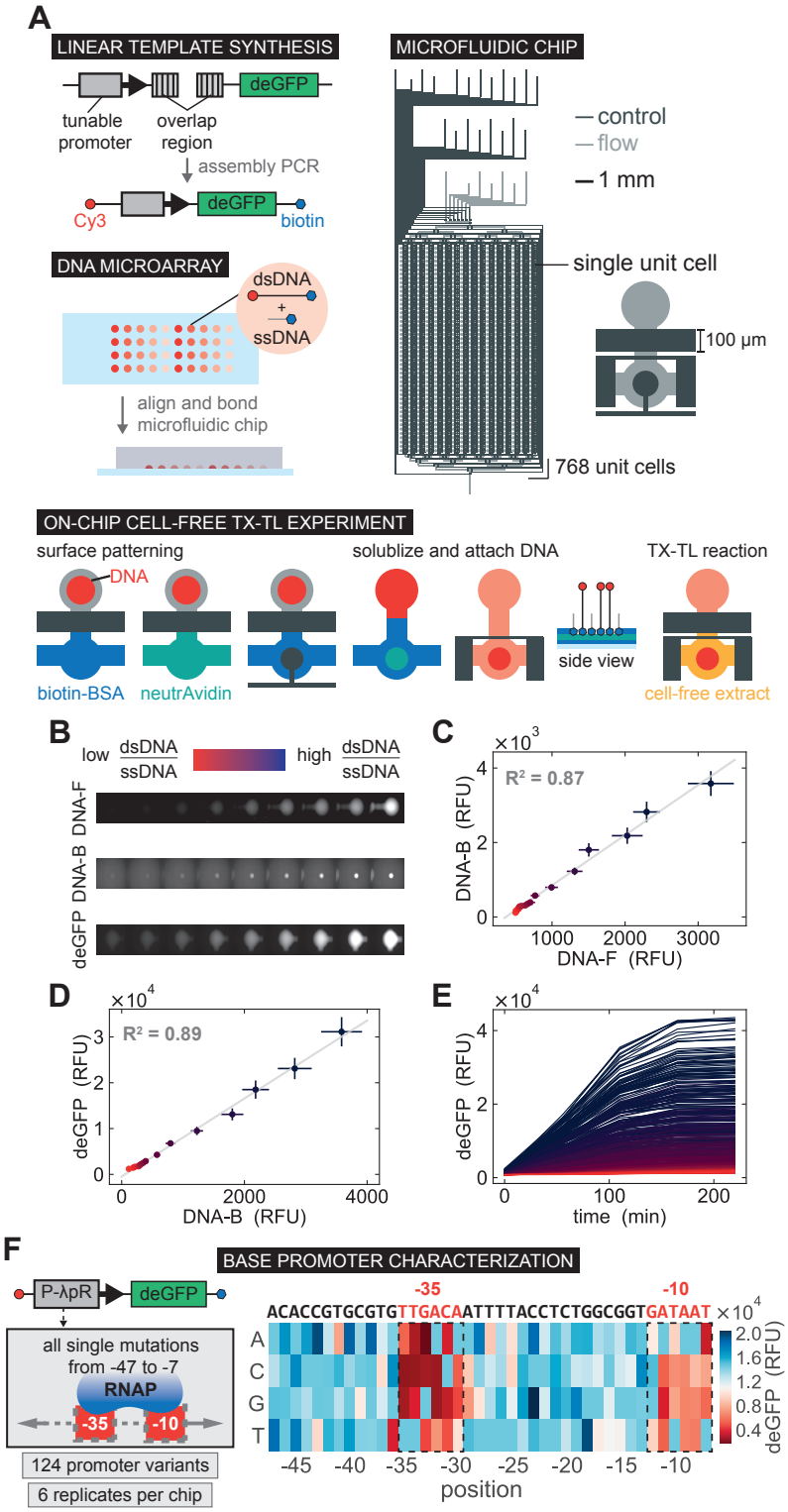

Figure 2.1: **High-throughput microfluidic cell-free reactions.**

Caption on the next page.

Figure 2.1: **High-throughput microfluidic cell-free reactions.** **(A)** A schematic overview of the experimental design including synthesis of DNA templates, DNA spotting, chip alignment, surface functionalization followed by DNA immobilization and on-chip cell-free TX-TL reactions. **(B)** Fluorescence images of Cy3-DNA_F, Cy3-DNA_B, and deGFP expressed for a range of ds-DNA:ssDNA ratios. **(C)** Quantification of surface immobilized DNA (DNA_B) as a function of free DNA in solution (DNA_F). **(D)** deGFP expression at the final time point as a function of DNA_B concentration. All values represent means ± SD ($n = 48$). **(E)** deGFP expression measured over time in all unit cells. **(F)** Schematic of a promoter library design and on-chip experimental throughput, followed by the deGFP expression for all single base mutations from position -47 to -7 of the λP_R promoter.

The affinity of a ZF repressor to DNA can be improved by increasing the number of finger domains [158, 159, 160, 161]. The same effect can also be achieved by engineering dimerizing ZFs that bind cooperatively. An early example used structure-based design to engineer a two-finger ZF which dimerized via a leucine zipper (LZ) motif to form a four-finger complex [162, 163]. Three-finger ZFs have also been dimerized using PDZ domains [149]. Cooperative interactions are of interest because they potentially increase the nonlinearity of regulation, as well as decreasing non-specific binding compared to extended arrays of ZFs. To study cooperative interactions we built several different ZFs fused to either PDZ or LZ domains (Fig. 2.2B).

In parallel, we designed corresponding repressible promoter libraries. As we use an *E. coli* cell-free system [164], we based our promoter designs on the strong λP_R promoter in combination with transcription and translation elements optimized for *E. coli* cell-free expression [96]. Previous work has shown that the most effective position for transcriptional repression is the space between the -35 and -10 boxes [152]; we thus generated a library with consensus ZF binding sites (ZFBSs) inserted into this location. Additionally, we built promoters with a second ZFBS upstream of the -35 box, allowing us to study the effect of multiple non-cooperative and cooperative ZFBSs (Fig. 2.2B). The promoters drive expression of a deGFP reporter, a GFP protein previously optimized for cell-free translation [165]. All constructs were built and tested using linear DNA templates generated by PCR in concordance with recommended guidelines for cell-free expression [96].

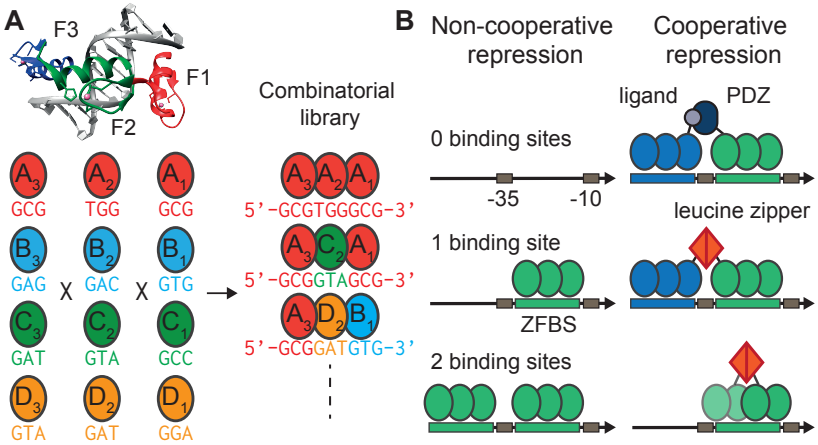

Figure 2.2: **Zinc-finger repressor and promoter design. (A)** Our repressor design is based on the Zif268 protein, whose three Zn-fingers (`F1`–`F3`) each recognizes a nucleotide triplet. We created a combinatorial library of repressors by shuffling individual Zn-fingers, starting from four initial ZF proteins (here labelled with the codes `AAA`–`DDD`). **(B)** We designed a library of repressible promoters based on the λP_R promoter. To test the effectiveness of repression we designed promoters containing single and dual sites with variable spacing, as well as engineering direct cooperativity between ZF proteins, which can be mediated by PDZ-ligand or LZ interactions.

2.3.3 Repression with single and multiple binding sites

We performed an in depth characterization of 11 synthetic ZFs by assessing their repressive capacity in cell-free reactions, and by measuring their respective dissociation constants (K_d) with MITOMI. We used MITOMI to measure the K_ds for each ZF against all possible target promoters. By localizing pre-synthesized his-tagged ZFs to the surface of each unit cell we are able to measure the binding of DNA sequences spanning the promoter region including the ZF binding site (Fig. 2.3A, Supplementary Fig. 2.8B). We obtained standard Gibbs free energies, $\Delta G = RT \ln(K_d)$, for each ZF – target promoter complex (Fig. 2.3B). A range of binding strengths was observed for the respective consensus ZF binding sequences, as well as low affinity off-target binding. The CBD zinc finger was included as a negative control as it does not bind to its own predicted binding site nor any of the other targets.

To test whether the relative binding strength of each ZF related to functional gene repression, we implemented cell-free TX-TL reactions screening the same matrix of ZFs versus promoters. Each microfluidic unit cell contained a linear template encoding the ZF to be tested and a sec-

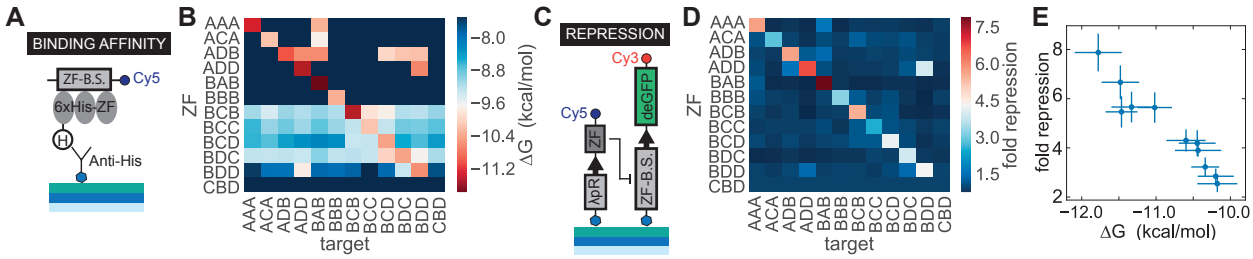

Figure 2.3: **Zn-finger binding affinities, functional repression and orthogonality. (A)** Schematic depicting the MITOMI assay used to determine TF - DNA binding affinities. **(B)** Affinity orthogonality matrix of ΔG values for all zinc fingers versus all possible DNA targets. **(C)** Schematic depicting the linear templates used to test functional repression in on-chip cell-free TX-TL reactions. **(D)** Fold repression orthogonality matrix for all zinc fingers versus all possible targets. **(E)** Fold repression values versus measured K_ds for all ZF - promoter consensus pairs. The fold repression data was collected from a single chip and all values represent means ± SD ($n = 5$). The error bars shown for the K_d values represent the 95% confidence interval for the fit to a single binding site model.

ond linear template encoding deGFP downstream of a promoter with a single ZF binding site (Fig. 2.3C). Binding of the expressed ZF to the target promoter would lead to down-regulation of deGFP expression. A common measure of repression performance is fold repression, or the ratio of unrepressed to repressed expression levels. Unrepressed measurements were obtained by co-expressing the target promoter template with the non-binding ZF_{CBD} template to control for loading effects [98]. Despite some off-target binding observed by MITOMI, functional repression of all ZF – target pairs was almost perfectly orthogonal (Fig. 2.3D), with one exception: the repression of promoter BDD by ZF_{ADD}. However the general trend of weak off-target affinities translated to no or minimal off-target repression, resulting in functional repression only for cognate pairs. Furthermore, on-target fold repression directly correlated with the measured MITOMI affinity values (Fig. 2.3E). Using two high-throughput microfluidic techniques we were able to characterize the binding affinity, repressive strength, and orthogonality of synthetic transcription factor – promoter pairs.

Promoters with a single ZF binding site achieved low to medium fold repression levels in the range of 1.5 to 7 (Fig. 2.4A). We tested whether placing an additional binding site upstream of the -35 box could further improve fold repression levels. While fold repression is a convenient measure used to describe the functionality of a given repressor – promoter pair, for applying these

repressors in genetic networks it is important to also consider basal promoter strength (unrepressed state) and leak (repressed state). These quantities are also shown in Figure 2.4, where we observed that variation in binding site sequence led to variations in basal promoter strength; this variation increased upon inclusion of the second binding site upstream of the -35 box. At the same time, the average leak from the repressed state decreased for the dual site library, resulting in higher fold repression values. Overall, fold repression improved for almost all two binding-site promoters, with the best promoters achieving a fold repression level of $7 - 10$ (Fig. 2.4B). These results showed that good repression levels can be achieved by synthetic ZF repressors with either single or double binding site promoters in a cell-free system.

Next we characterized the effect of binding site position on repression strength. We generated a library of promoters containing a single ZF binding site that was placed in various positions relative to the -35 box. Best fold repression was achieved by positioning binding sites directly proximal to the -35 box, in the range of -2 to +4 bps relative to the start and end of the -35 box, respectively. We also observe that repression is sensitive to single bp shifts in position. For instance, the site at the +5 position is effectively non-functional compared to repressing neighbouring sites at +4 and +6; and the site at the -5 position exhibited significantly stronger repression than its neighbours at -4 and -6. Based on the crystal structure alignment of ZF and RNA polymerase bound to DNA containing the binding site at position +5, we note that it is possible for both proteins to bind simultaneously with minimal steric interference. To ascertain that the observed repression strengths were not due to changes in binding site affinity of the ZF, as each binding site is located in a different sequence context, we measured the binding affinity of the ZF repressor to each promoter using MITOMI. The results showed only minor differences in affinity across all promoters, suggesting that the ZF repressor bound to these promoters with equal strength. Promoter repression thus appears to be primarily a function of the ability of the ZF to sterically hinder and compete with RNA polymerase. These data are consistent with an occlusion mechanism whereby RNAP binding is competitively inhibited by ZF binding [151], and the effectiveness of the competition is dependent on the relative positions of ZF and RNAP on the promoter.

2.3.4 Engineering cooperativity

We showed that incorporating a second binding site can result in improved fold repression. However, engineering certain types of genetic circuits often requires an additional increase in the nonlinear

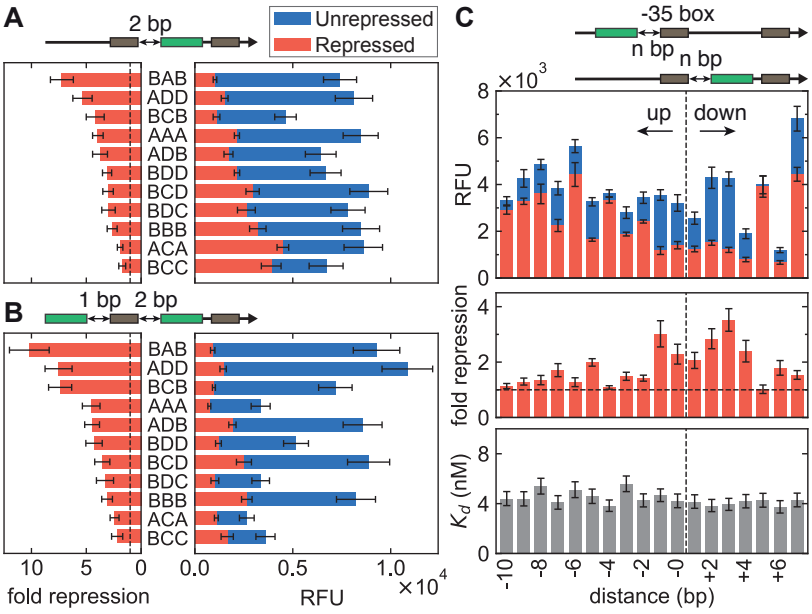

Figure 2.4: **Effect of binding site number and position on repression.** Shown are endpoint unrepressed and repressed levels for the single binding site library **(A)**, and the dual site library **(B)**. Within each library, the data are rank-ordered by fold repression values. Data were collected from two separate chips and all values represent means ± SD ($n = 10$). **(C)** A single BCB site was shifted up to 10 bp upstream and 7 bp downstream of the -35 box; position values are given by the number of nucleotides separating the 9-bp site from the -35 box. The binding affinities of the ZF to its target site remains approximately constant irrespective of target site position (**(C)**, bottom). Data from the top panel was measured from a single chip and all values represent means ± SD ($n = 7$). The error bars shown for the K_d values represent the 95% confidence interval of the fit to a single binding site model.

response, as well as a decrease in the leak for a given promoter – TF pair. Nonlinearity can be increased by introducing cooperativity via protein – protein interactions. We implemented two different protein interaction domains previously demonstrated to successfully dimerize ZFs.

PDZ domains enable natural protein – protein interactions by binding specific C-terminal peptide sequences with micromolar affinity [149]. We took advantage of this interaction to engineer cooperativity by linking ZF_{BCB} to a mammalian α1-syntrophin PDZ domain, and ZF_{ADD} to its corresponding cognate C-terminal peptide ligand (VKESLV). Furthermore, we linked ZF_{ADD} with a non-cognate ligand (VKEAAA) to use as a non-cooperative control. The second type of inter-

action we explored was dimerization by linking ZF_{BCB} and ZF_{ADD} to GCN4 LZ domains. The GCN4 LZ has previously been used in a structure-based design to enable homodimerization of two-finger ZFs [162], and we thus also tested this existing structure. In both cases, a mutated LZ was used as a negative control.

Preliminary studies on a plate reader demonstrated that ZFs containing interaction domains exhibited significantly increased fold repression and decreased leak (Fig. 2.5A, B). Whereas two non-cooperative repressors gave a maximum fold repression of ∼6, this value was increased to ∼30 for PDZ and ∼16 for LZ-mediated cooperativity. Concurrently, leak values decreased four-fold from around 4000 to <1000 RFUs. One critical parameter affecting PDZ cooperativity was the choice of linker, with an optimized glycine-serine linker vastly outperforming a rigid proline linker. The two-finger LZ transcriptional repressor also performed very well, achieving a fold repression ratio of ∼28.

To investigate cooperativity in more detail, we measured dose response curves by titrating repressor DNA concentration. To keep a fixed load on the transcription-translation machinery, the total ZF DNA concentration was kept constant by adding DNA coding for a non-binding ZF control (ZF_{CBD}). Figure 2.5C shows dose response curves of $ZF_{BCB} - PDZ$ and $ZF_{ADD} - L$ separately, together with those for the cooperative pair $ZF_{BCB} - PDZ + ZF_{ADD} - L$, and the non-cooperative pair $ZF_{BCB} - PDZ + ZF_{ADD} - NL$. An increase in the steepness of the dose response curve was observed as we proceeded from a single ZF to two non-cooperatively interacting ZFs, and finally to two cooperatively interacting ZFs. Similar results were obtained for the LZ designs (Fig. 2.5D, E). The effect of cooperativity can be quantified by determining the sensitivity (Supplementary Fig. 2.14), which measures the steepness of the dose response curve [166], as well as the effective Hill coefficient, which is obtained by fitting phenomenological Hill functions (Supplementary Fig. 2.15). The results of this analysis are shown in Table 6.3 (Appendix). We observe that cooperativity increased sensitivity by nearly 50% with respect to the non-cooperative repression, as well as slightly increasing the Hill coefficient.

We sought to understand this behaviour quantitatively by developing a thermodynamic model that relates protein expression to the equilibrium occupancy of the promoter by RNAP [167]. We extended the standard competitive model of repression to include a term for the interaction between repressor and RNAP, which is quantified by an effective interaction energy. As this energy tends to large positive values, DNA binding by either RNAP or the repressor is exclusive, and the model

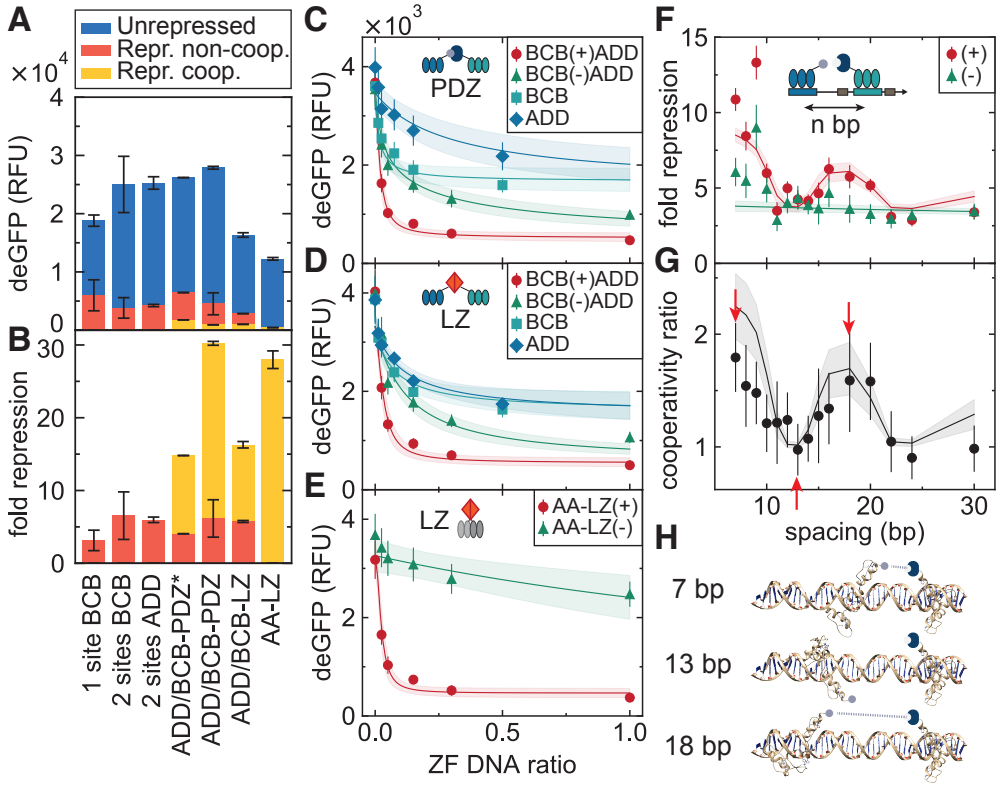

Figure 2.5: **Engineering cooperativity.** Comparison of unrepressed and repressed levels **(A)**, as well as fold repression **(B)**, for different cooperative zinc-finger designs. Three-finger ZFs dimerized using either PDZ-ligand or GCN4 LZ domains. ZFs were linked to interaction domains using proline (-PDZ*) or optimized glycine-serine linkers (-PDZ, -LZ). Additionally, two-finger ZFs were dimerized using LZs (AA-LZ). Data in panels A and B were taken from plate reader experiments; all values represent means ± SD ($n = 3$). **(C–E)** The dose response is shown for individual ZF repressors as well as non-cooperative (-) and cooperative (+) pairs of ZFs, for the three-finger PDZ, and two- and three-finger LZ designs. The maximum *a posteriori* values as well as 2 SD boundaries of the model predictions are represented as solid lines and shaded regions, respectively. Data in panels C–E were measured on a single chip; all values represent means ± SD ($n = 12$). Shifting the binding site upstream of the -35 box resulted in periodic modulation of the fold repression for the cooperative designs **(F)** as well as in the ratio between the cooperative and non-cooperative fold repressions **(G)**, likely due to periodic changes in relative ZF positioning **(H)**. All data were collected from a single chip and all values represent means ± SD ($n = 9$).

tends towards that of competitive inhibition. As the energy approaches zero, both RNAP and DNA can bind simultaneously, resulting in leaky expression at full repressor occupancy. This extension to the model was motivated by our results that a ZF with a fixed binding affinity represses with varying efficiency depending on the position of the binding site; the changing RNAP-ZF interaction energy therefore provides a simple description of this effect. We fit the model to the dose response curves using Markov chain Monte Carlo (MCMC) sampling (Supplementary Fig. 2.16), allowing us to consistently extract the posterior probability distributions of all parameters, which consist of fixed effective dissociation constants of each individual ZF, as well as the effective energies describing ZF-RNAP and ZF-ZF interactions. The fits are shown in Figure 2.5C–E as solid lines and shading, which represent the mean and 2 SD boundaries for model predictions, respectively. The values of all fitted parameters are given in Table 6.4 (Appendix), and a full description of the model is given in the Materials and Methods section. We find physically sensible values for all our parameters; in particular, the cooperative interaction energies for PDZ-L (-2.1 ± 0.2 kcal/mol) and LZ (-1.8 ± 0.2 kcal/mol) are consistent with literature values for similar domains (~ -2 to -10 kcal/mol [168, 169]).

Since the location of the ZF binding site, and hence the relative positioning of ZF and RNAP, is an important determinant of repression efficiency, it is likely that the relative positioning of the $ZF_{BCB} - PDZ$ and $ZF_{ADD} - L$ binding sites would also determine their ability to interact and subsequently alter their repressive strength. Keeping the $ZF_{BCB} - PDZ$ binding site position fixed, we shifted the $ZF_{ADD} - L$ binding site further and further upstream. If the two ZFs are positioned on the promoter such that the cooperative PDZ – ligand interaction is unfavorable, we would expect fold repression to be similar to that of the non-cooperative ZFs. In other words, the ratio between the cooperative and the non-cooperative fold repression, a quantity we call the cooperativity ratio, should go to unity when the PDZ – ligand interaction cannot occur.

We observed an effect due to this variation of spacing between the two binding sites (Fig. 2.5F), and this behavior corresponded to the relative orientation of the PDZ-ligand domains. As the binding site is shifted, $ZF_{ADD} - L$ rotates around the DNA, modulating its alignment with $ZF_{BCB} - PDZ$. The cooperativity ratio fell to 1 when the interaction was unfavorably aligned, but increased again as the domains began to realign (Fig. 2.5G). The cartoon in Figure 2.5H shows the predicted orientations of the two ZFs as the left-hand site is shifted. The ability of the ZFs to interact over distances of a few tens of bp is likely due to extension of the long flexible glycine-

serine linker used to join the ZF_{BCB} and the PDZ domain. It is unlikely that DNA bending plays a significant role at these distances, due to dsDNA's much longer persistence length of ∼150 bp.

We incorporated into our model a phenomenological exponential decay of interaction energies with distance, both between the two ZFs as well as between the ZF and the RNAP. Additionally, the ZF – ZF interaction energy was modulated by a periodic function at the frequency of the DNA helical pitch (10.5 bp/turn). Using previously inferred parameters for energies and K_Ds from the dose response measurements, we performed a fit to determine the decay constant and phase shift; the results are shown as solid lines and shading in Figure 2.5F and G, and in Table 6.4 (Appendix). Fitting a model with an explicit position dependence for the binding sites illustrates the importance of site positioning for functional repression. More generally, while simplistic, our model fits demonstrate that it is possible to understand cell-free gene expression in terms of thermodynamic occupancy.

2.3.5 Affinity tuning

In order to test whether fold repression levels could be precisely and predictively tuned, we investigated the effect of varying binding site affinity. In order to rationally tune binding site affinity, we first generated quantitative PWMs for three ZFs: ZF_{BCB}, ZF_{AAA} and ZF_{ADD}, covering the 9-bp core sequence plus three flanking bases on either side (Fig. 2.6A, Supplementary Fig. 2.17A, B). The sequence logo determined for ZF_{AAA} is in concordance with the consensus sequence determined by bacterial one-hybrid and *in vitro* SELEX assays [170, 171]. Based on our PWMs we designed a library of promoters that included a single binding site at a fixed position between the -35 and -10 boxes, with single or double mutations within or outside the core binding sequence. As binding site affinity decreased we observed corresponding decreases in fold repression for all ZFs tested (Fig. 2.6B, Supplementary Fig. 2.17C). By converting our macroscopically measured ΔG values into microscopic interaction energies $\Delta\epsilon$ we found that the fold repression data could be described by the same thermodynamic model presented in the previous section.

Mutating either a single base outside the core site, or one core position of low information content (high entropy), enabled fine tuning of fold repression, whereas a single mutation in the core site of high information content strongly decreased fold repression. Two core mutations decreased fold repression to baseline levels. Fold repression was therefore precisely tuneable over the entire dynamic range by modulating binding site affinity, and the affinity changes required to achieve

tuning were relatively small. Affinity changes of ~ 0.5 to 1 kcal/mol were sufficient to cover the entire dynamic range for each ZF repressor tested. The results are in line with previous findings that promoter tuning in *S. cerevisiae* can be accomplished by relatively subtle affinity changes in a single binding site created by mutations in flanking or single core site mutations of high entropy [172]. They also correspond to recent results obtained in *E. coli* [173].

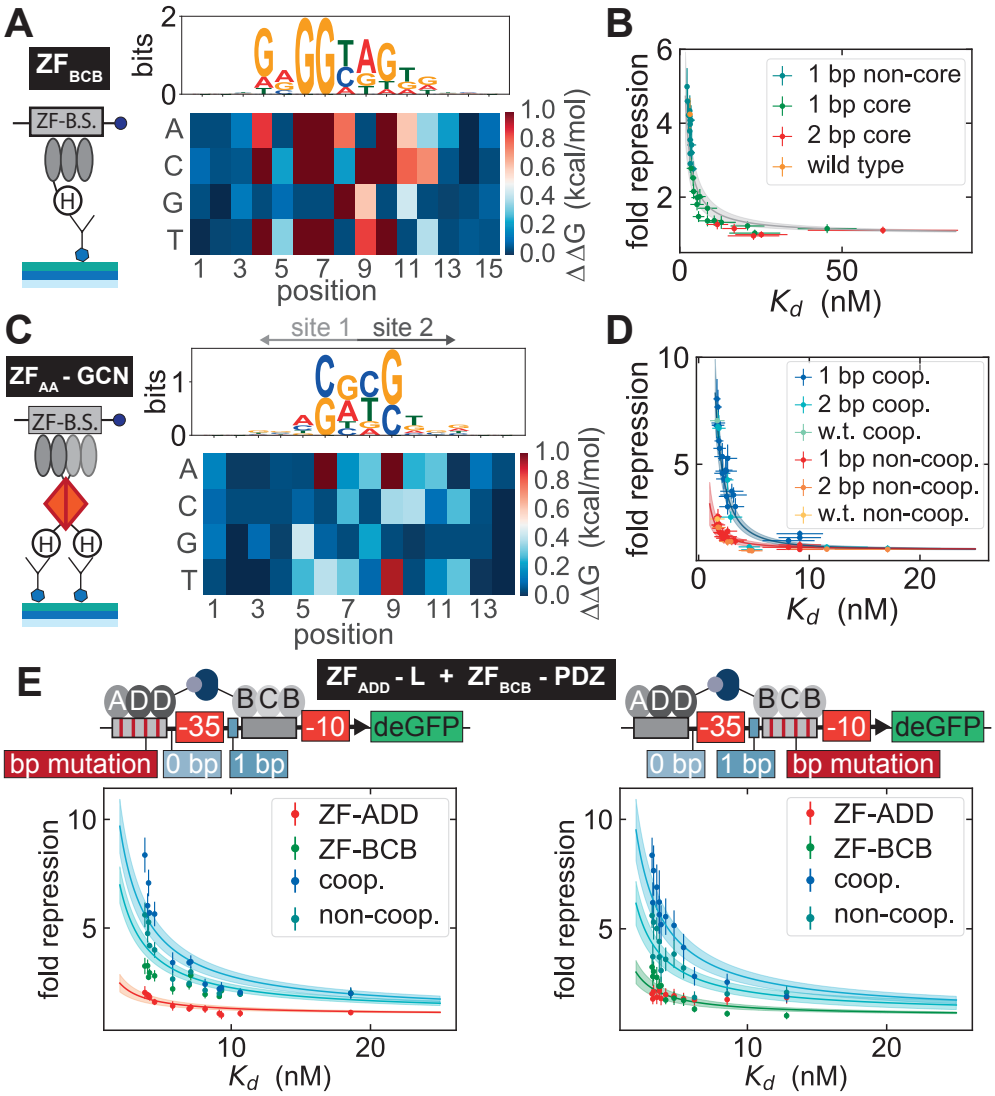

Figure 2.6: **Tuning repression by changing binding site affinity.**

Caption on the next page.

Figure 2.6: **Tuning repression by changing binding site affinity.** **(A)** Schematic of the MITOMI assay used for measuring the binding affinity of a ZF to a given DNA target. To the left, the sequence logo and PWM for ZF_{BCB}, where the core sequence is designated by positions 4-12. **(B)** The relationship between fold repression and K_d values for ZF_{BCB}. The fold repression data was collected from three separate chips and all values represent means ± SD ($n = 7$). **(C)** Schematic of the MITOMI surface used for measuring the binding affinity of the $ZF_{AA} - GCN$ homodimer to a given DNA target. To the left, the sequence logo and PWM for $ZF_{AA} - GCN$, where the core sequence is designated by positions 3-12. **(D)** The relationship between fold repression and K_d values for both the cooperative and non-cooperative variants of $ZF_{AA} - GCN$. The fold repression data was collected from a single chip and all values represent means ± SD ($n = 8$). **(E)** Fold repression versus K_d values for the $ZF_{ADD} - L$ - $ZF_{BCB} - PDZ$ heterodimer pair. On the left the K_ds refer to the K_d arising from the specific change made to the ADD binding site, whereas on the right the K_ds are associated with the BCB binding site. The fold repression data was collected from a single chip and all values represent means ± SD ($n = 4$). In all cases the error bars shown for the K_d values represent the 95 % confidence interval for the fit to a single binding site model, the solid lines are maximum *a posteriori* values from thermodynamic model fits, and the shaded region represents a 2 SD boundary.

Given that a single ZF binding site could be mutated to yield varying levels of repression we investigated whether the same tuning could be applied to cooperative ZFs. We measured the binding affinity of the $ZF_{AA} - GCN$ homodimer versus a library of DNA targets that consisted of all single point mutations for the 10-bp core binding sequence plus 2 flanking bases on either side. The resulting sequence logo and PWM reveal the symmetric binding profile of the homodimer (Fig. 2.6C). Mutating a single binding site within the -35 and -10 boxes led to a change in repression levels that reflected the measured K_ds for both the cooperative and non-cooperative $ZF_{AA} - GCN$ variants (Fig. 2.6D). As the two 6-bp binding sequences overlap, mutating a single base within the core site leads to a finer tuning of fold repression in comparison with the three-finger ZFs. Furthermore, we extended binding site tuning to the $ZF_{ADD} - L$ - $ZF_{BCB} - PDZ$ heterodimer pair, taking advantage of the PWMs generated for ZF_{BCB} and ZF_{ADD}. Implementing a subset of mutations to each ZF binding site yielded a range of fold repression values not only for the single ZF but also for the cooperative and non-cooperative ZF pairs (Fig. 2.6E). As the affinity of one ZF

is reduced we see that the fold repression observed for the cooperative and non-cooperative cases tends to the fold repression measured for the second ZF whose binding site remains constant.

2.3.6 Logic gate construction

Having established a well-characterized resource of transcriptional repressors and promoters, we applied them to designing logic gates. By combining two cooperative ZF repressors on a single promoter we were able to create NAND gates, which are of particular interest as they are functionally complete. An effective NAND gate should have low output only when both inputs are present (Fig. 2.7A). We therefore placed the binding site for a strongly binding ZF (ZF_{BCB}) 2 bp upstream of the -35 box, and second binding site for different ZFs between the -35 and -10 boxes. ZF_{BCB} cannot strongly repress by itself at the -2 position and the second ZF should also not strongly repress on its own. Only when both ZFs are bound to the promoter should they strongly repress, which can be achieved by including a cooperative interaction between the two ZFs. Using this general design we tested NAND gates for $ZF_{BCB} - PDZ$ in combination with the remaining ZFs (Fig. 2.7B). As expected, NAND gate performance improved as the affinity of the $ZF_{XXX} - L$ decreased. For instance the combination of $ZF_{BCB} - PDZ$ and $ZF_{BDD} - L$ gave rise to a functional NAND gate, whereas a combination with $ZF_{AAA} - L$ did not due to the high affinity of $ZF_{AAA} - L$, which led to functional repression even when only $ZF_{AAA} - L$ was present.

Since we showed that binding affinity could be precisely tuned (Fig. 2.6) we tested whether we could improve our non-functional NAND gates. Based on the PWM measured for ZF_{AAA} we mutated the $ZF_{AAA} - L$ binding site sequence in the NAND gate promoter and showed that we could achieve tuning in this context as well (Supplementary Fig. 2.17D). We then investigated the effect of tuning the $ZF_{AAA} - L$ binding site for all possible input combinations and showed that the NAND gate improved as we weakened $ZF_{AAA} - L$ binding affinity (Fig. 2.7C). Mutations +1C and +1A gave rise to functional NAND gates. Decreasing the binding site affinity increased the output when only $ZF_{AAA} - L$ was present; however, when the mutation resulted in a $\Delta\Delta G$ of greater than ~ 0.5 kcal/mol ($\Delta 2T$), the cooperative binding output also suffered. Our synthetic ZF repressors can thus be used to build functional NAND gates, which can additionally be rationally optimized and precisely tuned by modifying binding site affinities.

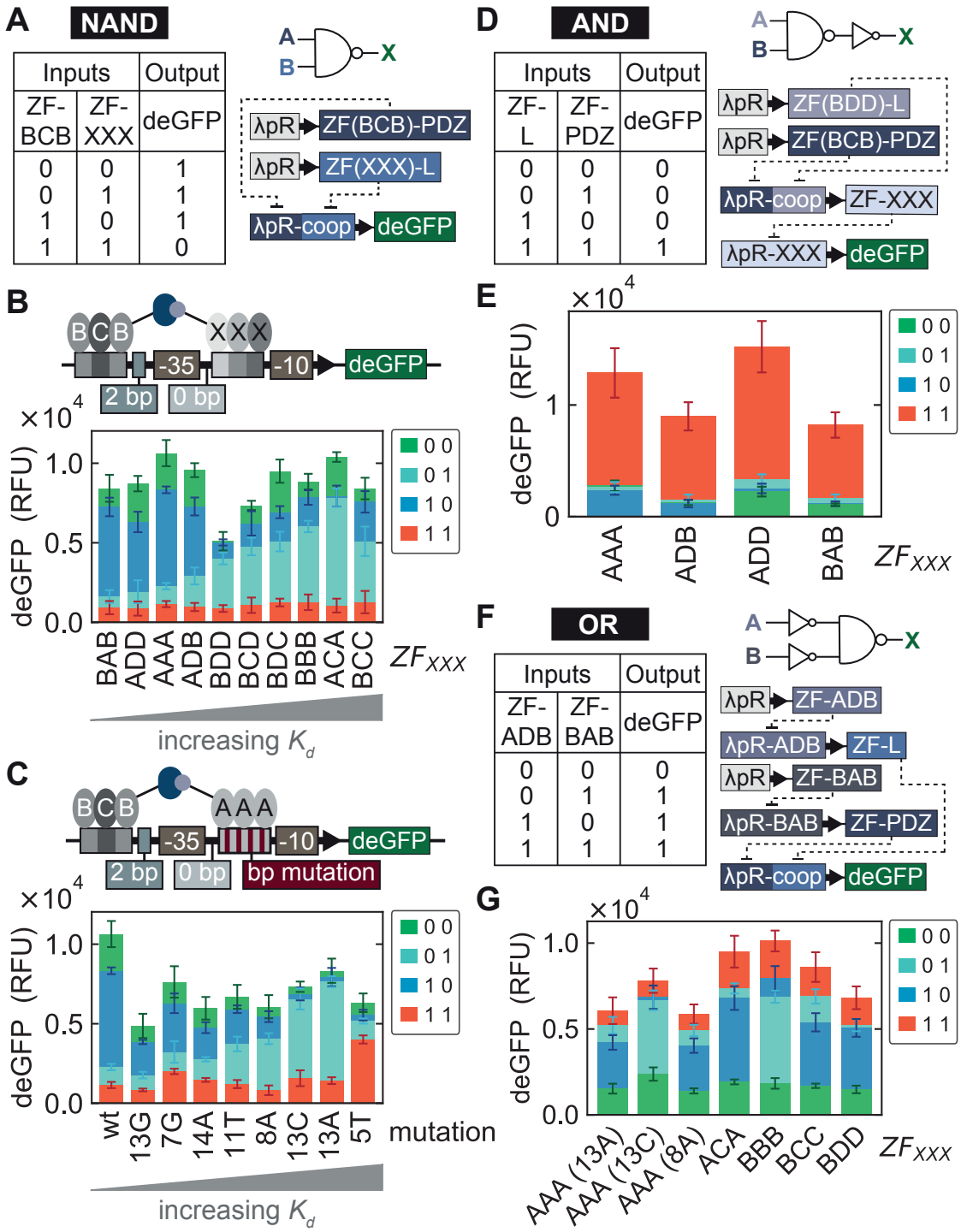

Figure 2.7: **Logic gates.**

Caption on the next page.

Figure 2.7: **Logic gates.** **(A)** Truth table, logic gate symbol and biological network design for constructing a NAND logic gate. **(B)** NAND gate design combining $ZF_{BCB} - PDZ$ with all other $ZF_{XXX} - L$s. Below, the output for each NAND gate tested. **(C)** The same NAND gate design as in **(A)** except that only $ZF_{BCB} - PDZ$ and $ZF_{AAA} - L$ are used as inputs and the $ZF_{AAA} - L$ binding site affinity is rationally adjusted to yield a functional NAND gate. The deGFP outputs for all NAND gates were measured from a single chip where all values presented correspond to the mean ± SD ($n = 5$). **(D)** Truth table, logic gate symbols and biological network design for constructing an AND logic gate. **(E)** The output for each AND gate tested. All output values were measured from a single chip and represent the mean ± SD ($n = 8$). **(F)** Truth table, logic gate symbols and biological network design for constructing an OR logic gate. **(G)** The output for each OR gate tested. When $ZF_{AAA} - L$ is used as part of the NAND gate, the mutation of the binding site is indicated in the parentheses. All output values were measured from a single chip and represent the mean ± SD ($n = 6$).

As a final example we generated compound logic gates by combining NAND and NOT logic gates as linear cascades in order to create AND and OR gates. We created an AND gate by appending a NOT gate to the output of a NAND gate (Fig. 2.7D). Specifically we combined the $ZF_{BDD} - L$ - $ZF_{BCB} - PDZ$ NAND gate with four different ZFs. Each AND gate was tested and yielded the expected outputs (Fig. 2.7E). We then generated OR logic gates by prepending two NOT gates in front of different NAND gates to invert the inputs (Fig. 2.7F). We used ZF_{ADB} and ZF_{BAB} as the two NOT gate inverters and a set of NAND gates, all of which gave rise to functional OR gates (Fig. 2.7G).

2.4 Conclusion

GRNs are of central importance in both native and engineered systems. They integrate, compute, and transduce input signals, leading to specific changes in gene expression. Many components contribute to the function of GRNs, and transcription factors and their interaction with promoters are core players. Due to the complexity of even a single transcription factor – promoter interaction it has proven difficult to quantitatively study these systems *in vitro* or *in vivo*. Although the development of new technologies is steadily enabling progress in this area, our understanding of GRNs remains limited as exemplified by our inability to predict *in vivo* gene expression levels

in essentially any organism, and the difficulty associated with *de novo* engineering of GRNs. Although methods exist for high-throughput *in vitro* characterization of transcription factor binding specificities [106, 174, 175, 176] and medium to high-throughput approaches are used to understand gene regulation *in vivo* [155, 172, 173, 177] both approaches have limitations. Both an advantage and disadvantage of *in vitro* methods is that they generally include only the smallest number of components necessary, i.e. a transcription factor, dsDNA target and a defined buffer solution. *In vivo* methods are on the other hand convoluted by cellular complexity. Furthermore, generating and analyzing defined libraries *in vivo* remains labor intensive and difficult. Here we explored the use of a cell-free transcription-translation system to build and characterize GRNs in an environment that bridges the gap between *in vitro* and *in vivo* methods. This cell-free approach also has the advantage of allowing complex assays to be performed in high-throughput, in a well-controlled and accessible environment. As a consequence, the ability to study functional transcriptional regulation in an *in vitro* system has allowed us to delve into much greater depth than comparable *in vivo* methods have been able to achieve [172, 178, 179]

We chose to build GRNs from the bottom up using ZF transcription factors for several reasons. First, in regards to GRN engineering, researchers have long been hampered by the relatively small number and poor characterization of available transcriptional regulators. Khalil *et al.* have previously engineered ZF regulators, showing that they are viable tunable transcriptional regulators *in vivo* [149]. We built on this concept, generating additional ZF regulators and interaction domains. More importantly, we quantified the binding energy landscapes of several synthetic ZF regulators and were able to show that repression can be precisely tuned with small changes in affinity. These small changes were achieved by mutating the flanking bases lying outside of the consensus core sequence or by mutating one consensus core base of low information content. Hitherto, only coarse tuning has been accomplished through varying the number of consensus sequence binding sites leading to rather large differences in output [149, 150]. The ability to predictively and precisely tune expression levels as demonstrated here is important in engineered GRNs where individual nodes of the network need to be matched in expression levels. For example, we show here that the ability to precisely adjust individual binding site affinities is crucially important for optimizing logic gate function.

With the advent of TALEs and dCas9, ZFs might be considered outdated technology, but there are a number of reasons why ZF TFs remain an appealing tool for GRN engineering. ZFs have

several advantages such as small size, relatively easy gene synthesis, and good expressability. The biggest advantage of dCas9 and TALEs is their programmability, allowing them to be precisely targeted to any DNA sequence. Conversely for ZFs, it remains relatively difficult to rationally design a particular binding site preference. For genome editing and *in vivo* targeting approaches, in which the target sequence is defined and immutable, programmability is crucial. In the context of bottom up GRN design, this ability becomes less important as target sequences can be easily adjusted to a particular TF specificity. We argue that it is actually more important to be in possession of a well-characterized TF binding energy landscape that can be obtained for ZF TFs using current methods [110].

A second argument in support of using ZF transcription factors over TALEs and dCas9 is the simple but important fact that ZFs are native transcriptional regulators and the most abundant class of transcriptional regulators *in vivo*. Cas9, to the best of our knowledge, has not been shown to be involved in gene regulation in native systems, while TALEs are injected into plant host cells to modulate gene expression by pathogenic bacteria [180]. If cell-free approaches are to be used to understand the function of native systems it is important to build GRNs with native transcription factors. For example, the protein – DNA interaction kinetics are very different in that dCas9 [181] and TALE [182] tend to have very slow DNA dissociation rates, while native transcriptional regulators have fast dissociation rates [183], which may make engineering dynamic GRNs using TALEs and dCas9 difficult.

In order to improve fold repression and to add more control over the system we engineered cooperative binding into our ZF TFs by including PDZ or LZ protein – protein interaction domains. These interactions improved repression from ∼10 to up to ∼30 fold and were functional for both two- and three-finger ZFs. We showed that the relative placement of binding sites for two cooperative TFs is a major determinant of interaction capacity and consequently repression strength. Repression was achieved when the TFs were located on the same face of the DNA, and repression strength followed the helical twist of DNA. Cooperative interactions consequently allowed us to engineer functionally complete NAND gates. In all cases we were able to explain our data with thermodynamic models. Combining these models with binding energy landscapes thus provides a viable and useful approach to rationally engineer GRNs.

One outstanding problem encountered during this study is the issue of composability. Although transcription factor binding sites were only introduced in regions outside the -10 and -35 boxes of

the original λP_R promoter, many of the synthetic promoters had considerably different baseline (non-repressed) expression levels. In the future it will clearly be important to better understand and predict basal promoter strength from the underlying sequence, which would lead to models that allow introduction of transcription factor binding sites without affecting basal promoter output. Here we have seen that basal promoter strength itself can be finely tuned over a relatively large range of expression levels (Fig. 2.1). It should therefore be possible to adjust promoter strength as desired: we demonstrate a basic example of this idea by tuning the basal expression level of a repressible promoter (Supplementary Fig. 2.18). Ultimately understanding the outcome of multiple base changes in close context with each other remains a complex issue. Evaluating a greater number of sequences and systematically addressing all factors affecting transcription efficiency similar to the approach taken by Cambray *et al.* towards translation could lead to an improved understanding of promoter sequence design principles [184].

In order to characterize and measure our synthetic ZF transcription factors and promoters in detail we repurposed a high-throughput microfluidic device that allowed us to measure 768 cell-free reactions in parallel. Eliminating cloning and transformation steps by relying on PCR-based assembly strategies allowed us to measure a large number of defined transcription factor and promoter variants. Over 13,000 on-chip cell-free TX-TL reactions were performed, encompassing replicates for ∼2000 unique reactions. We furthermore took over 8000 MITOMI measurements to provide binding energy landscapes for 4 synthetic ZF transcription factors. Together, these technologies allowed us to establish a quantitative and in-depth dataset and insights into transcriptional regulation that should be of general interest. The approach taken here nonetheless does not *per se* require these state-of-the-art technologies, and is easily transferable to standard lab equipment. Cell-free lysate can now be easily and cheaply generated, yielding sufficient material so that medium-scale screens in 384-well plates are feasible [164]. Commercial liquid handling equipment can also be used to scale up throughput. Binding energy landscapes can be generated by many approaches including PBMs [174], MITOMI [107], SELEX-seq [175], and HiP-FA [176]. While our binding energy landscapes are based on direct affinity measurements, it may be sufficient to use PWMs from indirect measurements as found in other high-throughput techniques.

Rapid progress is being made in the development and application of cell-free synthetic biology. Cell-free systems are being used to tackle fundamental problems in molecular engineering and are being applied to molecular diagnostics [185], therapeutics [186], synthesis [187], and are even be-

ing used for educational purposes [188]. Cell-free systems are an appealing alternative to cellular systems, as they eliminate many of the complexities associated with working with cells. Cell-free systems are also a rapid prototyping platform for engineering molecular systems destined to be applied in cellular hosts [131]. As engineered systems become more complex it will become increasingly important that a large number of standardized characterized components become available. It will be equally important to develop a comprehensive mechanistic understanding of these components and systems to allow parts to be standardized and rationally assembled without requiring extensive trial-and-error cycles or large screens, which may not be feasible for large systems. As work progresses on cellular sub-systems such as gene regulation, DNA replication, ribosome biogenesis, metabolic networks, and membrane and protein super-structures, it will be intriguing to contemplate whether it may be possible to integrate these individual systems to create a synthetic cell or cell-like mimic. Work in this area will not only provide tools and methods aiding engineering of synthetic systems, but is likely to provide insights into the function of native systems as well. Prior to being used as tools for protein synthesis and synthetic biology, cell-free systems have already had a rich history in deciphering fundamental aspects of biochemistry including DNA replication [189] and the genetic code [64]. It is likely that they will continue to provide fundamental insights into complex systems such as transcriptional regulation.

2.5 Materials and Methods

2.5.1 Microfluidic chip fabrication

The molds for each device layer were fabricated using standard photolithography. For the control layer, a silicon wafer was primed in an oxygen plasma processor for 7 minutes (TePla 300) and SU-8 photoresist (GM 1070, Gersteltec Sarl) was spin coated onto the wafer yielding a height of 30 μm. Following a soft bake the wafer was exposed to light (365 nm illumination, 20 mW/cm^2 light intensity) using a chrome mask for 10 s on a Süss MJB4 mask aligner. After a post exposure bake the wafer was developed with PGMEA (propylene glycol monomethyl ether acetate) to remove unexposed SU-8 and a hard bake was performed to remove unwanted cracks in the SU-8 structures. For the flow layer, a silicon wafer was treated with HMDS (hexamethyldisilazane) vapor in a YesIII primer oven and AZ 9260 photoresist (Microchemicals GmbH) was spin coated on the wafer to a height of 14 μm. After baking and a one hour relaxation period, the coated wafer was illuminated

with a broadband light using an MABA6 mask aligner with a total dose of 660 mJ/cm split into two exposures of 18 s with a 10 s wait period between (20 mW/cm^2 light intensity). The wafer was developed with AZ 400K developer and baked at 175 °C for two hours to re-flow and anneal the AZ structures.

Each of the wafers was subsequently treated with TMCS (trimethylchlorosilane) and coated with PDMS (polydimethylsiloxane, Sylgard 184, Dow Corning). For the control layer PDMS with an elastomer to crosslinker ratio of 5:1 was prepared and poured over the wafer to yield a height of ∼0.5 cm, while for the flow layer, PDMS with a 20:1 elastomer to crosslinker ratio was spin coated at 1800 rpm to yield a height of ∼50 μm. Both PDMS coated wafers were placed in the oven at 80 °C for 20 minutes. After an initial curing the control layers were cut out and the holes for each control line were punched using a 900 mm pin. Each control layer was then aligned by hand on top of a flow layer using a Nikon stereo microscope and the aligned devices were placed in the oven at 80 °C for 90 minutes, allowing the two layers to bond together.

2.5.2 Preparation of cell-free extract

BL21 Rosetta *E. coli* cell-free extract was a gift from the Murray lab (Caltech) and prepared according to a published protocol [164]. As described in the cited protocol, the addition of purified gamS protein is added to the final reaction mixture to prevent the degradation of linear DNA templates by nucleases.

2.5.3 Preparation of DNA templates

All promoters were generated by PCR from a pBEST-OR2-OR1-Pr-UTR1-deGFP-T500 plasmid [165] (Addgene #40019). Oligos containing the promoter variants were ordered from IDT. Assembly PCR was used to synthesize the complete template including a given promoter variant and the downstream deGFP gene. In the first step two linear DNA products are amplified with PCR where each product contains a 20 bp overlap region and one of the products contains the change to the base promoter. The overlap region was generally between the -10 box and the RBS. In the second step the two DNA products were annealed together and the entire template was amplified using global primers which were labeled with a fluorescent molecule (Cy3) on the 5' end and biotin on the 3' end. ZF repressor templates were generated by PCR from gBlock gene fragments (IDT) that included the λP_R promoter. Global primers labeled with Cy5 at the 5' end and biotin at the 3'

end were used to synthesize the ZF templates. To amplify ZF gene templates with cognate or non-cognate ligands a separate 3' primer was used to incorporate the ligand. However, to produce ZF - PDZ or LZ gene templates, an assembly PCR was performed to link the sequence encoding the ZF with that encoding the PDZ or LZ domain. The two-finger homodimer $AA - GCN$ was amplified from a gBlock gene fragment. All linear DNA templates contained 5' protection sequences of 250 bp (promoters) or 130 bp (zinc fingers); this slows degradation of DNA in the cell-free extract [96]. Complete sequences are given in Tables 6.5–6.11 (Appendix). Given that each linear template is tagged by a fluorescent molecule at the 5' end and a biotin molecule at the 3' end we can assume that all DNA which is immobilized at the surface of a given unit cell and we visualize via fluorescence is therefore full length.

2.5.4 Setting up high-throughput cell-free experiments

The concentration of linear template DNA was quantified by absorbance (NanoDrop, ThermoFisher) and PCR products were directly added to a 384 microwell plate along with short biotinylated ss-DNA oligos for spotting. For characterization of the λP_R promoter library, a single linear template was spotted. Simple repression assays involved spotting both a ZF template along with the deGFP target template and dose response experiments for cooperative ZFs required spotting up to 5 linear templates per unit cell. Taking the PDZ-ligand heterodimer case as an example, both $ZF_{BCB} - PDZ$ and $ZF_{CBD} - PDZ$ as well as $ZF_{ADD} - L$ and $ZF_{CBD} - NL$ templates were combined in varying ratios, in addition to the deGFP template. All ZF templates and the target template were spotted for the NAND logic gate experiments, however for the AND and OR gates the first ZF template was pre-expressed in a separate reaction while all other down-stream components of the logic gate were spotted. Linear DNA templates were spotted with a QArray2 (Genetix) microarrayer using an MP3 pin (Arrayit) onto epoxy coated glass slides. The DNA was diluted in 4% BSA in MilliQ H_2O to prevent the DNA from binding the epoxy functional groups and to aid visualization of the drops for alignment with the PDMS chip. Once the PDMS chip was aligned on top of the DNA microarray the chip was bonded to the glass by incubating the assembled device for 1 hour at 80 °C. Chips were then stored overnight at 45 °C and used the following day or up to 2-5 days later.

To prime the chip, control lines were filled with PBS and pressurized at up to 138 kPa. While isolating the spotted DNA with the neck valve closed, the lower half of the unit cell was patterned

with BSA-biotin and neutravidin (Thermo Fisher) [106]. First, BSA-biotin (2 mg/mL) was flowed for 15 minutes, then neutravidin (1 mg/mL) for 15 minutes, after which the button was closed and BSA-biotin was flowed again for 10 minutes. Between each of these three steps PBS was flowed for 5 minutes to wash away any unbound molecules. The pressure applied to the flow lines during this process was ∼24 kPa. This surface chemistry resulted in a circular area coated with neutravidin, whereas the remaining surface of the unit cell was passivated with BSA-biotin. Afterwards the spotted DNA was solubilized with PBS by closing the outlet and opening the neck valve while PBS was flowed into the device. To avoid cross-contamination of DNA between unit cells the neck valve was closed and the lower half was washed with PBS. The sandwich valves were then closed and the neck was released to allow the DNA to diffuse into the lower half of the unit cell. After an incubation of 90 minutes the button was opened and the DNA was allowed to attach to the neutravidin coated area. The unbound DNA could then be washed away while the button was pressurized. The surface immobilized DNA was imaged by fluorescence microscopy. A 10 μL reaction volume of cell-free extract was prepared according to a previous protocol [164] and flowed into the device. For the AND and OR logic gates, the pre-synthesis reaction made up 25% of the fresh cell-free reaction mixture. The chip was separated into four parts using a multiplexer to test all logic gate inputs on a single chip. All unit cells were isolated from one another by the sandwich valves before the button was released and the chip was incubated at 29 °C. The production of deGFP in each unit cell was monitored over time on an automated fluorescence microscope (Nikon). The pneumatic valves, microscope, and camera were controlled by a custom LabVIEW program throughout the experiment.

This platform has also been used to carry out cell-free TX-TL reactions using PURExpress (Section 6.1, Appendix). Additionally, a more detailed protocol for preparing epoxy-coated glass slides and the spotting parameters used are given in Section 6.2 of the Appendix.

2.5.5 MITOMI measurements

DNA targets were either amplified with PCR or Klenow reactions and diluted over a range of 2 nM to 1 μM. The DNA was then spotted and the chip was aligned in the same way as described in the previous section. The same surface chemistry was also performed, followed by an additional two steps. First, a biotinylated anti-His antibody (Qiagen, 15 nM) was flowed for 20 minutes, enabling its binding to the neutravidin coated region. Second, a 30 μL cell-free reaction, in which a

His-tagged ZF was expressed, was flowed for 25 minutes, immobilizing the ZF at the surface of each unit cell. The DNA targets were then solubilized and allowed to diffuse into the lower half of the unit cell where their binding to the ZF could be quantified via fluorescence microscopy. All image analysis was done using a custom MatLab script that either calculated the mean of the fluorescence signal at the button area or in the solution of the unit cell. K_ds were determined by fitting the data with a single binding site model

$$DNA_B = \frac{B_{max} DNA_F}{DNA_F + K_d},$$

where B_{max} is the maximum specific binding, DNA_F is the free DNA in solution, DNA_B is the DNA bound to protein at the surface and K_d is the dissociation constant. Absolute K_d values in molar units were subsequently determined according to a calibration made with known concentrations of Cy5-tagged DNA on-chip.

2.5.6 Thermodynamic models for repression

Following [167] we make the assumption that gene expression is proportional to RNAP occupancy, and that RNAP binding to promoters is at thermodynamic equilibrium. This allows the final protein expression level to be written as a function of the equilibrium occupancy of the promoters by RNAP, which itself is a function of the available microstates. Thus the model can be constructed by enumerating all possible binding states of RNAP and any transcription factor it interacts with. For concentrations of nonspecific sites and RNAPs given by N_{NS} and P, respectively, a third assumption $P \ll N_{NS}$ allows the occupancy to be written in the following simple form,

$$p_{bound} = \frac{1}{1 + \frac{N_{NS}}{PF_{reg}} e^{\beta \Delta\epsilon_{pd}}}, \tag{2.1}$$

where the effects of the microstate distribution are subsumed into a regulation function F_{reg}. $\Delta\epsilon_{pd}$ is the energy difference between RNAP binding to specific versus nonspecific sites. All energies are given in units of $k_B T$, and $\beta = 1/k_B T$.

Typically repression is modeled using a purely competitive model where RNAP and the repressor competes for exclusive binding on the promoter. Motivated by our experimental observations, we extend this standard formulation of repression by enumerating four possible states for repressor

binding, with the following energies:

$$\text{no binding} : 0$$
$$\text{repressor only} : \Delta\epsilon_{rd}$$
$$\text{RNAP only} : \Delta\epsilon_{pd}$$
$$\text{repressor + RNAP} : \Delta\epsilon_{rd} + \Delta\epsilon_{pd} + \epsilon_{rp}$$

In our model, the repressor and RNAP can thus both bind at the same time, and interact with an energy ϵ_{rp}. As ϵ_{rp} becomes large and positive, the repression tends to that of competitive inhibition, where either species excludes the other from binding. This formulation allows for a continuous transition between competitive and noncompetitive mechanisms of inhibition: as repression becomes noncompetitive, simultaneous binding is possible and thus the promoter exhibits a non-zero leak at full repression.

We can then write down the regulation functions. For a single repressor of concentration R we have

$$F_{reg,1} = \frac{1 + \frac{R}{N_{NS}} e^{-\beta\Delta\epsilon_{rd}} e^{-\beta\epsilon_{rp}}}{1 + \frac{R}{N_{NS}} e^{-\beta\Delta\epsilon_{rd}}}. \tag{2.2}$$

For repressors binding to two sites, we have

$$F_{reg,2} = \frac{1 + \frac{R_1}{N_{NS}} e^{-\beta\Delta\epsilon_{r_1 d}} e^{-\beta\epsilon_{r_1 p}} + \frac{R_2}{N_{NS}} e^{-\beta\Delta\epsilon_{r_2 d}} e^{-\beta\epsilon_{r_2 p}} + \frac{R_1 R_2}{N_{NS}^2} e^{-\beta(\Delta\epsilon_{r_1 d} + \Delta\epsilon_{r_2 d})} e^{-\beta(\epsilon_{r_1 p} + \epsilon_{r_2 p})} e^{-\beta\epsilon_{r12}}}{1 + \frac{R_1}{N_{NS}} e^{-\beta\Delta\epsilon_{r_1 d}} + \frac{R_2}{N_{NS}} e^{-\beta\Delta\epsilon_{r_2 d}} + \frac{R_1 R_2}{N_{NS}^2} e^{-\beta(\Delta\epsilon_{r_1 d} + \Delta\epsilon_{r_2 d})} e^{-\beta\epsilon_{r12}}} \tag{2.3}$$

where the two repressors can interact with an energy ϵ_{r12}. Positive values of ϵ_{r12} result in positive cooperativity, where the binding of one repressor facilitates the binding of the other.

We make two transformations to Equation 2.3. First, in dose response experiments, we assume that repressor concentration R is proportional to repressor DNA concentration $R = Bd_R$, as supported by on-chip DNA titration measurements (Fig. 2.1). This allows us to convert repressor concentrations to DNA concentrations, which is the experimentally varying quantity. Second, we simplify all our expressions by defining an effective dissociation constant

$$K_D = \frac{N_{NS}}{B} e^{+\beta\Delta\epsilon_{rd}}, \tag{2.4}$$

which gives the DNA, rather than the repressor concentration for half-maximum occupancy. The effective K_Ds in the model are related to standard physical dissociation constants $K_d = e^{\Delta G^{\ominus}/k_B T}$

by a multiplicative factor. These transformations result in the simplified equations

$$F_{reg,1} = \frac{1 + \frac{d_R}{K_D} e^{-\beta \epsilon_{rp}}}{1 + \frac{d_R}{K_D}}$$

$$F_{reg,2} = \frac{1 + \frac{d_{R1}}{K_{D1}} e^{-\beta \epsilon_{r_1 p}} + \frac{d_{R2}}{K_{D2}} e^{-\beta \epsilon_{r_2 p}} + \frac{d_{R1} d_{R2}}{K_{D1} K_{D2}} e^{-\beta(\epsilon_{r_1 p} + \epsilon_{r_2 p})} e^{-\beta \epsilon_{r12}}}{1 + \frac{d_{R1}}{K_{D1}} + \frac{d_{R2}}{K_{D2}} + \frac{d_{R1} d_{R2}}{K_{D1} K_{D2}} e^{-\beta \epsilon_{r12}}}.$$

Finally, the protein level is given by a direct proportionality with the occupancy $y = Ap_{bound}$, and fold repressions are given by ratios of protein levels. Thus,

$$y = \frac{A}{1 + \frac{C_0}{F_{reg}}} \tag{2.5}$$

with

$$C_0 = \frac{N_{NS}}{P} e^{\beta \Delta \epsilon_{pd}}. \tag{2.6}$$

For binding site tuning experiments, the independent variable is an experimentally measured K_d, in units of nM. The regulation functions become

$$F_{reg,1} = \frac{1 + \frac{R}{K_d} e^{-\beta \epsilon_{rp}}}{1 + \frac{R}{K_d}}$$

$$F_{reg,2} = \frac{1 + \frac{R_1}{K_{d1}} e^{-\beta \epsilon_{r_1 p}} + \frac{R_2}{K_{d2}} e^{-\beta \epsilon_{r_2 p}} + \frac{R_1 R_2}{K_{d1} K_{d2}} e^{-\beta(\epsilon_{r_1 p} + \epsilon_{r_2 p})} e^{-\beta \epsilon_{r12}}}{1 + \frac{R_1}{K_{d1}} + \frac{R_2}{K_{d2}} + \frac{R_1 R_2}{K_{d1} K_{d2}} e^{-\beta \epsilon_{r12}}},$$

where R is now an effective repressor concentration, in units of nM.

To extend the model to take into account the distance-dependent effects, as well as the dependence of cooperativity on the helical positioning of the ZF on the DNA backbone, we posit the phenomenological description

$$\epsilon_{r_1 p} = \epsilon_{r_1 p_0} e^{-\lambda \Delta x}$$

$$\epsilon_{r12} = \epsilon_{r12_0} e^{-\lambda \Delta x} [1 + \cos(k \Delta x - \phi)],$$

where λ is a distance decay constant, Δx the spacing between the two ZF binding sites, k the wavenumber corresponding to the DNA helical pitch of 10.5 bp/turn, and ϕ a phase shift. The model was parameterized using values obtained from dose response measurements before fitting to the helical data. Finally, to take into account varying experimental conditions between those measurements and the helical effect experiments, a third parameter R_0 was introduced as a multiplicative factor on DNA concentrations, $d^*_{R1} = R_0 d_{R1}$ and $d^*_{R2} = R_0 d_{R2}$. This parameterizes global changes such as a different total DNA concentration and protein production rates between the dose response and helical experiments.

2.6 Markov chain Monte Carlo inference of model parameters

Model fits to experimental data are carried out using Markov chain Monte Carlo (MCMC) sampling, using the python package `emcee` [190] which is an implementation of Goodman and Weare's affine-invariant ensemble sampling method [191]. We first found a maximum likelihood estimate (MLE) of parameters using the BFGS algorithm from the `scipy.optimize` package. We define our negative log-likelihood function as

$$\ln p(y|x, params) = -\frac{1}{2}\sum_n \left[\frac{(y_n - \hat{y}_n(x, params))^2}{s_n^2} + \ln(2\pi s_n^2)\right] \tag{2.7}$$

where $\hat{y}_n(x, params)$ is the model prediction and y_n the experimental data with errors s_n. In order to combine results from different experiments (for example, separate dose response curves), we added together the log-likelihood functions without normalization.

Uninformative, broad normal priors were used, centered on the MLE parameter values. 50 Markov chains were initialized in a tight ball around these MLE values, and allowed to run for 10,000 iterations. The first 5,000 points were considered as part of the burn-in period and discarded; equilibriation of the Markov chains was verified by inspection of the traces. Sampling the equilibrated Markov chains returns the posterior probability distributions of the parameters, which can be used to generate an ensemble of potential models (and hence, a distribution of fits as shown in Figure 2.5). The posterior distributions, as well as pairwise distributions of parameters are shown in Supplementary Figure 2.16.

All supporting data and code are available on GitHub.
https://github.com/lbnc-epfl/2019_Swank_analysis

2.7 Supplementary figures

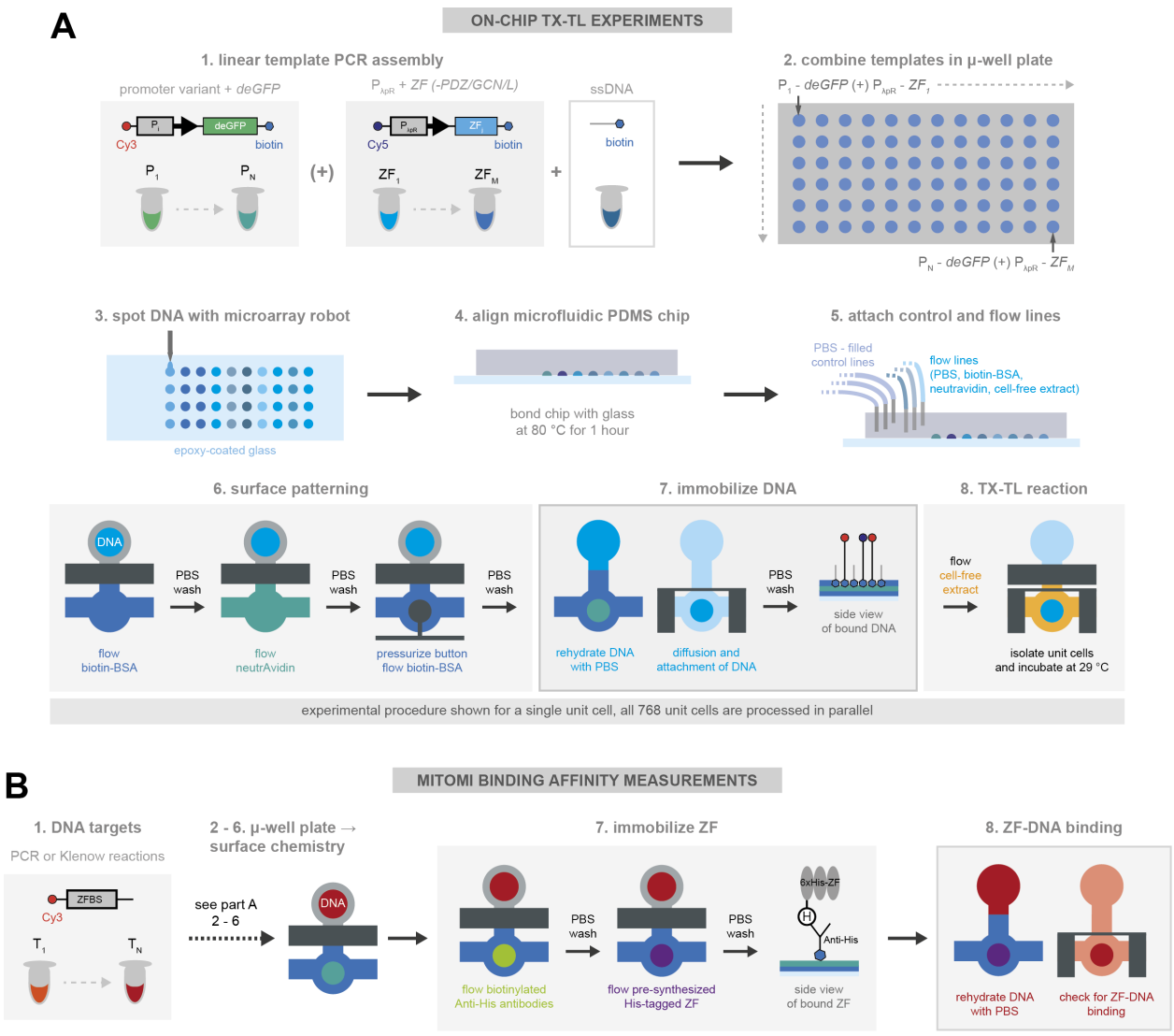

Figure 2.8: **Overview of experimental protocol.** Schematic showing the details of the experimental procedure for on-chip cell-free TX-TL reactions **(A)** and for measuring the binding affinity of ZF-DNA complexes with MITOMI **(B)**.

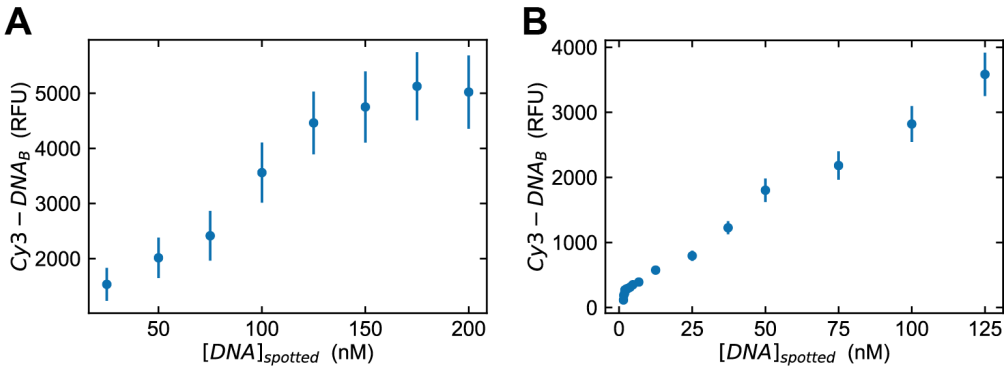

Figure 2.9: **DNA template spotting.** DNA concentration measured on-chip versus the concentration of DNA in the spotting plate, when a single dsDNA template was diluted **(A)** versus a mixture of dsDNA template and ssDNA **(B)**.

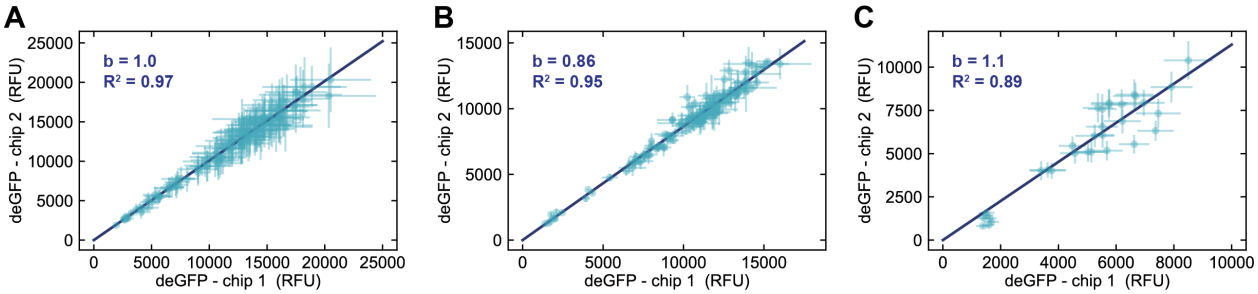

Figure 2.10: **Chip-to-chip reproducibility.** **(A)** deGFP expression values obtained from two separate chips for the λP_R promoter mutagenesis library. The same DNA microplate was used to spot both chips. **(B)** A comparison of two separate chips measuring the output of all possible ZF – promoter pairs. Similar to when only a single DNA template is present per unit cell (**(A)**), two templates could be added with good reproducibility between chips. **(C)** Data from two separate chips with two or more DNA templates per unit cell (NAND logic gate). Each chip was prepared using different DNA microplates, showing a slightly increased variability for DNA templates derived from different PCR reactions.

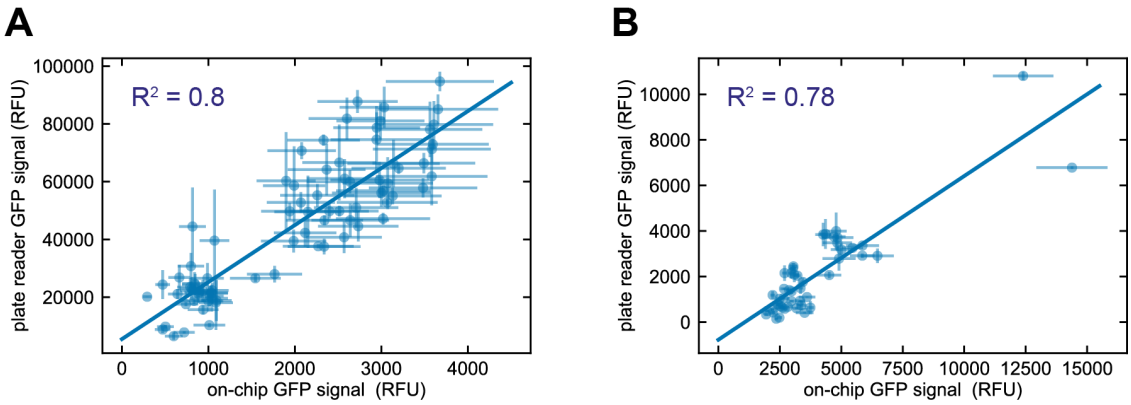

Figure 2.11: **Comparison of on-chip and plate reader measurements. (A)** Data collected from standard micro-well plate reader reactions versus data collected on-chip for a 9x9 ZF-target orthogonality matrix for targets with two binding sites in the promoter region. The 9 ZFs tested included AAA, ADB, ADD, BAB, BCB, BCC, BCD, BDD and CBD. **(B)** Plate reader versus on-chip data for cooperative, non-cooperative and control ZF PDZ-L heterodimers tested with a library of promoters that had variable spacing between the two ZF binding sites.

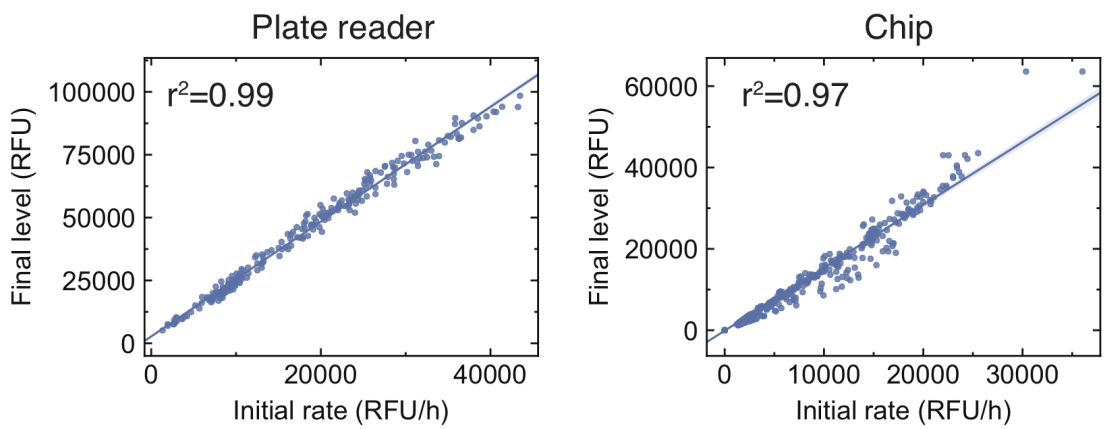

Figure 2.12: **Relationship between initial rates and final deGFP values.** We observe a linear relationship between the initial rate of deGFP production, as obtained by linear fits to the time course at early times (∼30 minutes), and the final steady state level of deGFP, on both plate reader and chip experiments. This suggests that final levels of deGFP are proportional to the production rate, and validates the use of endpoint protein levels as a proxy for transcription rates.

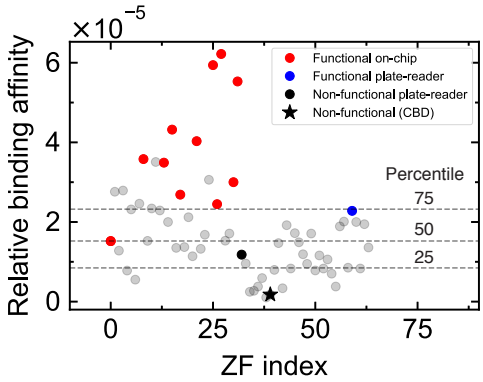

Figure 2.13: **Functional ZFs within the combinatorial library.** This figure shows the on-target binding affinity for all 64 members of our combinatorial library (data from [110]). In red are the 11 functional ZFs characterised on-chip. Additionally, the blue and black points are two other ZFs characterised in a separate plate-reader experiment. The black star corresponds to ZF_{CBD}. Horizontal dashed lines represent the 25th, 50th, and 75th percentile of binding affinity, and we observe that of the ZFs tested, all those with binding affinities greater than the 50th percentile exhibited functional repression. We therefore hypothesize that of the untested ones, those with affinities greater than approximately 1.5×10^{-5} in relative units should be functional. This would correspond to a total of 32 functional repressors.

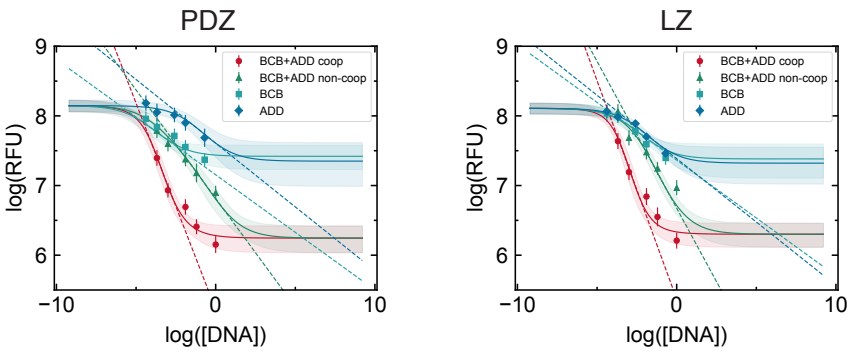

Figure 2.14: **Sensitivity calculations from dose response curves.** The slope of the dose response curve, as measured in the linear regime of a log-log plot, is defined as the sensitivity; this quantity increases in the presence of cooperative interactions. Values are given in Table 6.3.

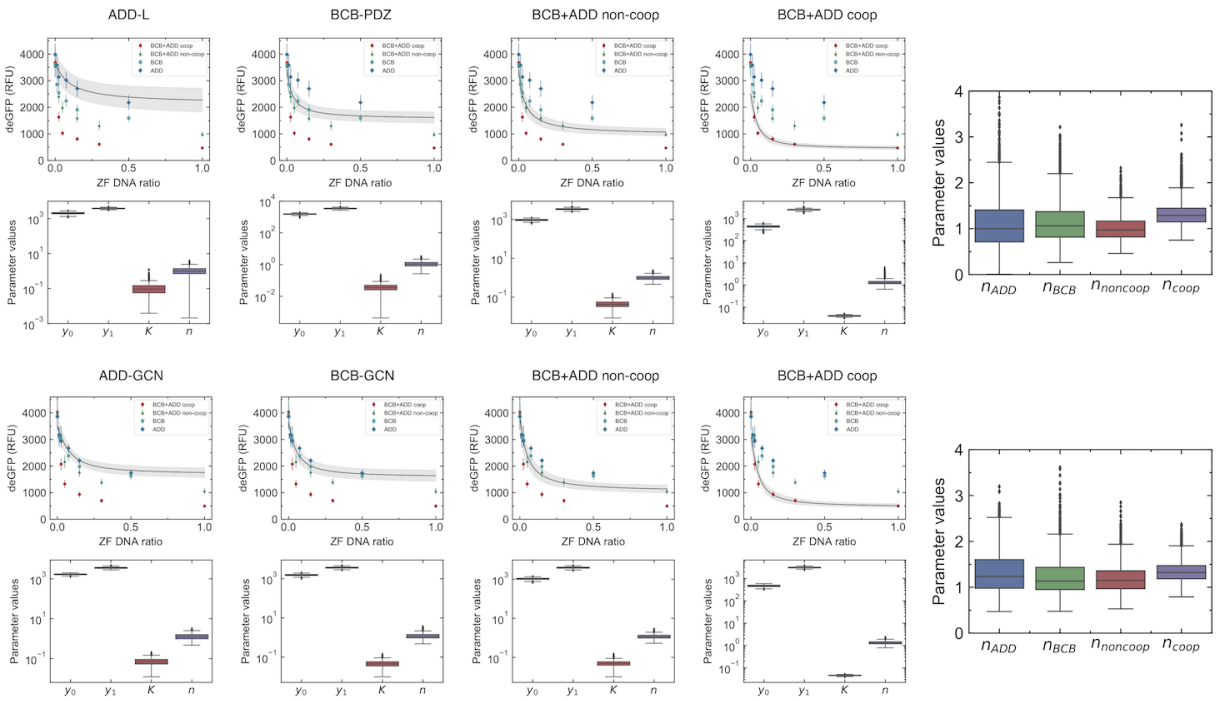

Figure 2.15: **Hill function fits to dose response curves.** Standard Hill functions take the form $y = y_0 + \frac{y_1 - y_0}{1+\left(\frac{R}{K_D}\right)^n}$, where y_0 is the leak, y_1 the maximum expression, R the repressor concentration, K_D the dissociation constant, and n the Hill coefficient. Unlike the thermodynamic model which proposes a mechanism to consistently fit the entire data set, Hill functions must be independently fit to each dose response curve. We first fit the single ZF data, followed by the non-cooperative BCB+ADD curve. Hill functions describe two-site binding using an effective K_D and varying n. We make the assumption that in both the cooperative and non-cooperative case, the effective K_D is the same. Thus the cooperative BCB+ADD curve is fit using the K_D value obtained from the non-cooperative BCB+ADD curve. Although the Hill coefficient is predicted to increase in the presence of cooperativity, we observe a minimal change in our data, within the error of the fits.

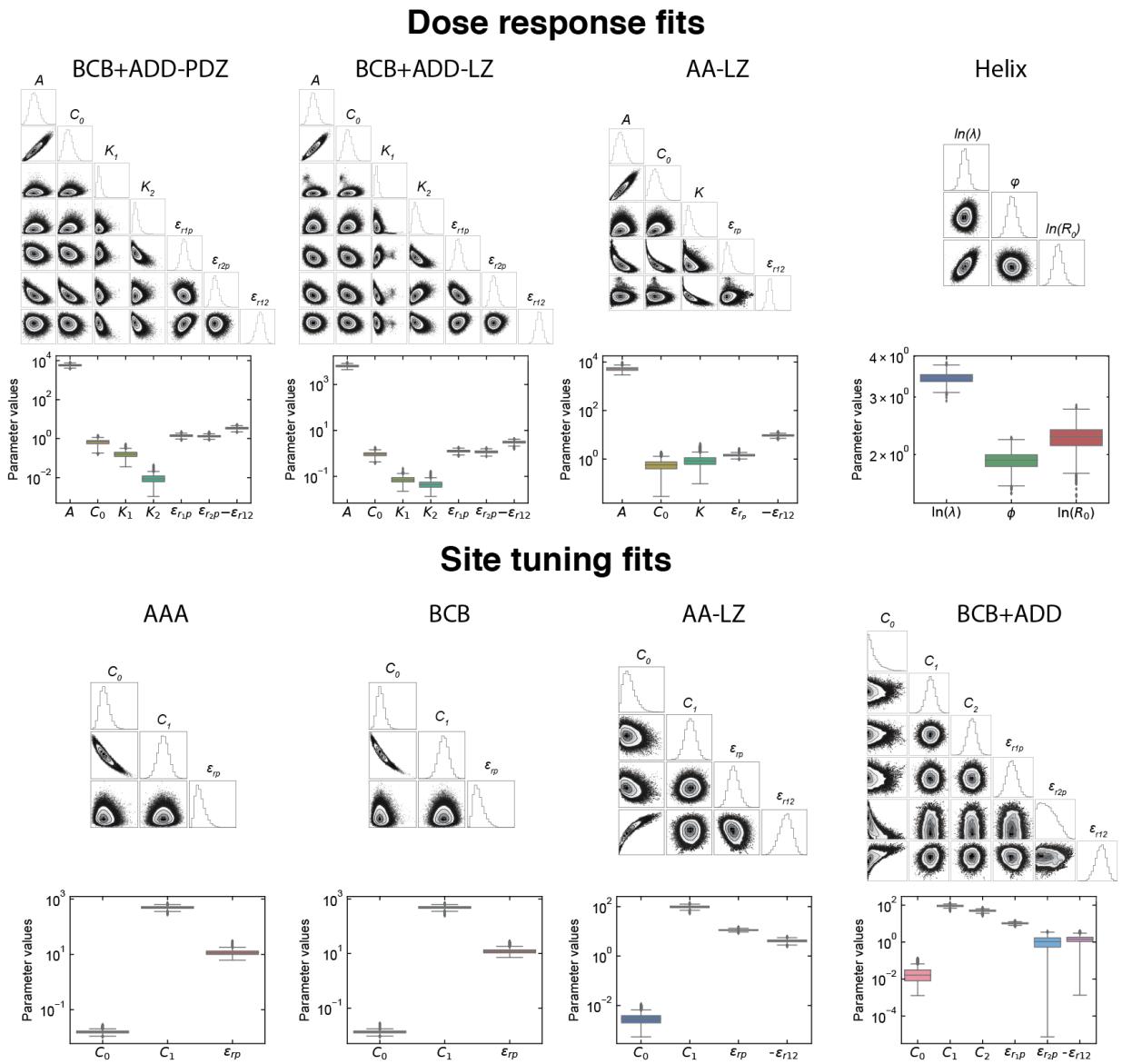

Figure 2.16: **Markov chain Monte Carlo inference of model parameters.** Matrix plots show pairwise posterior probability distributions of model parameters for each of the models fitted. The individual posterior distribution for each parameter can also be visualized using box plots; the top and bottom of each box represents the 75th and 25th percentile, respectively.

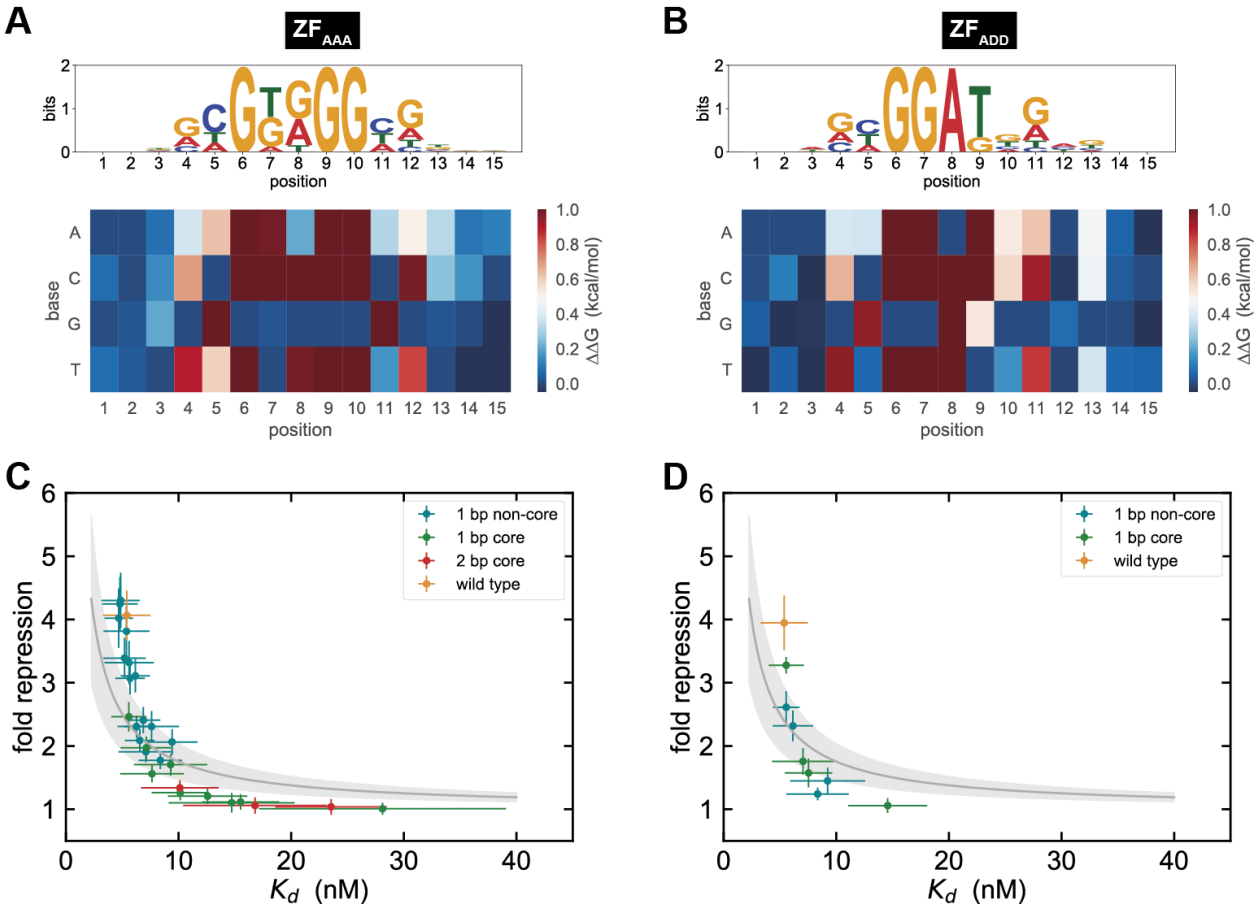

Figure 2.17: **PWMs for ZF_{AAA} and ZF_{ADD} and binding site tuning for ZF_{AAA}.** Sequence logos and PWMs measured by MITOMI for ZF_{AAA} **(A)** and ZF_{ADD} **(B)**. Fold repression versus K_d measured for mutations to a ZF_{AAA} binding site within a single binding site promoter **(C)** and a cooperative promoter **(D)**. Solid lines represent the model fits.

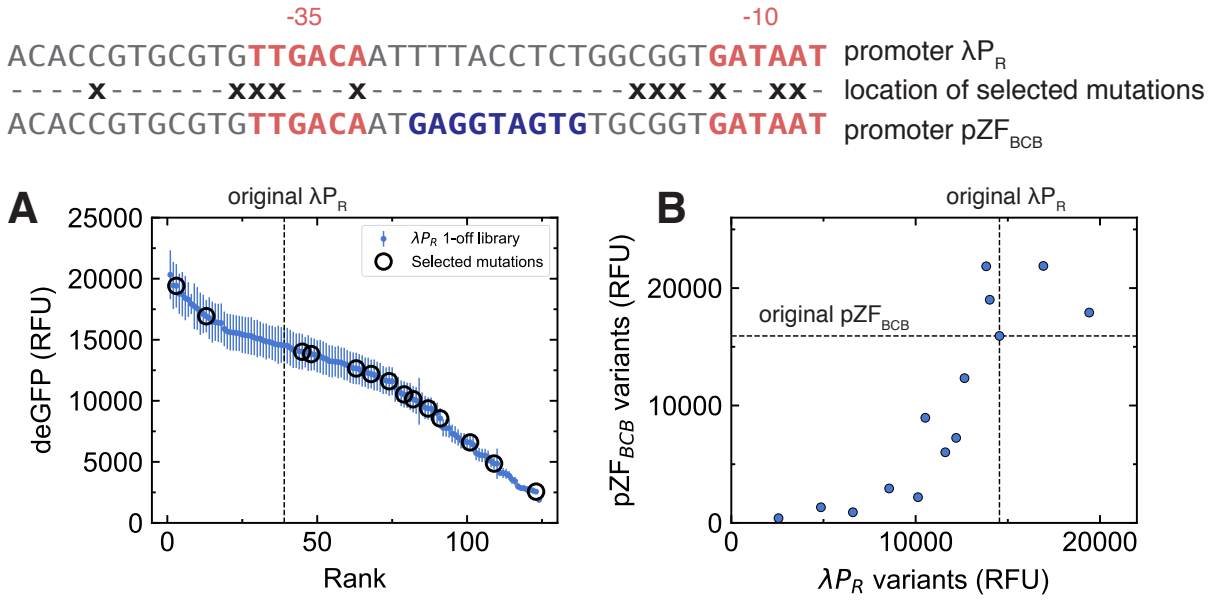

Figure 2.18: **Tuning promoter strength.** In Figure 1 we presented the one-off library data which contains all single base mutations from positions -47 to -7 of the λP_R promoter. **(A)** These data can be rank-ordered, and we observe that a large dynamic range of promoter output is accessible. A number of mutations were selected which both increased and decreased expression relative to the original promoter. **(B)** Introducing a single BCB binding site between the -35 and -10 boxes generates the pZF_{BCB} promoter. Applying the selected mutations to this new promoter changes the output in a correlated way when compared to the λP_R promoter; the new promoter can thus be roughly tuned in a predictive fashion.

3

A high-throughput microfluidic platform for programming cell-free gene expression at steady state

3.1 Abstract

Forward engineering synthetic gene circuits is often a process of trial-and-error that has been expedited with the use of cell-free TX-TL systems. Microfluidic technologies have made it possible to perform cell-free experiments with increasing sophistication and throughput, enabling the screening and characterization of gene regulatory elements. In this work, we developed a microfluidic chip that extends high-throughput screening capabilities to a steady state reaction environment, which can serve as a tool to aid in the design of increasingly complex synthetic biocircuits. The device consists of an array of unit cells with variable dimensions that can be individually programmed with specific DNA template(s) at controlled concentrations. Additionally we are able to periodically supply the unit cells with cell-free reagents mixed on-chip to generate predefined dilution gradients. Combining these features, we are able to tune repression at steady state and implement gene circuits inducible by small molecules.

3.2 Introduction

Engineering gene regulatory networks from the bottom-up is a cornerstone of synthetic biology and provides a means for an improved understanding of natural biological systems [1, 192]. Optimizing new circuit designs *in vivo* often requires several iterations leading to a time consuming process, considering that every iteration involves a molecular cloning step. For that reason cell-free systems have proved to be a useful tool for accelerating the design-build-test cycle [80, 98]. Recently there have been several technological advancements that both increased the complexity and throughput of cell-free batch experiments, including the use of acoustic liquid handling robots [111, 112], as well as new microfluidic platforms [113, 114, 193] to characterize the promoter and/or transcription factor landscape together with generating concentration gradients of various reaction components. Although these methods have facilitated detailed studies of certain biomolecular circuits, they will always be limited to the scope of batch reactions.

The necessity to implement continuous or steady state cell-free reactions has been realized in the form of novel microfluidic devices that were capable of programming oscillating protein expression patterns [100, 101]. However these devices function at relatively low throughput, creating a need for new platforms that can carry out steady state cell-free gene expression at higher capacities

that will aid the forward engineering of more complex biocircuits. Consequently we developed a microfluidic device that sought to combine the high-throughput potential of batch reaction chips [193] with the passive exchange of cell-free reagents inspired by microfluidic chemostats [101].

Here we present a microfluidic chip that enables the exploration of biocircuit parameter space at steady state in a cell-free system. Immobilizing DNA templates within an array of unit cells permits us to screen both DNA sequence variants in addition to different DNA concentrations. Furthermore, the two-layer device incorporates pneumatic valves that allow the use of pulse width modulation (PWM) for on-chip mixing of different reaction components [194, 195]. By varying the geometry of the unit cells we can alter the diffusion time of reagents into and out of the unit cell, providing a second way to affect protein expression levels apart from DNA concentration. We integrated controlled DNA surface attachment, variable unit cell dimensions and PWM-programmable reagent inputs into a single device that we applied to tuning repression at steady state and small molecule inducible gene circuits.

3.3 Results

3.3.1 Design and characterization of the microfluidic device

We fabricated a two-layer PDMS microfluidic device using soft lithography. The device consists of a control and a flow layer, whereby fluids inside the flow layer can be manipulated by applying pressure to the control lines (Fig. 3.1A). The flow layer contains a total of 280 unit cells that can each run a cell-free gene expression reaction. Each unit cell is connected to an exchange channel, through which fresh cell-free extract can flow. The length of the connecting channel, leading from the unit cell to the exchange channel ranges from 50 μm to 450 μm in length, while the width is kept constant at 25 μm. The inlets of the flow layer are optimized for mixing reagents with PWM [194]. The inlet lengths are equal and the length of the control lines for the top five inlets are also equal, ensuring that the valves used for PWM will actuate at similar speeds. Following the inlets, we have incorporated a serpentine channel to allow reagent plugs formed by PWM to mix before reaching the start of the exchange channel.

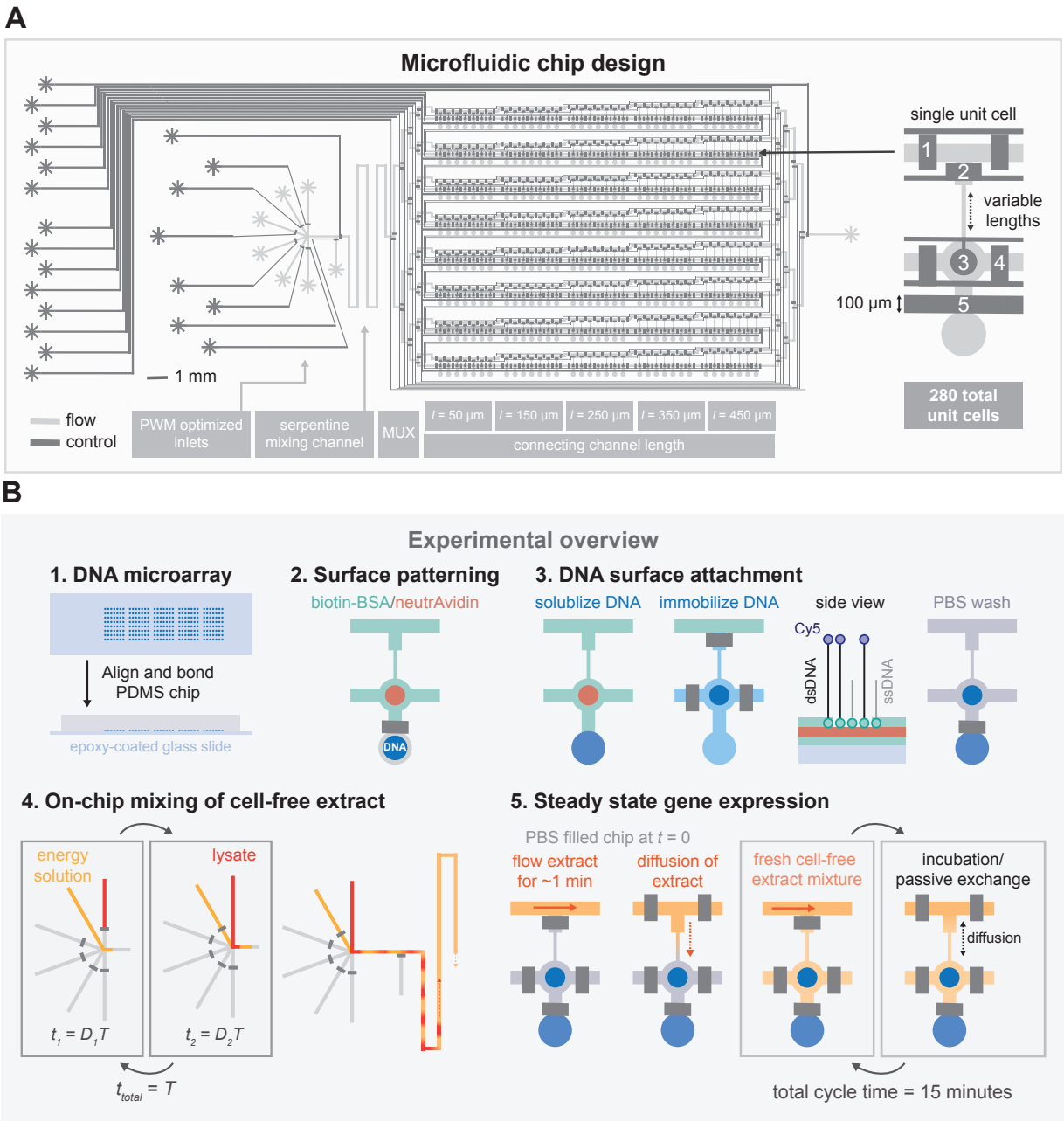

Figure 3.1: **Overview of the microfluidic platform.**

Caption on the next page.

Figure 3.1: **(A)** Illustration of the microfluidic chip design, highlighting the PWM optimized inlets, followed by the serpentine mixing channel and array of unit cells with variable connecting channel lengths. To the right a single unit cell is shown. The pnuematic valves are described from top to bottom: 1) a pair of valves separates each unit cell in the exchange channel, 2) a valve prevents flow into the unit cell while the exchange channel is replaced with fresh reagents, 3) the button valve enables surface patterning for DNA attachement, 4) sandwich valves separate the assay part of each unit cell from one another, and 5) the neck valve isolates the DNA spot until the surface patterning is complete. **(B)** A schematic summary of the experimental protocol: 1) DNA templates are spotted with a microarray robot onto an epoxy-coated glass slide, on top of which the PDMS chip is aligned. 2) The assay section of the unit cell is patterned with biotin-BSA and neutrAvidin. 3) The DNA spot is solubilized, permitting the DNA to diffuse into the upper half of the unit cell and bind to the surface, after which all unbound DNA is washed away. 4) Lysate and energy solutions are then flowed and mixed on-chip with PWM. Each solution is flowed for a time $t = DT$, where D and T represent the duty cycle and cycle period, respectively. 5) Initially a cell-free extract solution is flowed onto the chip and diffuses into a unit cell that is filled with PBS. Every 15 minutes fresh cell-free extract is flowed through the exchange channel for $\sim$1 minute followed by an incubation period that enables the exchange of reagents via diffusion.

Cell-free transcription-translation (TX-TL) reactions are performed on-chip by first spotting fluorescently labeled and biotinylated linear DNA templates onto an epoxy-coated glass slide using a microarray robot. The PDMS chip is then aligned on top of the DNA microarray and bonded to the glass. After bonding, the upper half of each unit cell is patterned with biotin-BSA and neutrAvidin, resulting in a circular region of neutrAvidin coating, to which biotinlyated DNA can bind. Throughout this process the DNA spot remains isolated in the lower chamber, sealed off by the neck valve. Once the surface patterning is completed, the DNA spot is solubilized, enabling the DNA to diffuse into the upper part of the unit cell and attach to the neutrAvidin coated area. Any unbound DNA is then washed from the device and cell-free extract is introduced into the exchange channel by mixing the energy and lysate solutions directly on-chip using PWM. While the exchange channel is being replaced with fresh cell-free extract the bottom half of the unit cell is separated with a valve that is then released to allow the diffusion of fresh reagents into the unit cell. During the incubation time another set of valves is actuated to isolate the unit cells from each

other. The process of flowing fresh cell-free extract followed by an incubation step is repeated for up to 20 hours to achieve steady state gene expression (Fig. 3.1B). By periodically flowing fresh cell-free extract we are able to use far smaller reagent volumes (∼60-80 μL total) compared to other methods that flow fresh reagents continuously. Additionally due to on-chip mixing of the lysate and energy components there is no need to cool the reagents off-chip.

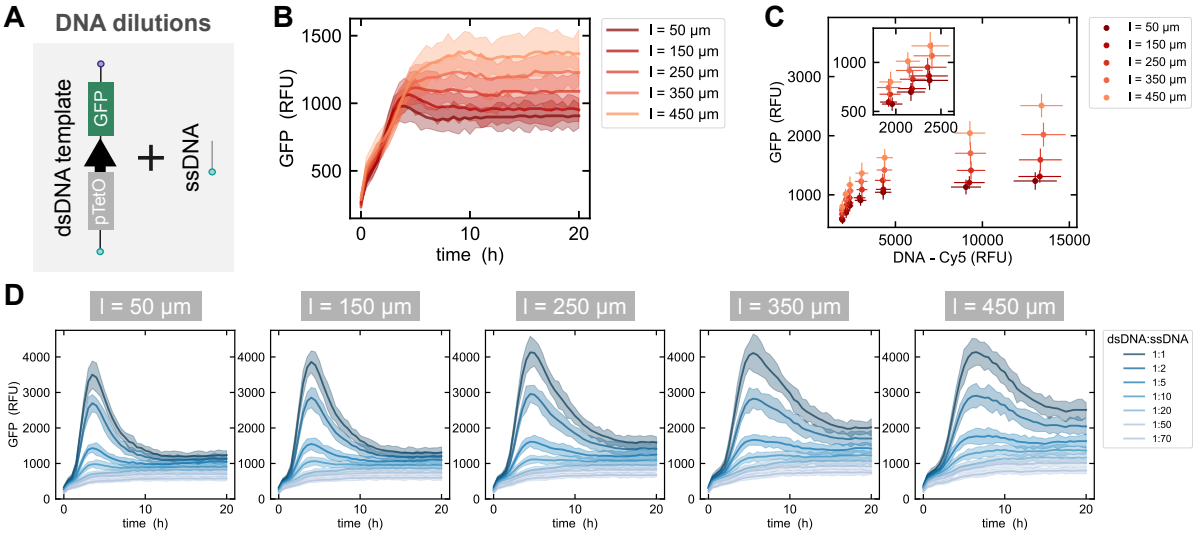

Figure 3.2: **Steady state GFP expression for a range of DNA dilutions. (A)** DNA dilutions are made by mixing different ratios of dsDNA templates with short biotinylated ssDNA oligos. **(B)** GFP expression versus time shown for a single DNA dilution (dsDNA:ssDNA = 1:10) and different connecting channel lengths. **(C)** The steady state GFP expression level versus the Cy5 fluorescence signal of dsDNA template attached to the surface for all connecting channel lengths and DNA dilutions. The inlaid plot zooms in on the three lowest DNA concentrations. **(D)** Time-lapse of GFP expression for a range of DNA dilutions and all connecting channel lengths. All values represent means ± SD ($n = 8$), where the SD is designated by either a shaded region or an error bar.

To confirm that the cell-free extract solutions could be adequately mixed on-chip we tested various PWM cycle periods with duty cycles fixed at 50%. We use mCherry and GFP as tracers (∼ 27 kDa) in the energy and lysate solutions, respectively, to monitor the on-chip mixing at different locations downstream of the inlets. Directly after the inlets, the energy solution and lysate plugs can be clearly visualized for cycle periods ranging from 600 to 1400 ms (Supplementary Fig. 3.5A).

After passing through the serpentine channel, the two solutions have been mixed for cycle periods less than 800 ms, and at the beginning of the exchange channel mixing is achieved for cycle periods up to 1200 ms long (Supplementary Fig. 3.5B, C). As the chip is separated into eight different rows, it is also important to check whether mixing is homogeneous across all rows. We found that for cycle periods of 600 and 1000 ms relatively uniform mixing is achieved across all rows of the device (Supplementary Fig. 3.5D, E).

As described previously [193], the attachment of DNA templates on the surface of each unit cell can be controlled by using a mixture of double stranded DNA templates and single stranded biotinlyated DNA oligos (Fig. 3.2A). For a given DNA template concentration we can see a range of steady state expression levels depending on the length of the connecting channel (Fig. 3.2B). This steady state can be disrupted by flowing PBS in place of the cell-free extract mixture (Supplementary Fig. 3.6). An increase in the connecting channel length correlates with an increase in the steady state GFP expression level. Furthermore the time it takes to reach steady state levels is increased for longer connecting channels, as it takes longer for the cell-free extract mixture to diffuse into the unit cell where the DNA template is immobilized. If we then vary the DNA template concentrations we can observe a wide range of GFP expression levels for the different connecting channel lengths (Fig. 3.2C). Additionally, we see a good correlation between steady state GFP values for two independent chips (Supplementary Fig. 3.7). Looking at the GFP expression over time we see that the higher the DNA template concentration the longer it takes until a steady state is reached (Fig. 3.2D). However at lower ratios of dsDNA template to ssDNA, steady state can be reached after ∼4-6 hours, depending on the connecting channel length. For that reason, all following experiments are performed with a dsDNA to ssDNA ratio below 1:5.

3.3.2 Steady state repression with predefined transcription factor concentrations

Forward engineering of gene regulatory networks often requires an in depth characterization of the transcription factors that will be incorporated into the network. For instance, we have shown that the level of repression from a zinc finger (ZF) transcriptional regulator can be tuned by varying both the concentration of ZF in the TX-TL reaction, as well as by tuning the ZF binding site in batch conditions [193]. As a preliminary application of our chip, we therefore wanted to see the effect of tuning ZF repression at steady state.

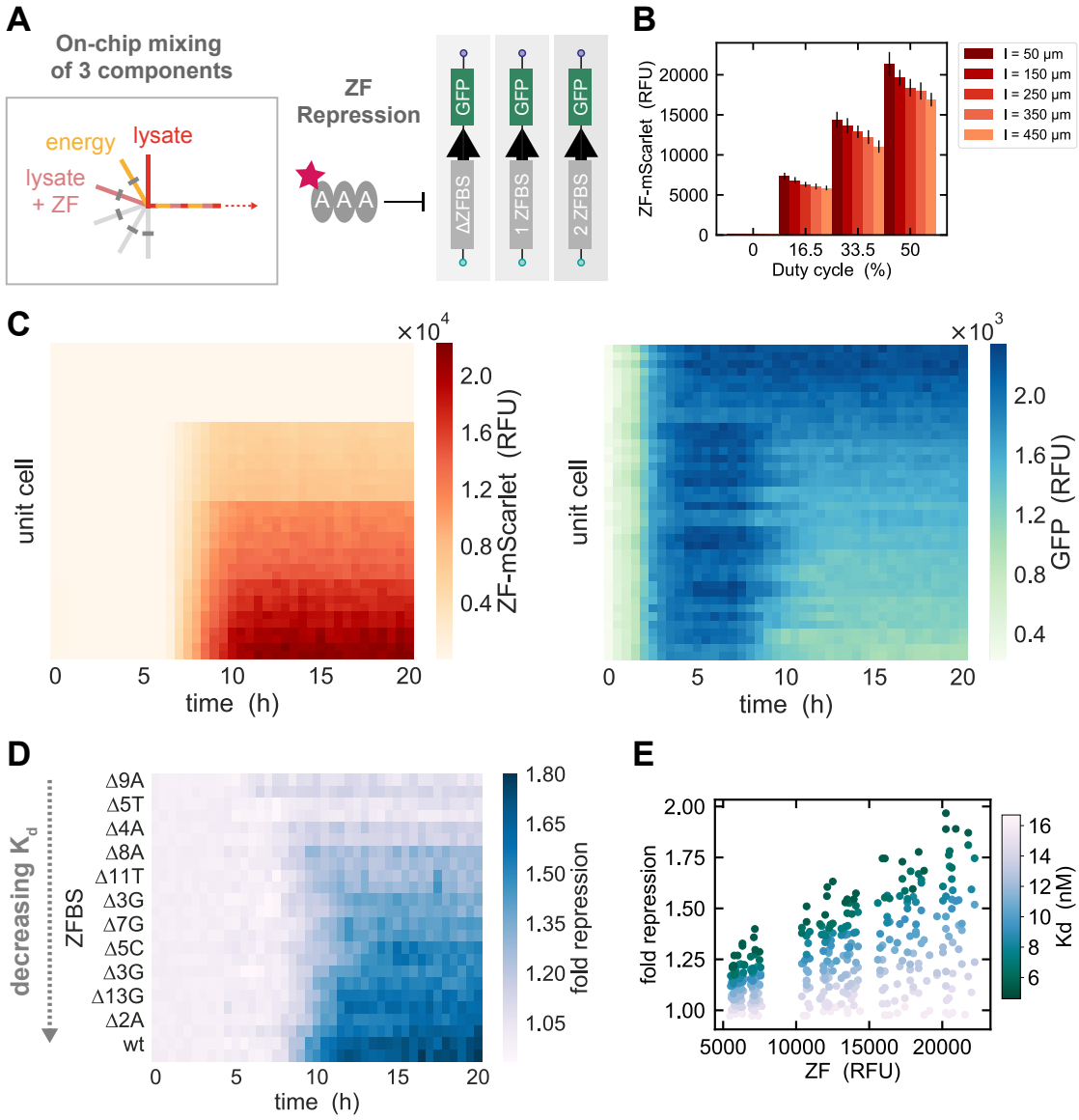

Figure 3.3: **Steady state ZF repression.** **(A)** Overview of the experimental design. PWM is used to mix three components on-chip to generate different concentrations of an mScarlet-tagged ZF which is then screened against targets with variable promoter sequences, including either one or two ZF binding sites or a single mutated binding site. **(B)** ZF-mScarlet signal for different duty cycles and unit cell dimensions. All values represent means ± SD ($n = 14$). **(C)** On the left, ZF-mScarlet signal over time for all unit cells containing a target template with 2 ZF binding sites in the promoter. To the right, GFP expression versus time for the same unit cells.

Caption continues on the next page.

Figure 3.3: **(D)** Fold repression over time for targets containing modified ZF binding sites, shown in order of decreasing K_d, with the wild type binding site sequence at the bottom. The fold repression is calculated by dividing the signal obtained from no added ZF by the signal obtained from the highest quantity of added ZF (Duty cycle = 50 %). The time-lapse data shown in this plot corresponds to unit cells with a connecting channel length of $l = 50$ μm. **(E)** All end-point fold repression values calculated for each duty cycle and connecting channel length, plotted according to the ZF binding site K_d.

To test whether we could add varying concentrations of a third protein component we mixed three different solutions on-chip with PWM: 1) a lysate solution containing a GFP tracer, 2) a second lysate solution and 3) an energy solution with an added mCherry tracer. As the ratio between the lysate and energy solution needs to be maintained at 1:1, the duty cycle of the energy solution is kept at a constant 50%, while the remaining 50% of the duty cycle is divided between the two lysate solutions to achieve varying levels of GFP. For a cycle period of 1 s we see the expected correlation as the duty cycle percentage is increased, the level of GFP also rises (Supplementary Fig. 3.8). At the same time the level of mCherry, which serves as a tracer in the energy solution, does not change, meaning the ratio of the energy and lysate solutions is maintained.

After confirming that we could accurately mix three components on-chip with PWM, we then designed an experiment that could measure the steady state repression for ZF_{AAA} at various concentrations and for different binding site sequences (Fig. 3.3A). We used a purified ZF tagged with mScarlet, enabling the visualization of ZF inside the unit cells. Three dilutions of ZF were generated on-chip and fed into separate rows of the device owing to the multiplexer upstream of the exchange channels. As a control, no ZF was added to the mixture in one quarter of the chip. Inside the unit cells linear DNA targets were attached, each comprised of a GFP gene downstream of a λPR promoter variant, containing either one or two ZF binding sites or a single binding site with a mutation known to tune repression to varying degrees. The mutations were chosen based on previously measured K_ds [193], including two mutations that completely ablated repression (Δ9A, 5T) and nine other mutations that led to a range of repression levels up to the wild type consensus. Initially the cell-free TX-TL reaction was brought to steady state without ZF, and then after 6.5 hours different ZF concentrations were added to each quarter of the chip. For a given duty cycle percentage we see an additional gradient across connecting channel lengths (Fig. 3.3B). For a given

reporter template, we have two replicates for a given ZF input concentration and unit cell dimension. To provide an example, we have shown the data for all unit cells with a template containing two ZF binding sites within the promoter (Fig. 3.3C). If we look at the ZF-mScarlet signal in each unit cell over time, we can observe four distinct partitions correlating with different duty cycles. However, within each quadrant we also notice a gradient which is associated with differences in connecting channel lengths. As the ZF diffuses into the unit cells we begin to see a decrease in GFP expression (Fig. 3.3C) that corresponds with the amount of ZF present. Furthermore if we consider a single unit cell dimension, we see that the fold repression for different target templates increases over time as the K_d associated with a given binding site mutation decreases (Fig. 3.3D). We observe a range of steady state fold repression values depending on the concentration of ZF within a given unit cell and we see a strong correlation between all fold repression values and the measured binding affinity for a given promoter (Fig. 3.3E). These results are in agreement with our previous findings [193] and they provide a proof of concept that our microfluidic platform can be used to simultaneously screen target sequence space in conjunction with transcription factor concentrations in a steady state cell-free system.

3.3.3 Implementing small molecule controlled gene circuits at steady state

After showing that we could introduce TF inputs into our chip at a predesignated time, we went on to test whether we could implement gene circuits that can be controlled by small molecule inputs. To start we set up a simple repression assay whereby TetR can repress a GFP encoding template that includes the Tet operon in its promoter region, unless a small molecule, anhydrotetracycline (aTc), is present and prevents TetR from binding to the operon (Fig. 3.4A). While holding the GFP target concentration constant, we vary the amount of TetR template present by adding a loading control template to maintain the same total DNA template concentration. After allowing the reaction to reach steady state, we introduce aTc into the unit cells for a 3 hour pulse. As the concentration of TetR template spotted is increased, we observe a corresponding decrease in the steady state expression levels of GFP (Fig. 3.4B). During the aTc pulse, repression is inhibited and GFP expression rises to the control level where no TetR template is present. Once aTc is no longer supplied to the unit cells, the GFP template is again repressed and the initial steady state is re-established. Furthermore, we can see that the reaction time to the aTc pulse differs according to the connecting channel length (Fig. 3.4C). As the connecting channel length increases, the time it

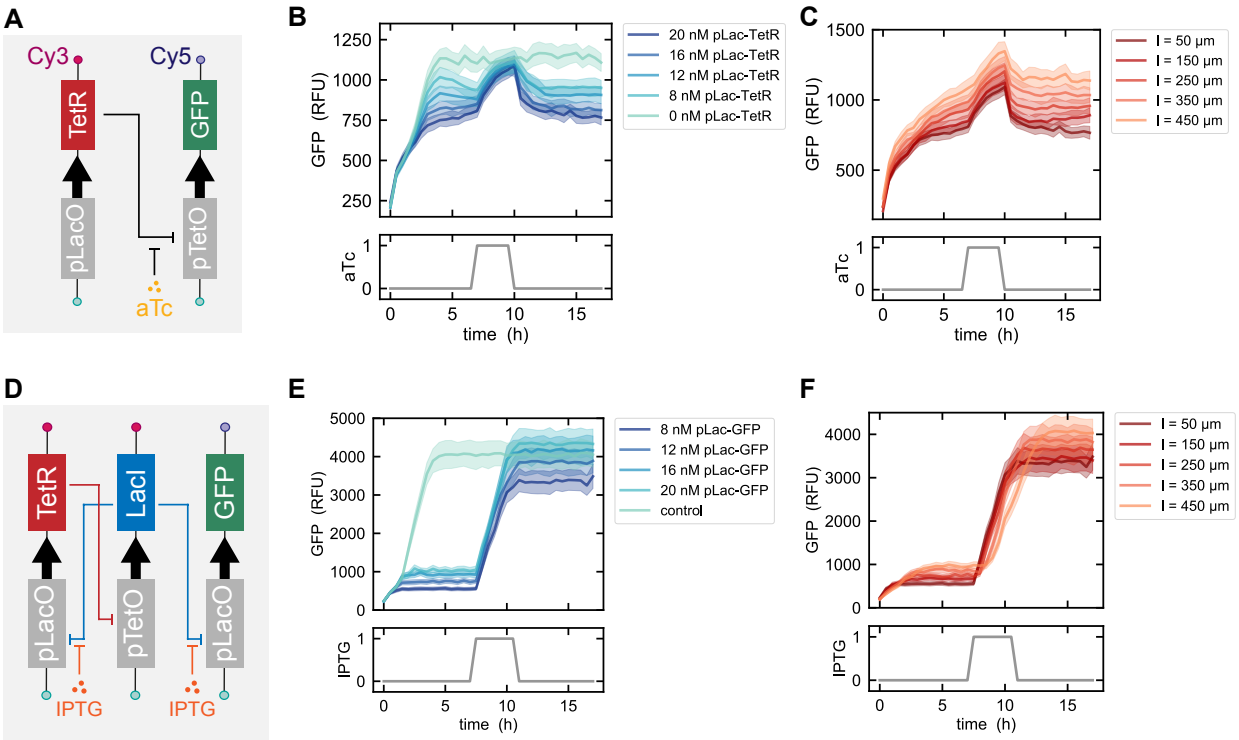

Figure 3.4: **Implementing gene circuits inducible by small molecules.** **(A)** Illustration of the gene elements making up the TetR repression assay, which can be controlled by aTc. **(B)** GFP expression versus time for variable concentrations of pLac-TetR DNA template spotted inside unit cells with a connecting channel length of $l = 50$ μm. **(C)** GFP expression profile over time shown for varying connecting channel lengths and a constant pLac-TetR DNA template concentration equal to 20 nM. **(D)** Sketch of the toggle switch gene circuit. **(E)** GFP expression versus time displayed for a range of pLac-GFP reporter concentrations spotted for unit cells with a connecting channel length of $l = 50$ μm. The concentration of the TetR and LacI templates are kept constant, giving a range of repressor to reporter template ratios from 1:2 to 3:1. **(F)** Time-lapse of GFP expression shown for different connecting channel lengths and a constant pLac-GFP reporter concentration equal to 8 nM. All data presented represents mean values $\pm$ SD ($n = 8$).

takes for the reaction to arrive at a steady state also increases, therefore we see sharper transitions upon the addition of aTc for shorter connecting channel lengths.

As a final application of our chip we then combined our ability to introduce small molecule inputs with dynamic gene circuits in order to implement a genetic toggle switch [27]. The toggle switch

is composed of two linear DNA templates that encode for two repressor proteins, TetR and LacI, where each protein encoding gene is downstream of mutually repressible promoters (Fig. 3.4D). A transient pulse of isopropyl-β-D-thiogalactopyranoside (IPTG) causes the circuit to switch from one state to another. Using different concentrations of a Lac-repressible GFP reporter we allow the reaction to reach steady state, observing increasing levels of leak for higher concentrations of reporter template spotted. After 7 hours IPTG is introduced into the chip, causing the GFP expression to switch from a low to high state (Fig. 3.4E). The toggle switch network remains stably in this state even after the IPTG pulse is complete. Similar to the varying response times we saw for aTc pulses before, the transition from one state to another occurs more slowly for longer connecting channel lengths, although we still observe switching from a low to high state in all cases (Fig. 3.4F). Considering that many genetic circuits incorporate small molecule control elements, we believe that our chip could serve as a useful platform for testing new network designs where it is necessary to explore the parameter space of DNA template concentration together with small molecule inductions.

3.4 Conclusion

As bioengineers attempt to construct exceedingly complex biomolecular circuits, the size of the parameter space necessary to explore grows larger and larger, requiring higher-throughput methods that can speed up the design-build-test cycle. Utilizing cell-free systems enables circuits to be optimized more quickly since timely molecular cloning steps can be bypassed. However, not all genetic networks can be tested in batch conditions and consequently need to be carried out in a system that mimics the dilutions which occur during cellular divisions. We have therefore developed a microfluidic device that can enable cell-free gene expression at steady state, facilitating the characterization of biological parts and circuits with increased throughput compared to previously fabricated microfluidic chemostat chips. By precisely controlling the amount of DNA template attached to the surface of each unit cell, we can effectively scan a range of DNA concentrations that correlate with variable steady state protein expression levels. Different levels of protein expression can also be achieved by modifying the geometry of a given unit cell. Furthermore, on-chip mixing of cell-free reagents with PWM makes it possible to introduce predetermined concentrations of different components. While we have shown different concentrations of ZF repressor can be generated

on-chip, this method could be extended to other proteins or small molecules. Moreover pneumatic valves provide a means to easily program a given input over a defined time period. Combining our capability to create concentration gradients of different reaction components with the potential to survey the DNA template sequence space, we believe that our device could be a powerful tool for aiding the design of novel gene regulatory networks.

3.5 Materials and Methods

3.5.1 Microfluidic chip fabrication

The designs for the flow and control layer of the device were drawn with AutoCAD software, we then used standard photolithography to fabricate the molds for each layer. SU-8 negative photoresist was used to create the control channel features (GM 1070, Gersteltec Sarl) with a height of 30 μm, while AZ 9260 positive photoresist (Microchemicals GmbH) was used to generate flow channel features with a height of 15 μm. Afterwards each of the wafers was treated with TMCS (trimethylchlorosilane) and coated with PDMS (polydimethylsiloxane, Sylgard 184, Dow Corning). For the control layer ~50 g of PDMS with an elastomer to crosslinker ratio of 5:1 was prepared, whereas for the flow layer a 20:1 ratio of elastomer to crosslinker was spin coated at 1800 rpm to yield a height of ~50 μm. Both PDMS coated wafers were then partially cured for 20 minutes at 80 °C, after which devices from the control layer were cut out and the inlets for each control line were punched. Each control layer is then aligned onto the flow layer by hand using a Nikon stereo microscope. The aligned devices were then placed at 80 °C for 90 minutes, allowing the two layers to bond together so that the entire device can then be cut out and removed from the flow wafer.

3.5.2 Cell-free extract preparation

E. coli cell-free extract was prepared according to a published method [196] and a 4x energy solution was prepared based on the protocol described by Sun *et al.* [164]. As Kwon *et al.* screened a number of different parameters, we will briefly describe the protocol we have used. Cells were cultured with 2xYTP medium. After an initial overnight 5 mL culture, 1 mL of the overnight culture was added to a 500 mL Erlenmeyer flask with 200 mL of fresh medium. Four 200 mL cultures were incubated at 37 °C until an OD of ~2 at 600 nm was reached. Each culture was then separated into falcon tubes and centrifuged at 4 °C for 20 minutes at 4000 rpm. Cells were resuspended with a wash

buffer (10 mM Tris, 14 mM magnesium glutamate, 60 mM potassium glutamate and 2 mM DTT) and centrifuged again at 4 °C for 10 minutes at 4000 rpm. Following three wash steps, all excess liquid is removed and the weight of each pellet is measured. The pellets are then flash frozen in liquid nitrogen and stored at -80 °C. The following day the cell pellets are thawed on ice and resuspended with 1 mL wash buffer per gram of cell pellet. Sonication was used to lyse the cells by applying a total energy input of ∼400 J for a total cell suspension volume of ∼1-1.5 mL. Cells were sonicated in an ice water bath with an amplitute of 50% with 10 s pulses interupted by 10 s wait periods (Vibra-cell 75186 sonicator). Next the lysate solutions are centrifuged at 4 °C for 10 minutes at 12000 x g. The supernatent is removed and placed at 37 °C for 60 minutes to perform the run-off reaction. Lastly, the solution is centrifuged again at 4 °C for 10 minutes at 12000 x g and the supernatent is then aliquoted into 50 μL volumes, flash frozen and stored at -80 °C. A more detailed protocol is given in Section 6.3 of the Appendix.

We prepared two different cell-free extracts originating from BL21 (DE3) and MC4100 cell strains. Lysates made from BL21 (DE3) cells were used for DNA dilution and ZF repression experiments, whereas MC4100 cell lysates were used for the small molecule inducible circuits as that strain is Lac- [28].

3.5.3 Preparation of linear DNA templates

Linear DNA templates were generated by assembly PCR in order to link a downstream gene with a given promoter variant. The methods for generating the pλPR-GFP reporter templates used in the ZF repression assays have been previously described [193]. Gene specific PCR fragments were obtained for TetR and LacI from the repressilator plasmid [28] and combined thereafter with promoter PCR fragments that contained either the Lac or Tet operons, respectively. Using global primers we were able to tag each full linear template at the 3' end with biotin and at the 5' end with either Cy3 or Cy5.

3.5.4 Setting up high-throughput steady state cell-free TX-TL experiments

The process of DNA spotting, chip alignment and bonding, followed by chip priming, surface patterning and DNA immobilization has been explained before [193]. Once the DNA templates had been immobilized at the surface of the unit cells, the button valve was actuated and the chip was washed with PBS for 15 minutes to ensure that any unbound DNA was removed and the

DNA spot was visualized with fluorescence microscopy (Nikon Ti-SH-U). Before the experiment was started the button valve was released and the sandwich valves were closed.

A lysate solution was prepared by combining lysate with wash buffer in a 1:1 ratio and the energy solution was made up of 50% 4x energy solution, 2.5 μM chi decoy DNA [97] or 3.5 μM purified gamS [96] and water. The total volume of each solution should be between 30-40 μL in order to run the reaction for 15-20 hours. Each solution was drawn into a separate piece of FEP tubing (OD 1/16", ID 1/32", Upchurch) and connected to the microfluidic device inlet with a small piece of PEEK tubing (OD 1/32", ID 0.18 mm, Vici). The pressure applied to the lysate and energy solution tubings was ~20 kPa during the experiment. A custom LabView program was written to control the pneumatic valves, the camera and the microscope. Every 15 minutes a fresh mixture of cell-free extract was flowed through the exchange channel using a cycle period of 600 ms and a duty cycle of 50% for 100 total cycles (or ~60 s) to ensure that the entire channel volume has been replaced (Supplementary Fig. 3.5F, G). To mix three components for the ZF repression experiment a cycle period of 1 s was used for a total of 60 cycles to result in the same overall flow time. Before the cell-free mixture was flowed, valve (1) was opened and valve (2) was closed, followed by a 10 s wait period to assure that valve (1) opened completely in all rows (Fig. 3.1A). Once the exchange channel was replaced with fresh reagents, valve (1) was closed and valve (2) was released permiting the diffusion of reaction components into and out of the unit cells. This process of exchange followed by incubation was carried out continuously for up to 20 hours while the chip was maintained in a temperature controlled box set to 33 °C. GFP expression was monitored in all unit cells over time by acquiring a fluorescence image every 30 minutes.

Switching from one cell-free mixture to another could be programmed in our LabView script. For instance, if a pulse of aTc or IPTG should be delivered to the unit cells at a given time then three solutions were prepared: 1) a lysate solution, 2) an energy solution and 3) an energy solution plus either 5 μM of aTc or 250 μM of IPTG. During the small molecule pulse the cell-free mixture will be generated from solutions (1) and (3), whereas at all other times it will be produced from solutions (1) and (2). For the ZF experiment three solutions were also used: 1) a lysate solution, 2) a lysate solution plus 5 μM ZF-mScarlet and 3) an energy solution. Initially solutions (1) and (3) are used to reach steady state GFP expression levels, then all three solutions are used to generate different concentrations of ZF-mScarlet within the cell-free mixture. Furthermore the multiplexing valves are actuated accordingly to replace each exchange channel with a cell-free mixture containing

a predefined ZF concentration. To ensure that the dead volume inside the serpentine mixing channel does not affect the next mixture generated, a PBS wash step is included every time the duty cycle percentage changes.

3.6 Supplementary Figures

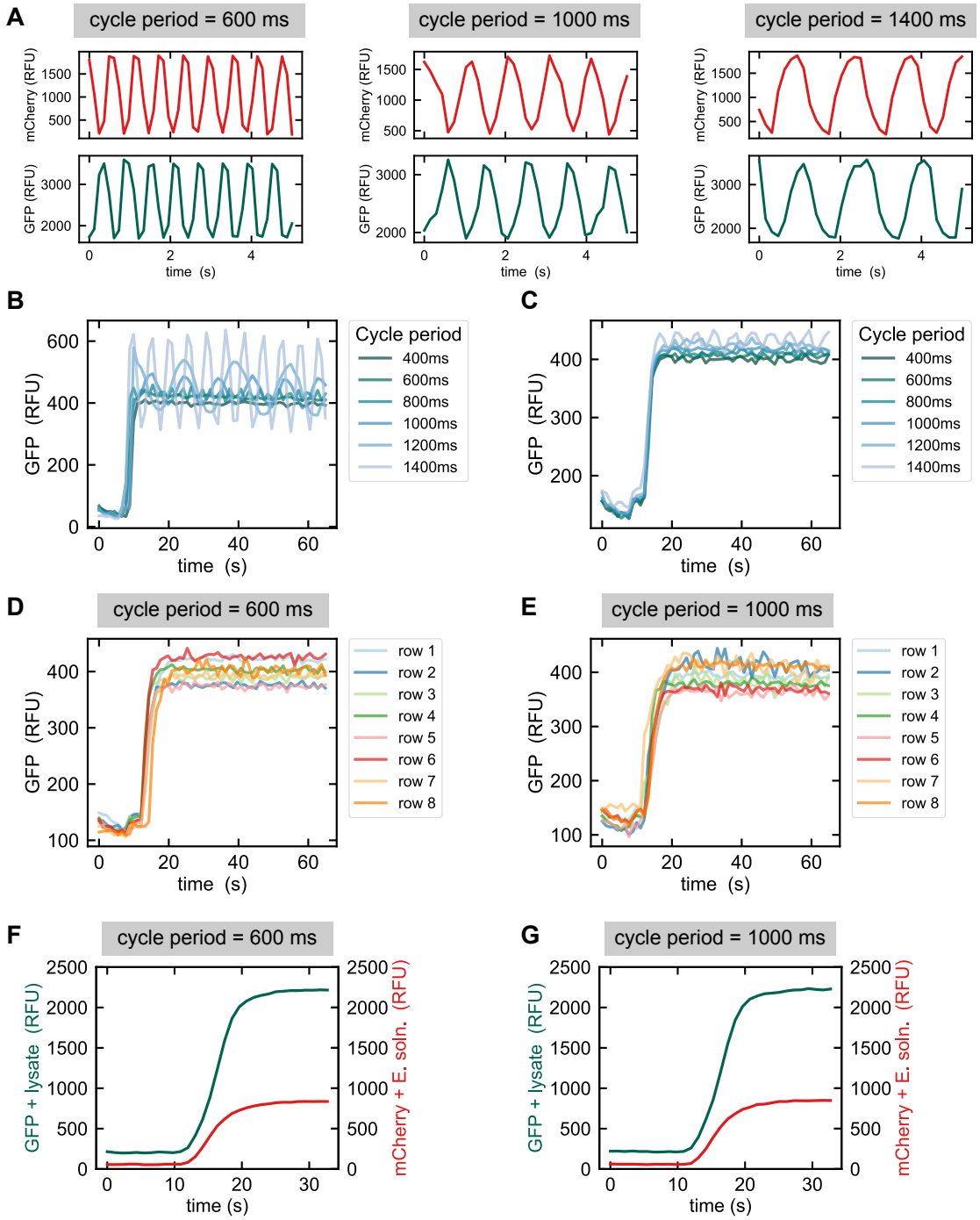

Figure 3.5: **Characterization of PWM for on-chip mixing of lysate and energy solutions.**

Caption on the next page.

Figure 3.5: **(A)** GFP (lysate) and mCherry (energy solution) signals versus time for cycle periods equal to 600, 1000 and 1400 ms. Images were acquired directly after the inlets, just before entering the serpentine channel. **(B, C)** GFP (lysate tracer) signal over time for a range of cycle periods as visualized at the end of the serpentine channel **(B)** and at the beginning of the exchange channel. **(D, E)** Time-lapse of the GFP (lysate tracer) signal acquired at the beginning of each exchange channel for cycle periods equal to 600 ms **(D)** and 1000 ms **(E)**. **(F, G)** GFP (lysate) and mCherry (energy solution) signals versus time for cycle periods equal to 600 ms **(F)** and 1000 ms **(G)** for images acquired at the end of the exchange channel. In all cases a duty cycle of 50% was maintained.

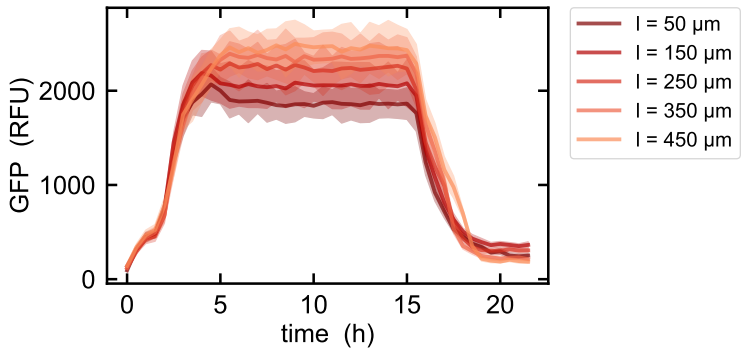

Figure 3.6: **Disrupting steady state expression.** Here we show the expression of GFP versus time for different unit cell connecting channel lengths. After 15 hours we stop flowing cell-free extract and instead flow PBS, showing that we can effectively terminate steady state GFP production in the absence of fresh reagents.

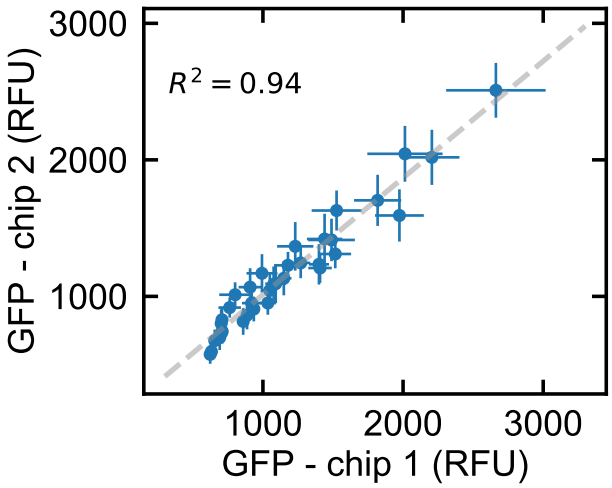

Figure 3.7: **Chip-to-chip reproducibility.** Steady state GFP expression values obtained for two separate chips for a range of DNA template dilutions. The same DNA microplate was used to spot both chips.

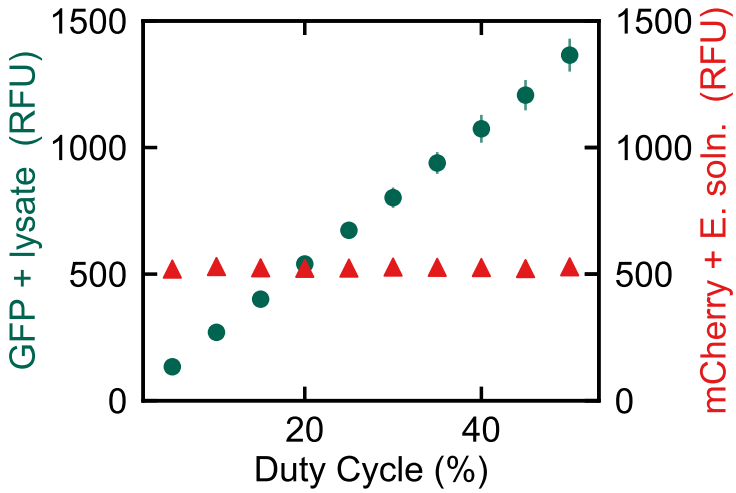

Figure 3.8: **Mixing 3 components on-chip with PWM.** Fluorescence intensity measured for GFP (lysate) and mCherry (energy solution) versus the duty cycle percentage corresponding to the lysate solution. The duty cycle for the energy solution was held constant at 50%.

4

Microfluidic device for real-time formulation of reagents and their subsequent encapsulation into double emulsions

This work has been published in *Scientific Reports*, 2018.

Authors: Jui-Chia Chang, Zoe Swank, Oliver Keiser, Sebastian J. Maerkl and Esther Amstad

Reference: Chang, J.-C., Swank, Z., Keiser, O., Maerkl, S. J., and Amstad, E. (2018). Microfluidic device for real-time formulation of reagents and their subsequent encapsulation into double emulsions. *Scientific reports*, 8(1):1–9.
DOI: 10.1038/s41598-018-26542-x

4.1 Abstract

Emulsion drops are often employed as picoliter-sized containers to perform screening assays. These assays usually entail the formation of drops encompassing discrete objects such as cells or microparticles and reagents to study interactions between the different encapsulants. Drops are also used to screen influences of reagent concentrations on the final product. However, these latter assays are less frequently performed because it is difficult to change the reagent concentration over a wide range and with high precision within a single experiment. In this paper, we present a microfluidic double emulsion drop maker containing pneumatic valves that enable real-time formulation of different reagents using pulse width modulation and consequent encapsulation of the mixed solutions. This device can produce drops from reagent volumes as low as 10 μL with minimal sample loss, thereby enabling experiments that would be prohibitively expensive using drop generators that do not contain valves. We employ this device to monitor the kinetics of the cell-free synthesis of green fluorescent proteins inside double emulsions. To demonstrate the potential of this device for real-time formulation, we perform DNA titration experiments to test the influence of DNA concentration on the amount of green fluorescence protein produced in double emulsions by a coupled cell-free TX-TL system.

4.2 Introduction

Emulsion drops are well-suited containers for performing chemical and biochemical reactions under well-defined conditions and in volumes that are significantly smaller than those required to conduct reactions in bulk. This is especially beneficial for high throughput screening assays [197, 198, 199]. The accuracy of such assays depends on the degree of control over the composition and concentration of reagents contained inside the drops, as well as their size distribution. Drops with a narrow size distribution can be produced using microfluidics [200, 201, 202]. These drops have, for example, been employed as containers for drug screening assays [203, 204], to perform polymerase chain reactions (PCR) from viruses [205, 206], or single cells [207, 208, 209, 210], for directed evolution of enzymes [51], to study the secretion of proteins or other signaling molecules on the single cell level [211, 212], or to identify genes that are responsible for a cellular phenotype [213]. To perform these screening assays, reagents are often pre-mixed before they are injected into the device. Pre-mixing

limits drop-based assays to characterizing very slow reactions or late stages of faster reactions because reagents start to react before they are loaded into drops. Moreover, pre-mixing prevents in situ changes of the relative reagent concentrations such that only one solution composition can be screened per experiment. A possibility to overcome these shortcomings is the injection of reagents into drops after they have been formed, for example through the application of high electric fields [214, 215, 216, 217, 218, 219], the addition of chemicals that destabilize drops [220], or the use of gas bubbles to spatially separate adjacent drops [221]. Using AC electric fields, the concentration of reagents in drops can also be oscillated through consecutive fusion and fission processes [222]. However, the number of different reagents that can be controllably added to intact drops is limited. Moreover, it is difficult to accurately and continuously vary the concentration of injected reagents.

The reagent concentration can be gradually changed by co-flowing two fluids under laminar conditions; in this case, the reagent exchange is diffusion limited [223, 224, 225, 226]. However, because mixing relies on diffusion, the spatio-temporal control over the solution composition is poor. This control can be improved if mixing is enhanced, for example by introducing turbulences into the fluid flow using structured microchannels [227, 228] or active mixers, such as micropumps, or micromixers [229]. However, it always takes some time to equilibrate injection flow rates especially if multiple fluids are involved. Thus, even with mixing features being implemented, it is difficult to controllably and continuously change the concentrations of different reagents with a high temporal resolution.

The concentration of reagents can be changed over a wide range and on very short time scales if microfluidic channels are equipped with integrated pneumatic valves that can be rapidly opened and closed [230]. The large-scale integration of micromechanical valves [231] fabricated by soft-lithography [232] has led to the development of a wide range of microfluidic devices and their applications in areas such as single cell analysis [233], protein biochemistry [109], drug discovery [234], systems biology [172, 235], synthetic biology [100, 131] and molecular diagnostics [236]. These valves allow the formation of a train of alternating plugs of different types of miscible liquids that can subsequently be mixed. The length of the plug of each fluid scales with the duty cycle, corresponding to the pulse width of the corresponding valve divided by the entire cycle period, and can be adjusted in situ and in real-time. Hence, the relative reagent concentrations can be varied over a wide range within a single experiment by gradually changing the duty cycle. This method of mixing fluids, based on pulse width modulation (PWM), has been implemented in microfluidic

devices [237, 238] and is often employed to synthesize biopolymers, to study the influence of their composition on their function, and to test the effect of certain molecules on cell behavior [113, 239, 240, 241, 242, 243]. Recent advancements of this technology enable independent injection of up to six different reagents and changing their concentrations by up to five orders of magnitudes [194]. This level of compositional control over such a wide concentration range is difficult to achieve with co-flowing fluids. The ability to rapidly and controllably change the concentration of reagents contained in the cores of double emulsions by PWM would open up new possibilities for high throughput screening assays. However, to the best of our knowledge, pneumatic valves have never before been implemented into microfluidic flow focusing drop makers and consequently PWM has thus far not been used to control the concentration of reagents contained in the cores of double emulsions.

In this paper, we present a microfluidic flow focusing drop maker that has three inlets for reagents, each of them controlled by a pneumatic valve. This device allows real-time mixing of multiple reagents using PWM, and encapsulates the resulting solution containing a homogeneous mixture of reagents in double emulsions. The pneumatic valves provide an additional benefit: they enable encapsulation of liquids with volumes as low as 10 μL at an efficiency approaching 100%. To test the performance of the device, we encapsulate lysates that synthesize green fluorescent protein (GFP) inside double emulsion drops. We demonstrate the potential of the device by conducting DNA titration assays to measure the influence of DNA template concentration on the amount of GFP produced in double emulsion drops.

4.3 Results

4.3.1 Design and characterization of the microfluidic device

We fabricate microfluidic devices using soft lithography [232]. Devices contain three inlets for aqueous solutions that form the inner phase, one inlet for the oil that constitutes the middle phase, and one inlet for an aqueous phase that forms the surrounding liquid. To control the fluid flow in the three inlets for the innermost phase, we introduce pneumatic valves on top of these channels, as schematically shown by the blue features in Figure 4.1A [231]. The valves enable alternating flow of fluids into the main channel using pulse width modulation, as exemplified in the optical micrograph in Figure 4.1B [194, 230, 244]. To accelerate the mixing of the sequentially injected

reagents, herringbones are introduced to the serpentine-like section of the main channel located between the inlets for the innermost phases and that for the oil phase [228], as schematically shown in Figure 4.1A. To separate reagent-loaded drops from empty ones, the device has a T-junction used as a sorting unit, as shown schematically in Figure 4.1A and in the optical micrograph in Figure 4.1C. The flow of double emulsions is again controlled with pneumatic valves that change the hydrodynamic resistance of the outlet channels.

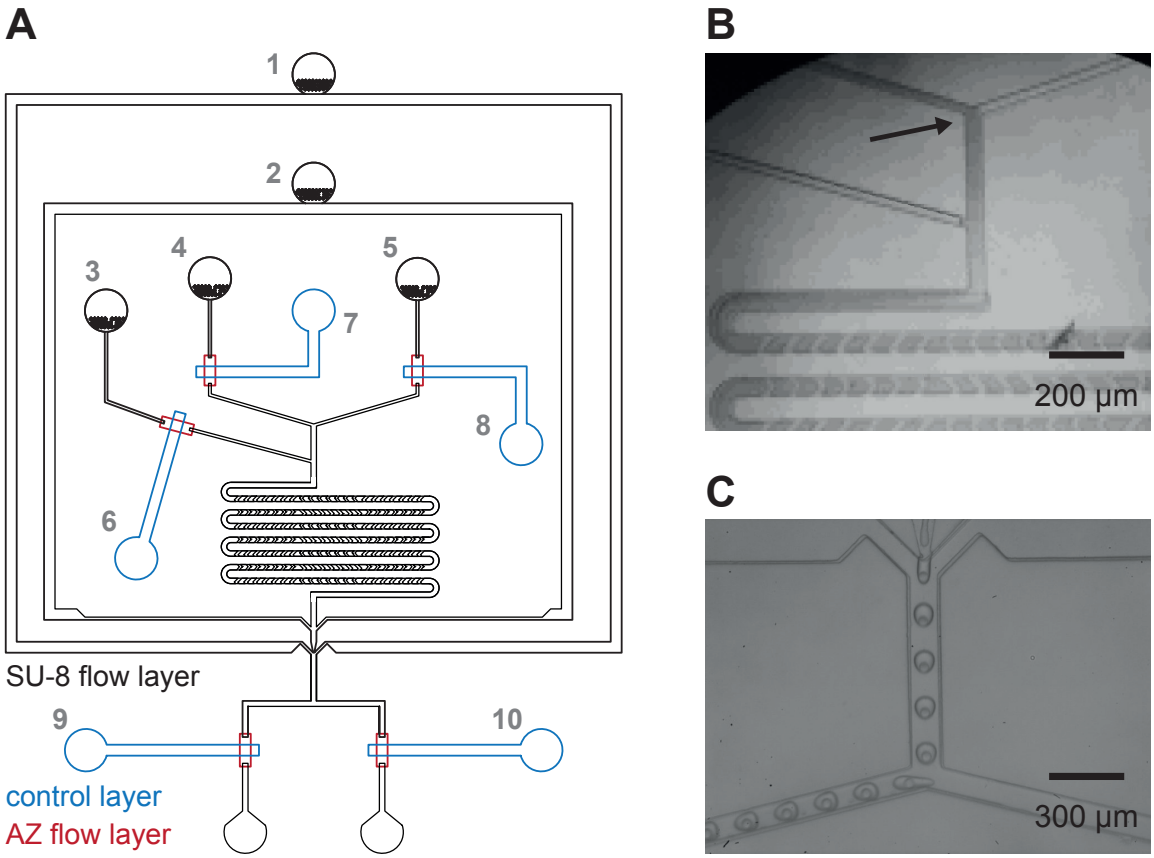

Figure 4.1: **Schematic illustration of the microfluidic device. (A)** Overview of the device with the inlet for (1) the outermost aqueous phase, (2) the oil phase and (3–5) the three innermost aqueous phases. On top of each inlet for the innermost phase is a pneumatic valve that enables controlling the fluid flow (6-8); the control lines are indicated in blue. Drops exit the device through one of the two outlet channels that also contain pneumatic valves (9, 10). **(B)** Optical micrograph of an operating device where an aqueous phase and a dye are alternatingly injected using PWM. **(C)** Optical micrograph of double emulsions that are collected through the left outlet.

To precisely vary the relative amounts of reagents injected into the main channel, the lengths of the sequentially injected plugs must be controlled. This can be achieved by tuning the duty cycles of the valves that control the flows of the inner phases. Valves close if their control channels are pressurized such that the valves are pressed towards the bottom of the fluid channel. We employ software-controlled solenoid valves to pressurize and depressurize the control channels [183, 245, 246]. To determine the response time of the microfluidic valves, we use a colored fluid and quantify the intensity profile across the fluid channel underneath the valve as a function of the pulse width, which is the time the valve is open. If the valve is open, the entire inlet channel underneath the valve is colored, as shown in the optical micrograph in Figure 4.2A; in our device, the inlet channel section below the valve is 200 μm wide. If the valve is closed, the fluid is pushed aside such that this section becomes transparent, as shown in Figure 4.2B. If we keep the duty cycle constant at 50% and set the cycle period to 40 ms, no fluid can pass, as demonstrated by the flat red curve in Figure 4.2C. If we increase the cycle period to 60 ms, some fluid passes and even more fluid passes if the cycle period is increased to 80 ms, as indicated by the increased peak intensity of the blue and green curves in Figure 4.2C. A further increase in the cycle period broadens the intensity peak but does not increase its amplitude any more, as shown in Figure 4.2C. These results indicate that the minimum time each valve must be open and hence the minimum pulse width is 40 ms, corresponding to a minimum cycle period of 80 ms for duty cycles of 50%. This minimum pulse width is limited by the time required to depressurize the control channel and sets a lower limit to the size of plugs that can be formed. This plug size also depends on the fluid flow rate that we set to 250 μL/h; in this case, the minimum plug volume is 3.5 nL. To test if we can control the concentration of reagents in drops, we vary the pulse width of the valve that controls the flow of the color from 50 ms to 200 ms. Indeed, the color of the resulting drops increases linearly with a change in pulse width and hence, with increasing duty cycle, as shown in Supplementary Figure 4.5. These results indicate that we can control the composition of the drops by tuning the duty cycles of the valves.

A key feature of the device is its ability to in situ change the composition of encapsulated reagents in real-time and with high precision. This degree of control is only possible to obtain, if adjacent plugs that contain different reagents are homogeneously mixed before the solution is compartmentalized into drops. The time required to achieve a homogeneous mixing of reagents increases with the plug length because their diffusion length increases. To quantify the maximum

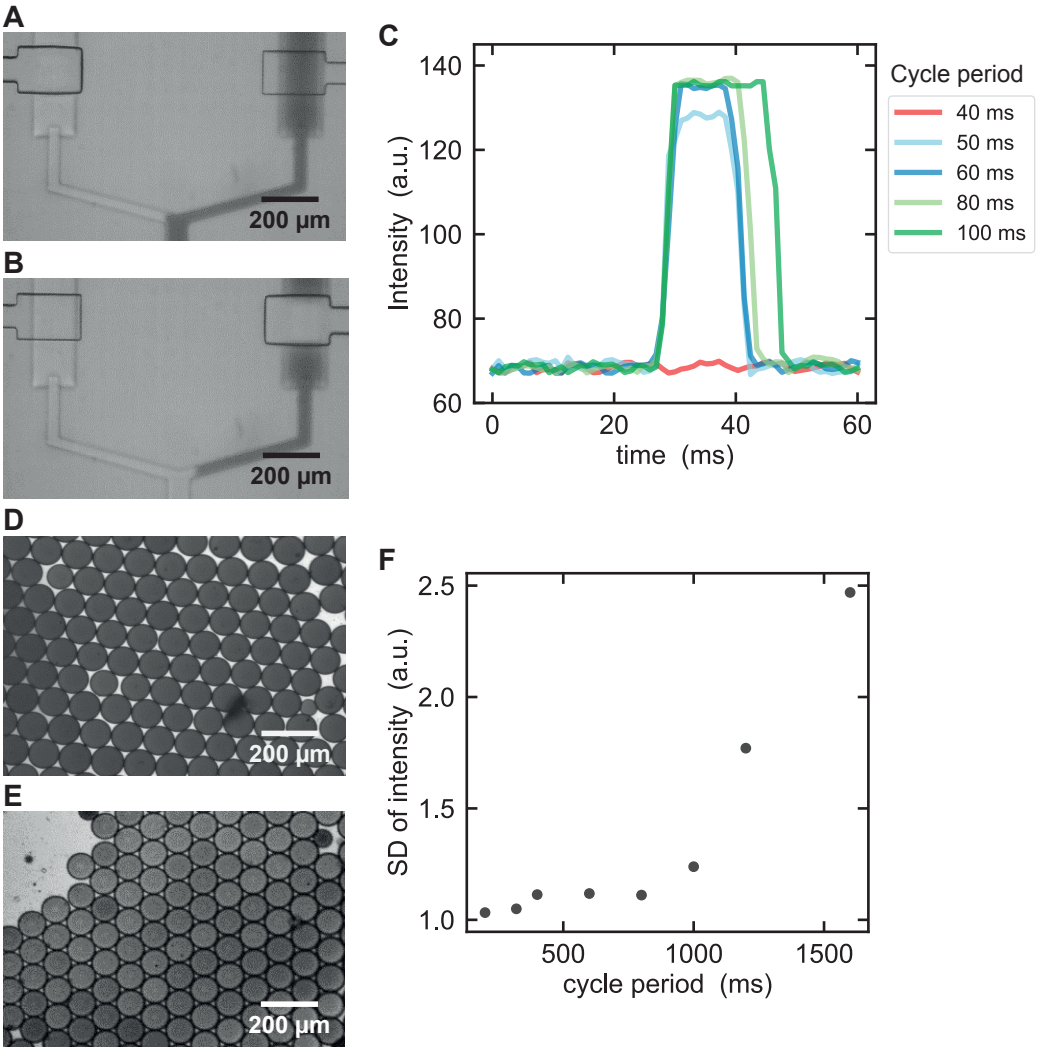

Figure 4.2: **Characterization of the pneumatic valves.** **(A, B)** Optical micrographs of a pneumatic valve that is **(A)** opened and **(B)** closed. **(C)** The intensity of the colorant measured underneath the valve as a function of time for duty cycles of 50% and cycle periods ranging from 40-100 ms. **(D, E)** Optical micrographs of drops formed with a cycle period of **(D)** 200 ms and **(E)** 1600 ms. **(F)** The standard deviation of the dye intensity in drops as a function of the cycle period.

length of plugs that our device can process into a homogeneous mixture before the solution is broken into drops, we employ two liquids, water and a water-soluble dye, as an inner phase. The lengths of the plugs are varied by changing the cycle periods while we keep the duty cycles constant at 50%. If the cycle period is short such that the liquid plugs are small, the two aqueous phases are

fully mixed when the solution reaches the water-oil junction. As a result, the intensity of the 70 μm diameter drops that form at this junction is homogeneous, as indicated in Figure 4.2D. However, if we increase the cycle period above a certain value where plugs become too long, the composition of the solution at the oil-water junction starts to vary over time such that the intensity of the resulting drops is heterogeneous, as shown in Figure 4.2E.

To quantify the maximum length of aqueous plugs that can be fully mixed in our device, we measure the standard deviation of the drop intensity as a function of the cycle period; these experiments are performed using liquids whose viscosity is close to that of water. If the cycle period is below 800 ms, the drop intensities are uniform, as shown in the optical micrograph in Figure 4.2D and summarized in Figure 4.2F. By contrast, if the cycle period is increased above this value, the intensity becomes heterogeneous, as shown in the optical micrograph in Figure 4.2E and summarized in Figure 4.2F. These results indicate that the maximum cycle period where reagents are still homogeneously mixed before the solution is broken into drops is 800 ms; this corresponds to a maximum pulse width of 400 ms and a maximum plug volume of 35 nL. Hence, in our device, we can vary the plug volumes from 3.5 to 35 nL. However, these are not fundamental limits. The dynamic range of the device could be increased by prolonging the mixing unit, or by altering the channel dimensions.

Droplet microfluidics allows encapsulation of reagents with high efficiency. However, in most cases, between 50 and 100 μL of reagents are lost during device start-up. This fluid loss is no problem if reagents are inexpensive and available in large quantities. However, some biological assays involve expensive reagents or samples that are only available in very small volumes. To process these solutions with microfluidic drop makers, sample losses should be minimized. The loss of reagents can be reduced essentially to zero if microfluidic devices contain pneumatic valves: using these valves, the device can be initialized with an aqueous solution while the channels containing expensive or rare samples are closed. These reagent-containing channels are opened only when the device runs stably, such that no reagents are lost during start-up. To separate reagent-loaded drops from empty ones, we again employ pneumatic valves that are incorporated into the collection channels. To test the performance of these valves, we form aqueous single emulsion drops and collect them through the right outlet. To avoid that drops break while they pass the channel underneath the valve, that is only 14 μm tall and hence acts as a constriction, we increase this height to 20 μm [247]. These valves do not completely close the outlet channels even if they are fully

pressurized. Instead, they decrease the height of the channel, thereby increasing its hydrodynamic resistance. As a result of the high hydrodynamic resistance of one of the outlet channels, the vast majority of the fluid flows through the other outlet channel whose valve is open and hence, whose hydrodynamic resistance is much lower. We exemplify this behavior by closing the valve of the left collection channel and opening the one of the right channel. Indeed, drops remain intact if they pass these modified valves. Using these valves, the flow direction of drops can be switched from right to left, as indicated in the optical micrograph in Supplementary Figure 4.6A, demonstrating that these modified valves are well suited to sort drops.

To maximize the accuracy of the sorting, we close the valve of the right channel 10 ms before we open the valve of the left channel. This procedure reduces pressure differences between the two collection channels and therefore allows the drops to flow into the desired collection channel as soon as the corresponding valve is opened. If the injection rate is below 600 μL/h, drops can be sorted without any loss, as shown by the optical time-lapse images in Supplementary Figure 4.6A. Under these operating conditions, no sample is lost whatsoever. By contrast, if the injection rate exceeds 600 μL/h, some drops split at the sorting junction during the switching operation, as shown in the optical time-lapse images in Supplementary Figure 4.6B, resulting in some sample loss. The volume loss increases with increasing injection rate, as summarized in Supplementary Figure 4.6C. Hence, if appropriate flow rates are used, our device enables a loss-free compartmentalization of fluid volumes as small as 10 μL into well-defined drops and the separation of reagent-containing drops from empty ones.

4.3.2 Loading droplets with reagents for cell-free TX-TL

To test the performance of our device, we employ it to produce drops loaded with reagents that form proteins through cell-free TX-TL. If drops are used as containers to screen synthesis conditions, they must be stable during the reaction. Biological drop-based screening assays are most frequently performed using single emulsion drops that are dispersed in a fluorinated oil [213, 248]; these drops are often stabilized with a perfluorinated triblock copolymer surfactant [249]. To test if such aqueous drops remain intact during the synthesis of proteins, we loaded them with lysates [164, 196] and an energy solution containing 30 mM 3-PGA and incubate them at 29 °C for 3 h. We observed that most single emulsion drops coalesce during their incubation such that the resulting sample is polydisperse. This coalescence limits the use of drops for many screening applications. We assign

the limited drop stability to the high concentration of ions present in the emulsion drop [250]. To test if we can increase drop stability, we decrease the concentration of 3-PGA to 4 mM. However, also in this case, single emulsion drops tend to coalesce albeit to a smaller extent, as summarized in Figure 4.3A and shown in the fluorescence micrographs in Supplementary Figure 4.7A and B.

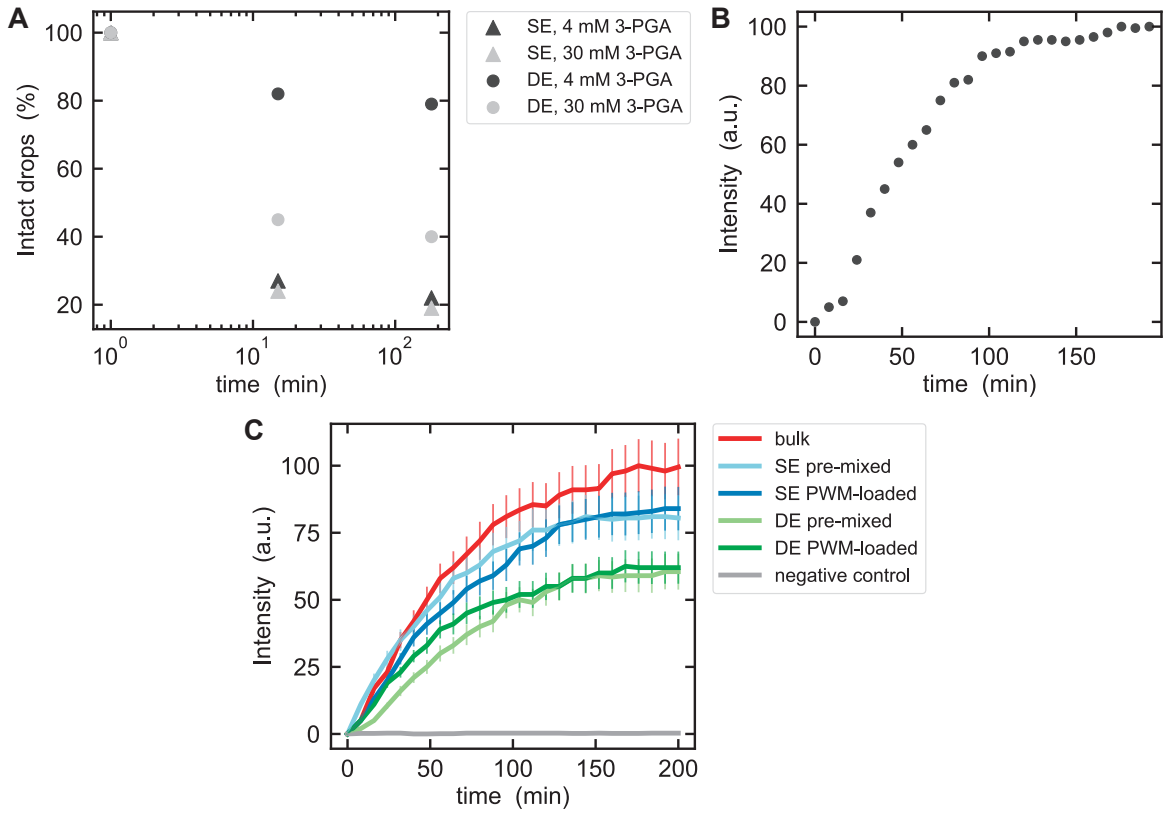

Figure 4.3: **Synthesis of GFP in drops.** **(A)** The percentage of drops that remains intact as a function of the incubation time for single and double emulsion drops (SE and DE, respectively) loaded with either 4 or 30 mM 3-PGA. **(B)** The normalized fluorescence intensity measured in double emulsion drops loaded with PURE as a function of the incubation time. **(C)** The normalized fluorescence intensity of lysate solutions in bulk compared with either single or double emulsion drops loaded with lysates through PWM or pre-mixed lysate solutions as a function of incubation time. As a negative control, lysate extract was loaded into drops in the absence of DNA.

To screen synthesis conditions inside drops, they should be stable against coalescence. The coalescence of single emulsion drops is likely caused by ions that are in close proximity to the

surfactants or the drop interfaces. If this is the case, double emulsions should be more stable against coalescence because their outer liquid-liquid interface is spatially separated from ions by the oil shell. Indeed, the percentage of intact double emulsions is significantly higher than that of single emulsion drops, even if a solution containing 30 mM 3-PGA is used as an innermost phase, as summarized in Figure 4.3A. These results indicate that double emulsions are potentially more suitable screening vessels if reactions are conducted at high salt concentrations and elevated temperatures because they are more stable against coalescence.

To test if we can use these double emulsions as picoliter-sized vessels to produce proteins through cell-free synthesis, we employ PURE, a cell-free transcription / translation reaction mixture generated from purified components [86]. PUREexpress is now commercially available (NEB) but is a relatively expensive reagent with a cost of over 1 USD per μL. Therefore, it is beneficial to only consume small volumes. Yet, small volumes are difficult to handle with standard microfluidic drop makers where volumes between 50 and 100 μL can easily be lost during start-up. To prevent sample loss during start-up of our device, deionized water is injected through inlet 3 (Fig. 4.1A). To ensure proteins are only produced inside double emulsion drops and do not start to form in the bulk solution prior to their injection in the device, we do not pre-mix reagents but co-inject two solutions containing complementary reagents. When the device runs stably, valve 6 (Fig. 4.1A) that controls the flow of pure water is closed, and the two solutions are sequentially flowed using PWM with duty cycles of 50% and a cycle period of 100 ms. One aqueous solution contains PURE and is injected through inlet 4 (Fig. 4.1A). The other aqueous solution contains DNA and is injected through inlet 5 (Fig. 4.1A). The reagents are mixed in the channel section that contains herringbones and the resulting solution is employed to form the cores of 65 μm diameter double emulsion drops. These drops are incubated at 29 °C for 3 h and the synthesis kinetics of GFP is measured by acquiring a fluorescent micrograph every 8 min. Within 2 h fluorescence reaches a plateau as shown in the fluorescence intensity trace in Figure 4.3B. These experiments demonstrate the potential of our device for the economic use of expensive reagents such as PUREexpress.

Double emulsions are significantly more stable than single emulsions. Nevertheless, a large fraction of the cores containing 30 mM 3-PGA merges with the surrounding aqueous phase such that all the encapsulants are released, as exemplified in Figure 4.3A. To increase the fraction of intact double emulsion drops, we reduce the 3-PGA concentration to 4 mM. This reduction in 3-PGA concentration significantly increases the percentage of intact double emulsions, as exemplified

in the fluorescence micrographs in Supplementary Figure 4.7C, D and summarized in Figure 4.3A. Hence, solutions containing 4 mM 3-PGA are employed for the following experiments.

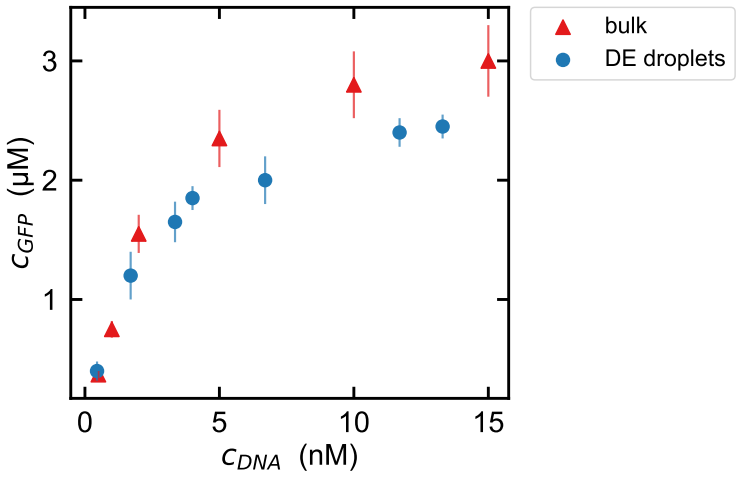

Figure 4.4: ***In situ* DNA-titration.** The influence of the DNA concentration on the amount of GFP synthesized inside double emulsions (DE) and in bulk. For GFP synthesized in double emulsions, the DNA concentration was varied in situ by pulse width modulation.

To investigate the kinetics of synthesized GFP, we quantify the fluorescence intensity of each drop. Encapsulation of lysates into 65 μm diameter drops does not alter the kinetics of GFP synthesis, as summarized in Figure 4.3C. However, the amount of GFP produced in double emulsions is significantly lower than that produced in single emulsion drops and in bulk, as indicated by the green curves in Figure 4.3C. In our experiments, single emulsion drops contain approximately 0.55 μM functional GFP whereas double emulsion drops contain only approximately 0.39 μM functional GFP, as quantified using a calibration curve and summarized in Supplementary Figure 4.8. This difference might be caused by a partial leakage of reagents through the shell of double emulsions, by analogy to the crosstalk observed between aqueous drops that are dispersed in perfluorinated oils [251]. Nevertheless, there is a significant amount of functional GFP synthesized in double emulsion drops, indicating that they can be used to screen effects of synthesis conditions on the amount of functional GFP produced.

One of the main features of our microfluidic device is its ability to change the concentrations of reagents contained in double emulsion drops in real-time and with high accuracy. To exploit this feature, we perform DNA titration experiments: Water is injected through inlet 4, an aqueous

solution containing lysate extracts from E. coli, 30 mM 3-PGA, and an energy source through inlet 3, and an aqueous solution containing 15 nM DNA through inlet 5. The total cycle period is kept constant at 400 ms while the duty cycle of valve 5 is varied from 10% to 80% in four steps. Using this procedure, we screen four DNA concentrations, 13.3, 11.7, 6.7, and 1.7 nM, within a single experiment that consumes as little as 10 μL of lysates and similar volumes of the energy solution. From these reagents, we produce approximately 100 drops for each DNA concentration. We repeat the same experiment using a solution containing 7.5 nM DNA to screen four additional DNA concentrations. The resulting double emulsions are incubated for 3 h at 29 °C and their intensity is quantified using fluorescence microscopy. The amount of protein produced in a drop increases with increasing amounts of DNA up to a concentration of 6 nM and levels off thereafter, as shown by blue circles in Figure 4.4. A similar trend is seen in the experiments performed in bulk, as shown by red triangles in Figure 4.4. However, using drops, we obtain a 25-fold improved statistics while consuming 8-fold less reagents than if the screening is performed in bulk. These results demonstrate the potential of our device to screen different reaction conditions with very low volumes of reagents.

4.4 Conclusion

We have presented a microfluidic drop maker that allows real-time formulation of three solutions using pulse width modulation and processes the resulting mixture into cores of double emulsion drops. The device allows processing solutions with volumes as low as 10 μL into cores of double emulsions without suffering from sample loss. To demonstrate the potential of the device to characterize the influence of the reagent concentrations on the products synthesized in double emulsion drops, we synthesize GFP using a cell-free reaction and titrate DNA template concentrations. The economic use of expensive reagents that includes the ability to change the reagent composition within a single experiment are of particular importance for the production of expensive biomolecules and for screening and characterization of samples that are only available in very small quantities. Hence, this device might open up new possibilities to screen synthesis conditions for reactions that involve expensive or rare reagents.

4.5 Materials and Methods

4.5.1 Cell-free TX-TL materials

GFP is synthesized by mixing an aqueous solution containing cell-free reagents and an energy solution. The cell-free reagent solution contains lysate extracted from *E. coli* and GFP DNA templates. The energy solution is composed of water containing 10.5 mM magnesium glutamate, 100 mM potassium glutamate, 0.25 mM dithiothreitol (DTT), 1.5 mM of each amino acid except leucine, 1.25 mM leucine, 50 mM HEPES, 1.5 mM adenosine triphosphate (ATP), and guanosine-5'-triphosphate (GTP), 0.9 mM cytidine triphosphate (CTP) and uridine triphosphate (UTP), 0.2 mg/mL tRNA, 0.26 mM coenzyme A (CoA), 0.33 mM nicotinamide adenine dinucleotide (NAD), 0.75 mM cyclic adenosine monophosphate (cAMP), 0.068 mM colonic acid, 1 mM spermidine, 2% PEG-8000, 4 mM 3-Phosphoglyceric acid (3-PGA). Further information regarding the preparation of *E. coli* lysate can be found in the Section 6.3 of the Appendix.

4.5.2 Fabrication of the microfluidic device

The microfluidic device is made of poly(dimethylsiloxane) (PDMS) using soft lithography [232, 252]. It contains five inlets, one for the outer phase, one for the middle phase, and three for the inner phases. The fluid flow of the inner fluids is tuned with control valves through which air is injected at a pressure of 25 psi to close the pneumatic valves located on top of the respective fluid channels. The three inlets for the inner phases lead into a 50 μm wide channel that contains herringbone structures to enhance the mixing of the reagents. Downstream the herringbone structures, the main channel is intersected by two inlets for oil that forms the shell of the double emulsions. The oil and the aqueous solution are processed into double emulsion drops at a 3D junction [252] that leads into a 100 μm wide collection channel.

The masters used for the bottom part of the device containing the liquid channels is fabricated from two layers of negative photoresist, SU-8; the first layer is 14–20 μm tall, the second layer is 100 μm tall. The masters employed to fabricate the top part of the device is made of three layers of photoresist: The first layer is 14 μm tall and composed of a positive photoresist, AZ9260, each of the second and third layer is 20 μm tall and composed of a negative photoresist, SU-8.

The microfluidic device is made from Sylgard 184 PDMS (Dow Corning). The three parts are

joined through reactive bonding: To fabricate the top part of the device, we employ a base:crosslinker ratio of 1:5, the middle part is made at a base:crosslinker ratio of 1:20, and the bottom part at a base:crosslinker ratio of 1:1036. The middle part must be thin to ensure that the valves are sufficiently flexible to close the fluid channels if the control channels are pressurized. To control the thickness of the middle part, we spin coat PDMS to form a 100 μm thick layer. PDMS is cured at 80 °C for 25 minutes. The top and middle parts are aligned and bonded by incubating them at 80 °C for 2 hours. The resulting part is removed from the mold and bonded to the bottom part using oxygen plasma followed by incubation at 65 °C for 12 hours. The resulting devices have 100 μm tall control channels. The inlet liquid channels are 20 μm tall and lead into the three dimensional junction where the outermost liquid phase meets the main channel; at this junction the channel height increases to 60 μm.

To produce water-oil-water double emulsions, the part upstream the junction where the outermost phase flows into the main channel must be hydrophobic whereas the main channel further downstream must be hydrophilic. To render the top part of the device hydrophobic we inject fluorinated oil (Novec 7500, 3 M, MN) containing 1 vol% trichloro(1H,1H,2 H,2H-perfluorooctyl)silane (Sigma-Aldrich, MO) into this section of the device. To render the remaining part of the device hydrophilic, the surfaces are treated with an aqueous solution containing 2 wt% poly(diallyldimethylammonium chloride) and 1 M sodium chloride. Fluids are injected into the device through polyethylene tubing (PE/5, Scientific Commodities Inc., AZ) using syringe pumps.

4.5.3 Encapsulation of cell-free reagents

We employ an aqueous solution containing 10 wt% of poly(vinyl alcohol) (PVA), M_w 13000–23000 Da, 87–89% hydrolyzed, as an outer phase, a perfluorinated oil, HFE7500 (Novec 7500, 3 M, MN), containing 1 wt% of surfactant [249, 250] as a middle phase, and an aqueous phase as an inner phase. To initialize the device, we use deionized water as an inner phase. Once the device runs stably, we close valve 6 (Fig.4.1A) that controls the fluid flow of the deionized water. Simultaneously, the two other valves, 7 and 8, are alternatingly opened to inject the aqueous solutions containing the reagents from the two other inlets for the inner phase. Within one experiment, we inject 10 μL of an aqueous solution containing lysate extract solution through inlet 4 and 10 μL of an aqueous solution containing DNA and energy source through inlet 5. Thereby, we keep the duty cycles constant at 50% and the total cycle period is 100 ms.

4.5.4 DNA titration

To perform DNA titration experiments, we employ three different aqueous phases as inner phases: Inlet 3 contains lysate with an energy source, inlet 4 contains an aqueous solution with 15 nM of DNA, and inlet 5 contains pure water (Fig.4.1A). We change the DNA concentration, without changing the concentration of any other reagent, by varying the duty cycles of valves 7 and 8 that control the flow of the aqueous solutions containing DNA and water respectively. The cycle period is 400 ms and the duty cycles vary from 10% to 80% in four steps. To enlarge the range of DNA concentrations that are screened, we repeat the same experiment but inject an aqueous solution containing 7.5 nM of DNA through inlet 4. Drops are subsequently incubated at 29 °C for 3 h. During this incubation, we monitor the formation of green fluorescence protein using fluorescence microscopy where one image is acquired every 8 minutes.

4.5.5 Analysis of the formation of GFP

The formation of GFP is quantified using fluorescence micrographs. The average fluorescence intensity of each drop is quantified and normalized for its size and shape. To correct for lensing effects that occur at the drop interfaces, we perform control experiments where the fluorescence intensity of solutions containing known amounts of fluorescein is measured in bulk, in single emulsion, and double emulsion drops. Lensing effects increase the fluorescence intensity in single emulsions by 11%, compared to the bulk and in double emulsions by 15%. We correct for these lensing effects and convert the fluorescence intensity into a protein concentration for each drop using a calibration curve measured in bulk. For each data point reported, we analyze the protein concentration of at least 25 drops to calculate the error bars.

4.6 Supplementary information

4.6.1 Influence of duty cycle on the amount of reagent contained in drops

To determine if the amount of reagent that is contained in drops scales with the duty cycle of the valve, corresponding to the fraction of time the valve is open relative to the entire cycle period, we employ an aqueous solution containing fluorescein. We co-inject this solution with an aqueous solution that does not contain any fluorophore. We keep the pulse width of the valve controlling the flow of the pure aqueous phase constant at 50 ms and vary that of the valve controlling the flow of the fluorescent phase between 50 and 200 ms. Indeed, the measured fluorescence linearly increases with the duty cycle, as shown in Figure 4.5.

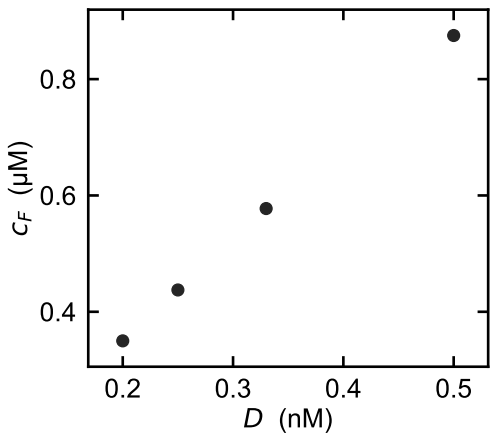

Figure 4.5: Influence of the duty cycle (D) on the concentration of fluorescein, c_F, contained in the drops.

4.6.2 Drop sorting

To separate reagent-containing drops from empty ones, we introduce a T-junction downstream of the drop generation junction. By pressurizing the left control channel of the sorting unit, the left valve partially closes the channel such that its hydrodynamic resistance increases and drops flow into the right outlet. To switch the direction of the fluid flow, we close the right valve 10 ms before we open the left one. If the fluid flow upstream of the T-junction does not exceed 600 μL/h, drops follow the fluid flow and remain intact even when the fluid flow switches direction, as shown in the time lapse optical micrographs in Figure 4.6A. By contrast, if the injection flow rate exceeds 600 μL/h, some drops split at the T-junction while the direction of the fluid flow is changed, resulting in some loss of reagents, as shown in the time lapse optical micrographs in Figure 4.6B. The amount of sample that is lost increases with increasing injection rate, as summarized in Figure 4.6C.

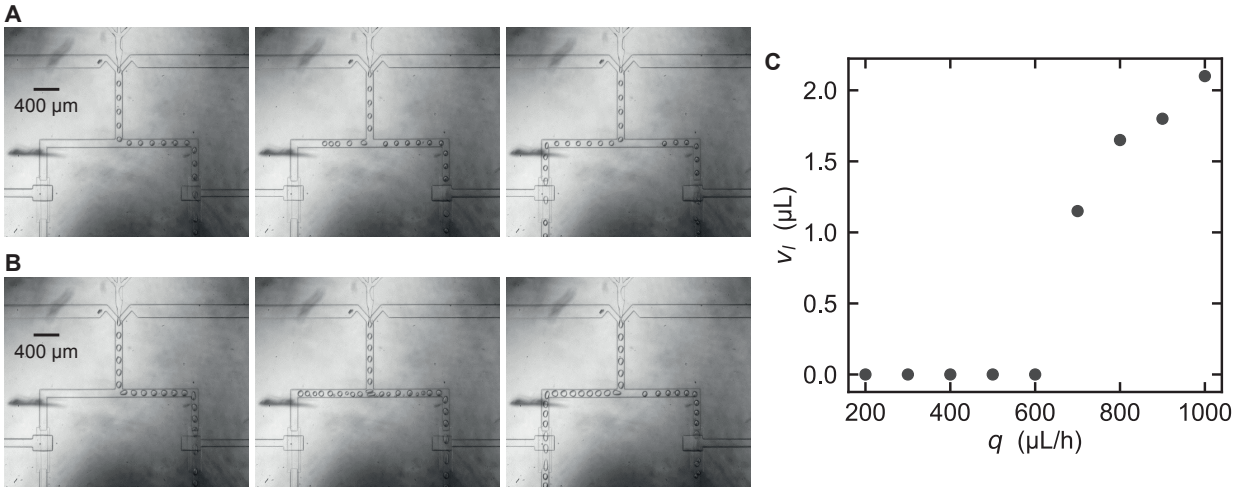

Figure 4.6: **Drop sorting.** Time lapse optical microscopy images illustrating the change in the flow direction of drops if the total injection speed is **(a)** 600 μL/h and **(b)** 900 μL/h. **(c)** The amount of fluid lost during the switching process (v_l), as a function of the injection flow rate, q, is shown.

4.6.3 Synthesis of GFP in drops

To test if we can track the formation of GFP inside drops, we form monodisperse single emulsion drops with a diameter of 70 μm that are loaded with lysates and 4 mM of 3-PGA. Even though the 3-PGA concentration in these drops is almost an order of magnitude below the 3-PGA concentration typically used, most of the drops coalesce, as indicated by the high polydispersity of drops incubated at 29 °C for 30 min, shown in Figure 4.7A and the even higher polydispersity of drops after they have been incubated at this temperature for 3 h, as shown in Figure 4.7B. Coalescence of drops hampers their use for screening assays. We expect the high concentration of ions that are in close proximity to the liquid-liquid interface deters drop stability. To test this expectation, we produce double emulsion drops containing lysates and 4 mM 3-PGA in their core; the outer liquid-liquid interface of these drops is separated from ions by their oil shell. Indeed, double emulsions are much more stable against coalescence, as indicated by their narrow size distribution after they have been incubated at 29 °C for 30 min and 3 h, as shown in Figure 4.7C and D, respectively.

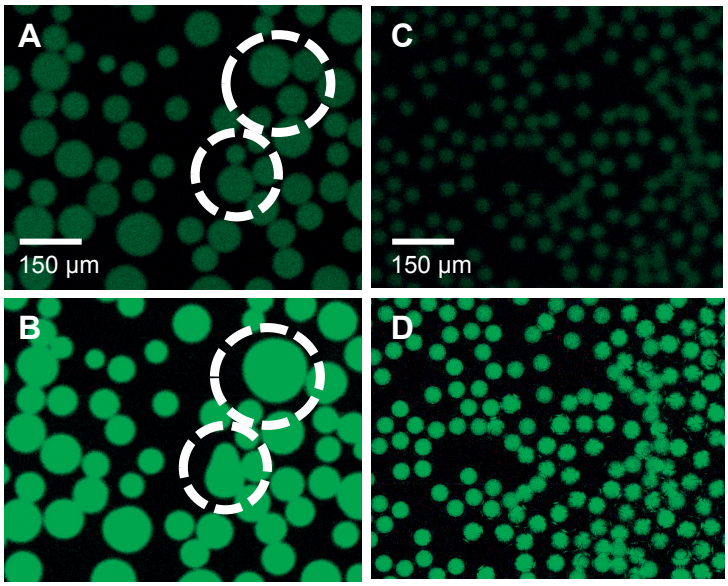

Figure 4.7: **Synthesis of GFP in drops with 4 mM 3-PGA. (a-d)** Fluorescence micrographs of **(a, b)** single emulsion and **(c, d)** double emulsion drops loaded with lysates and incubated at 29 °C for **(a, c)** 30 min and **(b, d)** 3 h.

4.6.4 Quantification of GFP concentrations

To quantify the amount of GFP produced in single and double emulsion drops we measure a calibration curve in bulk. The amount of GFP produced in solutions containing 4 mM 3-PGA is approximately 50% lower compared to solutions containing 30 mM 3-PGA, as summarized in Figure 4.8. By contrast, the kinetics of the GFP production is not affected by the concentration of 3-PGA, as shown in Figure 4.3C in the results section.

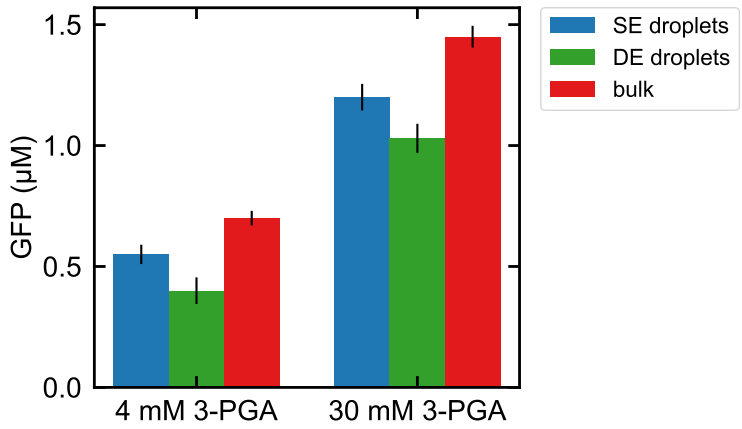

Figure 4.8: Concentration of GFP synthesized in 65 μm drops containing 4 mM and 30 mM 3-PGA for single emulsions (SE), double emulsions (DE), and bulk solutions.

5

Conclusions and outlook

To conclude, we have developed three microfluidic platforms that we used in conjunction with cell-free systems to gain a quantitative understanding of gene regulation that serves to guide the rational design of synthetic gene circuits. Many components contribute to the function of gene regulatory networks, though transcription factors and their interactions with promoters and each other are of central importance. In cell-free systems we can study transcription factors independently before considering the multi-component network, however the interactions that arise when a single transcription factor is paired with a given promoter are already considerably complex. Taking into account the sequence space of the promoter, together with the transcription factor binding site and the relative concentrations of both the target promoter and the transcription factor, acquiring quantitative measurements is simplified, but still challenging *in vitro*. Moreover, gaps in our understanding must be filled in by studying each network element with enough detail to enable the functional integration of separate parts. In addition, the composability of different circuit components is often unreliable, requiring several alternative network architectures to be tested and underlining the necessity for high-throughput techniques that can adequately screen and characterize a variety of parts and their piece-wise assembly together.

The DNA sequence space of gene regulatory networks is vast and includes promoters, transcription factor binding sites and the gene sequences of transcription factors among other components. Using the device presented in Chapter 2, we began by characterizing a base promoter using a site-directed mutagenesis library, yielding a range of expression profiles associated with specific point mutations. Often the design of functional gene circuits entails tuning the basal expression level of a given promoter, thus the reliable correlation between sequence and output could profoundly affect

our ability to rapidly design functional circuits. While we show that adjusting promoter strength is possible, it becomes less predictable when multiple base changes are made in close context to one another, for example with the incorporation of a transcription factor binding site. Bacterial promoters are relatively small, but a more in depth study would be necessary to improve our understanding of the principles that govern promoter sequence design. A complete understanding of the entire promoter sequence space would likely require characterizing far bigger libraries. However, given that we are often placing transcription factor binding sites in the same general positions, a closer look at a particular sequence subspace may suffice for current bioengineering needs. For instance, it could prove useful to collect cell-free expression data for another set of promoters that vary two or three bases at a time within and directly next to the -10 and -35 boxes. Perhaps only a subset of the possible permutations involving multiple base changes would need to be sampled and could then be combined with the single point mutation data to build a model that would predict the relative promoter strength associated with the inclusion of a given transcription factor binding site. While a fully predictive DNA sequence to protein output model was unattainable during the timeline of this project, we were able to postulate how single point mutations could help to offset the deviation in promoter strength that occurs with the insertion of certain binding sites. Thus without significantly expanding our DNA library, we collected enough information to continue with the step by step construction of gene regulatory networks.

Next, we decoupled the transcription factor binding site sequence from the promoter to determine the binding energy landscapes for a library of synthetic ZFs using another microfluidic technique known as MITOMI. Equipped with basic information regarding promoter strength and ZF binding affinities, we then went on to test how each ZF functioned as a transcriptional repressor for the simplest case involving a single binding site within the target promoter. We saw a strong correlation between the measured dissociation constants and fold repression levels and we demonstrated that our library of synthetic ZFs was mostly orthogonal. Owing to the high-throughput methods we employed, we only needed to run a few experiments to discover that different repression profiles can be achieved using ZFs with a range of binding affinities and these ZFs could be combined together in circuits with minimal cross-reactivity. Given the speed associated with this basic characterization, we could test additional ZF variants to increase the size of our transcription factor library with relative ease in the future. Furthermore, there are more variants available to test, as up to now we utilized less than one quarter of the ZFs stemming from the original 64-

member library. Bioengineers are often constrained by a limited number and poor characterization of transcriptional regulators, therefore the possibility to augment a collection of already functional ZFs is advantageous. Though engineering ZFs to reliably bind a specific target sequence continues to pose difficulties, their small size linked with increasingly inexpensive gene synthesis makes it easy to rapidly screen for functional variants. In any case, the predictable programming of transcription factors is not imparative to construct synthetic gene circuits, but on the other hand, a well-characterized transcription factor binding energy landscape, which we could obtain for ZFs, proves to be extremely useful.

Building upon our initial characterization we then proceeded to investigate higher order interactions by increasing the number of ZF binding sites within the promoter and by engineering coopertivity between ZFs. Engineering certain types of genetic circuits often necessitates an increase in the nonlinear response and a decrease in the leak for a given promoter – TF pair. While adding a second binding site led to an overall increase in fold repression, introducing cooperative protein – protein interactions resulted in an additional increase in nonlinearity. Furthermore, we observed that the relative positioning of the two binding sites with and without coopertivity is an important determinant of repression efficiency. Lastly, we sought to tune repression predictively by varying the binding site affinity. Utilizing MITOMI, we were able to generate position weight matrices for different ZFs and with this information we could precisely modify a given binding site, which related to a corresponding change in fold repression. Having established a well-characterized collection of transcriptional repressors and promoters, we were then able to design functional NAND, AND and OR logic gates. Moreover, we were able to explain our data with thermodynamic models, demonstrating that merging models with binding energy landscapes offers a viable and effective approach to rationally engineer gene regulatory circuits. Our library of well-defined genetic parts serves as a powerful resource for designing other types of networks in the future, though the introduction of more cooperative protein – protein interaction domains may be needed. With additional cooperative interactions and the present ability to balance ZF transcriptional regulation through affinity tuning, we are poised to rationally engineer increasingly complex networks in the future.

After illustrating the level of characterization we could achieve with a device operating in batch-mode, we were motivated to extend these capabilities to a steady state reaction environment, providing the means to implement other types of genetic circuits that do not function in batch reactions. Consequently, in Chapter 3 we describe an adapted device that facilitates cell-free TX-

TL at steady state, while maintaining the capacity for high-throughput screening. As a proof of concept, we make use of information gleaned in Chapter 2 in order to tune repression at steady state by modifying the binding site for a single ZF. With the added advantage of on-chip mixing, we can program the concentration of different inputs over time, allowing us to screen ZF concentration versus binding site sequence. Additionally, we showed that we could implement small molecule inducible gene circuits, such as the toggle switch. We forsee that devices of this nature will have great potential in the future, as we have the ability to characterize variable gene regulatory parts and circuit designs to the same extent at steady state as we have shown in batch-mode with the device presented in Chapter 2. Furthermore, we have the means to program the concentration of small molecule or protein inputs in real-time and measure the corresponding effect on gene expression for different cell-free gene circuit designs. One straight-forward application of this device could involve the systematic study of the toggle switch circuit in terms of promoter sequence space linked with inducer concentration and pulse length, providing a way to map the switching landscape. Alternatively, we could consider building a toggle switch composed of ZFs. The most obvious problem is that ZF – DNA binding cannot be inhibited by small molecules as with the Tet and Lac repressors, however with the use of new protein – protein interactions it may be possible. For example, two ZFs could be fused with complementary protein binding domains whose interaction is inhibited by a small molecule, thus the transition from cooperative to non-cooperative binding could shift the circuit from one state to another. Balancing promoter expression and binding affinities is made easier, owing to the characterization of our ZF – promoter resources in batch and screening new protein – protein interactions along with inducer molecule concentrations could be efficiently carried out with our steady state device.

Apart from the promoter sequence and transcription factor interactions, the concentration of DNA templates is another important parameter to consider when constructing gene regulatory networks. In particular, when multiple DNA templates are present, loading effects can manifest in the form of TX-TL resource constraints and an imbalance can result in circuit dysfunction. We were able to precisely control the amount of DNA template(s) immobilized on the surface of our reaction compartments using the devices presented in Chapters 2 and 3. Together with our high-throughput capabilities we could easily test a range of concentrations for a single DNA template or different ratios of multiple templates, enabling us to correlate different functional outputs with a given amount of DNA input. The device we described in Chapter 4 can also accurately control

the concentration of DNA template that is encapsulated into a given droplet by mixing different reagents on-chip using pulse width modulation. Though we only applied this device to study the effect of DNA titration, it provides an optimal platform for screening concentration gradients of other reaction components. For instance, it would be possible to titrate different cell-free protein components or energy substrates in order to link extract performance with system composition. This strategy could be particularly useful for optimizing recombinant systems since only very small volumes of often costly reagents are necessary. Furthermore, given the recent technological advancements applied to the spatial control of cell-free systems, it should be feasible to amend our platform for implementing gene expression at steady state. More specifically, DNA components could be tethered inside the droplets while artificial pores incorporated into the membrane would allow the exchange of cell-free substrates and products over time.

Each microfluidic device presented in this work provided the means to characterize gene expression and regulation at different levels and capacities. We have placed a considerable focus on the DNA sequence space encompassing the promoter and transcription factor binding sites, however gene expression can also be tuned with adjustments to the ribosomal binding site and the transcription terminator among other sequence elements. Although we used a streamlined PCR assembly method to generate linear templates with variable promoter sequences, we were still limited by the time it takes to carry out these reactions efficiently by hand, constraining the overall amount of sequence variability we could test. As the cost of DNA oligos and pippetting robots decreases, we will be able to generate larger libraries of genetic parts in an automated fashion, saving more time for carrying out the experiments to characterize these parts. Consequently, discerning how each of these sequence elements work independently and together will undoubtedly increase the reliability of gene network engineering in the future. In parallel, the process of building gene regulatory circuits offers another route to deconstruct and improve our understanding of natural biological systems.

While there are countless facets of gene regulation left to explore, we are convinced that the steady increase in the number of well-characterized genetic parts and their increasingly reliable piece-wise assembly will one day lead to predictable network engineering from the bottom-up. Using cell-free and microfluidic platforms, we have expanded the pool of resources available for engineering gene circuits and in doing so we generated quantitative data that could one day serve as the foundation for a fully predictive model. Rather than relying on a single microfluidic technology,

we have shown that the accumulation of data obtained from multiple methods can lead to a greater increase in mechanistic understanding. As improved technologies and cell-free systems coalesce in the future to create even larger libraries of well-defined genetic parts, we will be able to rationally design increasingly complex gene regulatory networks that function similar to natural systems or with novel applications.

6

Appendix

6.1 High-throughput cell-free TX-TL with PURE

The chip presented in Chapter 2 was also used to carry out *in vitro* TX-TL using PURExpress (NEB). Using mRNA binding probes [253], we were able to track transcription and translation over time and we again saw a correlation between the ratio of dsDNA:ssDNA spotted and the expression profiles of mRNA and GFP (Fig. 6.1A, B). Furthermore, if we quantify the amount of DNA template attached to the surface of our unit cell, we see a corresponding increase in the amount of GFP produced (Fig. 6.1C). We used this platform in combination with PURExpress to screen a small library of T7 promoters for different concentrations of DNA template. Two natural T7 bacteriophage promoters, phi10 and phi13, were tested and several other variants of the phi13 promoter were generated. Based on previously published data that investigated the relative utilization of promoter mutants [254], we introduced one, two or three point mutations to create a range of protein expression levels. While we did not perform a very extensive study, it was possible to see variable GFP expression depending on the mutation(s) introduced and the DNA concentration (Fig. 6.1D, E). In some cases a given mutation was associated with no GFP expression (-9A), while in other cases making multiple point mutations resulted in very little change with respect to the wild type (-17CTT). All extension primer sequences including the T7 promoter variants are given in Table 6.1.

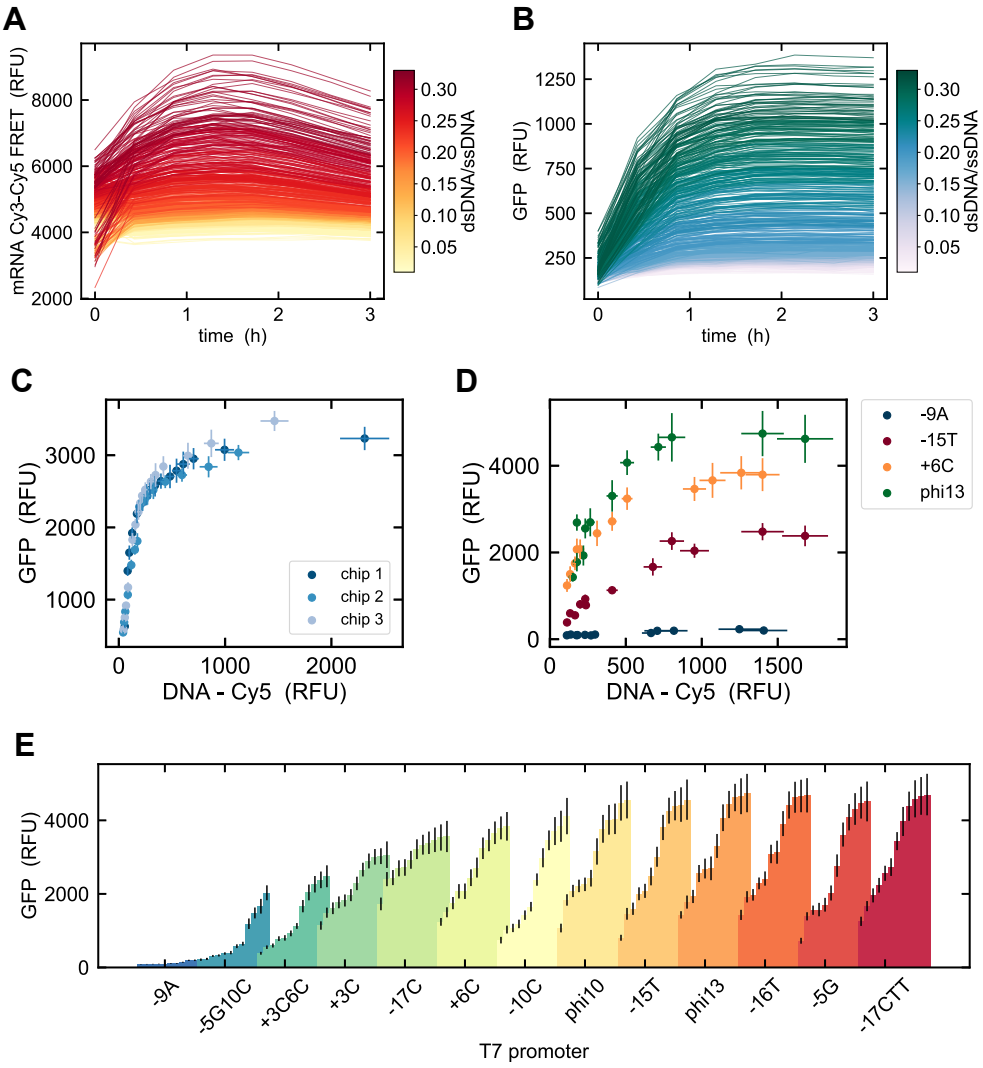

Figure 6.1: **On-chip TX-TL with PURE. (A)** mRNA expression over time in all unit cells using fluorescently tagged single stranded DNA oligos that emit a Cy3-Cy5 FRET signal when bound to the 3' region of an mRNA molecule. **(B)** GFP expression versus time in all unit cells. In both **(A)** and **(B)** the color bar shows the ratio of dsDNA template to ssDNA spotted. **(C)** End-point GFP measurements versus the fluorescence signal of dsDNA template attached to the surface for three separate chips. All values represent the mean ± SD ($n = 48$). **(D)** End-point GFP measurements versus DNA template signal for four different T7 promoter variants. **(E)** The GFP signal measured after 3 hours for 13 different T7 promoter variants and each at 12 different DNA template concentrations. The dsDNA to ssDNA ratio ranged from 1/90 to 1/3. For **(D)** and **(E)** all values represent the mean ± SD ($n = 4$).

Table 6.1: T7 promoter extension primers.

name	sequence
-9A	gatcttaaggctagagtacaaat**taatacgaatcactatagggaga**acaatacgacctctagaaataattttgtttaac
-5G	gatcttaaggctagagtacaaat**taatacgactcagtatagggaga**acaatacgacctctagaaataattttgtttaac
-10C	gatcttaaggctagagtacaaat**taatacgcctcactatagggaga**acaatacgacctctagaaataattttgtttaac
-5G10C	gatcttaaggctagagtacaaat**taatacgcctcagtatagggaga**acaatacgacctctagaaataattttgtttaac
+3C	gatcttaaggctagagtacaaat**taatacgactcactataggcaga**acaatacgacctctagaaataattttgtttaac
+6C	gatcttaaggctagagtacaaat**taatacgactcactatagggagc**acaatacgacctctagaaataattttgtttaac
+3C6C	gatcttaaggctagagtacaaat**taatacgactcactataggcagc**acaatacgacctctagaaataattttgtttaac
-15T	gatcttaaggctagagtacaaat**tattacgactcactatagggaga**acaatacgacctctagaaataattttgtttaac
-16T	gatcttaaggctagagtacaaat**ttatacgactcactatagggaga**acaatacgacctctagaaataattttgtttaac
-17T	gatcttaaggctagagtacaaat**caatacgactcactatagggaga**acaatacgacctctagaaataattttgtttaac
-17CTT	gatcttaaggctagagtacaaat**cttacgactcactatagggaga**acaatacgacctctagaaataattttgtttaac
phi13	gatcttaaggctagagtacaaat**taatacgactcactatagggaga**acaatacgacctctagaaataattttgtttaac
phi10	gatcttaaggctagagtac**taatacgactcactatagggaga**ccacaacgctttccctctagaaataattttgtttaac

Table 6.1: The T7 promoter is shown in bold and any mutations are colored red. For all sequences based on the phi13 promoter, the upstream aaat region was conserved.

6.2 Notes on epoxy glass slide preparation and spotting

6.2.1 Protocol for cleaning glass slides

- Heat 600 mL of milliQ water plus 120 mL of 25% ammonia (AnalaR NORMAPUR, VWR) on a hot plate inside a chemical hood until the solution reaches 80 °C.
- Load up to 50 glass slides (cut edges, VWR) into a metallic slide holder.
- Add 150 mL of hydrogen peroxide to the solution, which will cause the solution to bubble. Then add the glass slides into the solution, causing the solution to bubble more intensely.
- Cover the solution and let the slides incubate for 30 minutes.
- Remove the glass slides and place them in a room temperature milliQ water bath to cool.
- Dry each glass slide with nitrogen and place them into another metallic holder inside a clean

glass container.

6.2.2 Epoxysilane deposition

- Rinse a glass container, graduated cylinders (500 mL and 10 mL), and a small glass funnel with acetone. Then allow them to dry inside an oven at 80 °C for a few minutes.
- Once the glassware has cooled to room temperature, add 891 mL of toluene plus 9 mL of 3-GPS ((3-glycidyloxypropyl)trimethoxy-silane, Sigma Aldrich) to the clean glass container. (The small glass funnel can be used for pouring the 3-GPS into the graduated cylinder.)
  - Depending on the batch of 3-GPS, the surface created for spotting DNA can be variable. For example the spots made with the same pin may spread onto larger areas, sometimes causing neighbouring spots to come in contact with one another. If this happens, adding less 3-GPS (6-7 mL) can ameliorate the situation.
- Incubate the glass slides in this solution for 20 minutes.
- Rinse each glass slide with toluene to remove any unbound 3-GPS and dry with nitrogen. Load each dry glass slide into another clean glass container.
- Heat the glass slides at 120 °C for 30 minutes.
  - If spotting DNA on the prepared slides results in unusually large spots, another possible solution is to heat the slides for an additional 1-2 hours at 120 °C. This seems to dry the slides and decrease the size of deposited spots. Furthermore, using less humidity while spotting or no humidity can also prevent the spots from spreading.
- Let the glass slides cool to room temperature and then store them under vacuum.

6.2.3 Spotting parameters

- Linear DNA templates (direct PCR products or purified) were mixed with a 4 % BSA solution (sterile filtered) in round-bottom microwell plates (MMP384, Arrayit). If using these 384-well microarray plates, as little as 15 μL of DNA solution can be used per well for spotting.
- A QArray2 microarray robot (Genetix) was used to spot DNA with an MP3 pin (Arrayit) onto epoxy-coated glass slides. The parameters used are listed below:

- Humidity = 50-60%
- The stacker was not used for the Arrayit plates mentioned above.
- Max stamps per ink = 4
- Number of stamps per spot = 2 (Cyclic)
- Stamp time = 50 ms
- Inking time = 100 ms
- Print depth adjustment = 120 μm
- Wash between samples with water for 1000 ms.
- For the batch-mode cell-free TX-TL chip (Chapter 2) or MITOMI 768 use the following parameters for the spotting design:
  * 48 rows by 16 columns
  * row pitch = 373, column pitch = 746
  * Calculate the row and column pitch by measuring the distance in μm between spotting chambers in the original design on Autocad or similar software and multiply that distance by 0.98.
- For the steady state cell-free TX-TL chip (Chapter 3) use the following parameters for the spotting design:
  * 39 rows by 8 columns (every 8th spot along a given row should be left blank)
  * row pitch = 392, column pitch = 1666

6.3 Lysate preparation protocol

The following protocol has been adapted from the methods published by Sun *et al.* [164] and Kwon *et al.* [196]. If the cell-free reaction is carried out with the energy solution prepared according to Sun *et al.*, then any type of medium can be used to culture the cells. However cell-free reactions can also be implemented with a more minimal energy solution as presented by Cai *et al.* [255], in which case 2xYTP or 2xYTPG medium must be used (Fig. 6.2A). Although for many cell strains tested the more simplified Kwon *et al.* protocol has yielded functional lysates, it is important to note that the protocol may lead to variable results depending on the cell strain. An overview of the

different strains that were used to produce lysate and which protocols were tested to be functional is given in Table 6.2.

Table 6.2: *E. coli* strains tested.

	no RO rxn.	RO rxn.	buffer exchange	dialysis	energy soln.
BL21 (DE3)	not tested	functional	not tested	not tested	Sun et al. and Cai et al.
BL21 Rosetta2	not tested	functional	not tested	not tested	Sun et al.
Top10	not tested	functional	not tested	not tested	Sun et al.
JS006	not functional	not functional	not functional	functional	Sun et al.
MC4100	not functional	functional	functional	functional	Sun et al.

Day 1

- Prepare 1 L medium
  - LB - 10 g Tryptone, 10 g NaCl, 5 g Yeast extract per 1 L H2O
  - 2xYTP - 10 g Tryptone, 5 g Yeast extract, 5 g NaCl, 80 mL of 1M potassium phosphate dibasic (for a final concentration of 40 mM), 44 mL of 1 M potassium phosphate monobasic (for a final concentration of 22 mM)
  - 2xYTPG - prepare 2xYTP medium and a glucose solution (18 glucose per 250 mL H2O). Autoclave separately and combine 375 mL 2xYTP + 125 mL glucose solution.
- Prepare wash buffer A or B
  - buffer A - 10 mM Tris, 14 mM magnesium glutamate, 60 mM potassium glutamate
  - buffer B - 50 mM Tris, 14 mM magnesium glutamate, 60 mM potassium glutamate, titrate with acetic acid to reach pH $\sim$ 7.7
- If preparing wash buffer B, prepare dialysis buffer - 5 mM Tris, 14 mM magnesium glutamate, 60 mM potassium glutamate, if necessary titrate with 2M Tris to reach pH $\sim$ 8.2
- Start overnight culture of 5 mL from glycerol stock of desired *E. coli* strain.

Day 2

- Prepare 4 x 200 mL cultures in 500 mL Erlenmeyer flasks with 200 mL medium + 1 mL of overnight culture and incubate at 37 °C with shaking > 200 rpm.
  - If using BL21(DE3) cells, T7 RNAP expression can be induced by adding 400 μL of 100mM IPTG after 2 hours of incubation.
  - If using Top10 cells transformed with pBAD-gamS encoding plasmid [96] (Addgene #45833) then induce the expression of gamS by adding 5 mL of 10% arabinose.
- Culture cells for approximately 4 hours or until OD 600 is greater than 1.5. Depending on the *E. coli* strain the OD may be as high as 3-4, however the OD did not seem to be a significant indicator of lysate functionality.
- Weigh four 50 mL falcon tubes.
- Divide each 200 mL culture into 4 x 50 mL aliquots in falcon tubes and spin at 4 °C for 20 minutes at 4000 rpm.
- Resuspend pellets in 10 mL of wash buffer by pippetting and vortexing. Combine the cell suspension from each culture into one pre-weighed falcon tube. Spin at 4 °C for 10 minutes at 4000 rpm. Repeat two more times for a total of three washes.
- Remove all liquid from the cell pellet after the final wash. Empty updside down on a paper towel for a few minutes to allow excess liquid to drain out.
- Weigh the falcon tubes to calculate the weight of each cell pellet before freezing each tube in liquid nitrogen. Store the tubes at -80 °C. Pellets can be stored at -80 °C for several weeks before continuing with day 3 of the protocol.

Day 3

- Prepare 3 - 5 mL wash buffer with fresh DTT (final concentration of 2 mM)
- Add 1 mL wash buffer per gram of cell pellet and resuspend by vortexing. Transfer the solution to a 2 mL eppendorf tube for sonication. Place the tube in an ice water bath and sonicate the cells with an amplitute of 50% with 10 s pulses followed by 10 s wait periods for

approximately 1.5 minutes. Stop the sonication when the total energy input has reached ∼ 400 J for a total cell suspension volume of ∼1-1.5 mL.

  - Note: Ensure that the sonicator tip is submerged in the cell solution without touching the bottom or side of the test tube. The solution should change from an opaque cream color to a more transparent darker brown color after lysis.

- Spin the lysate solution at 4 °C for 10 minutes at 12000 x g. Afterwards the pellet should have two distinct layers. Remove the supernatent and place it in a clean eppendorf tube.
- Perform the run-off reaction by placing the tubes in a 37 °C incubator with shaking for 60-80 minutes.
- Spin the tubes again at 4 °C for 10 minutes at 12000 x g.
- If wash buffer A was used, remove the supernatent and skip to the last step.
- If wash buffer B was used, remove the supernatent and either perform a buffer exchange or dialysis.
  - Buffer exchange: Add up to 500 μL of supernatent to an Amicon Ultra 0.5 mL centrifugal filter with a 3 kDa molecular weight cutoff (Merck Millipore). Spin at 4 °C for approximately 45 minutes at 12000 x g until the volume goes to around 100-150 μL. Remove the buffer from the collection tube. Add dialysis buffer (plus fresh DTT to a final concentration of 2 mM) up to 500 μL. Repeat the spin and resuspension in dialysis buffer two times. After the last spin add dialysis buffer to reach a total volume of 500 μL again and flip the filter unit upside down in a clean collection tube and spin at 1000 x g to collect the buffer-exchanged lysate.
  - Dialysis: Add the supernatent to Slide-A-Lyzer MINI dialysis units (Thermo Scientific) and place them in a beaker with dialysis buffer (plus fresh DTT to a final concentration of 2 mM) and a stir bar. Use a low speed setting on the stir plate and dialyze for 3 hours at 4 °C. Collect the lysate from the bottom corner of the dialysis unit and transfer to an eppendorf tube. Spin the lysate at 4 °C for 10 minutes at 12000 x g. There is a small white pellet after spinning. Remove the supernatent.

- Aliquot the lysate into 25-50 μL volumes and flash freeze in liquid nitrogen. Store the aliquots at -80 °C.

Cell-free TX-TL reactions

Cell free TX-TL reactions consist of 25% lysate, 25% 4x energy solution, 25% wash buffer A (plus fresh DTT to a final concentration of 2 mM), DNA template and H2O. If the DNA template is linear then 3.5 μM of gamS protein [96] or 2.5 μM of chi decoy DNA [97] should also be added to the reaction to prevent the degradation of the linear DNA templates. Alternatively lysate can be made from Top10 cells transformed with the pBAD-gamS plasmid and induced for gamS expression. This lysate can then be used in conjunction with BL21 (DE3) lysate rather than adding purified gamS (Fig. 6.2B). In addition, an example of the importance of performing the run-off reaction followed by a buffer exchange or dialysis for two different *E. coli* strains is shown in Figure 6.2C, indicating the difference in expression profiles for varying strains and preparations.

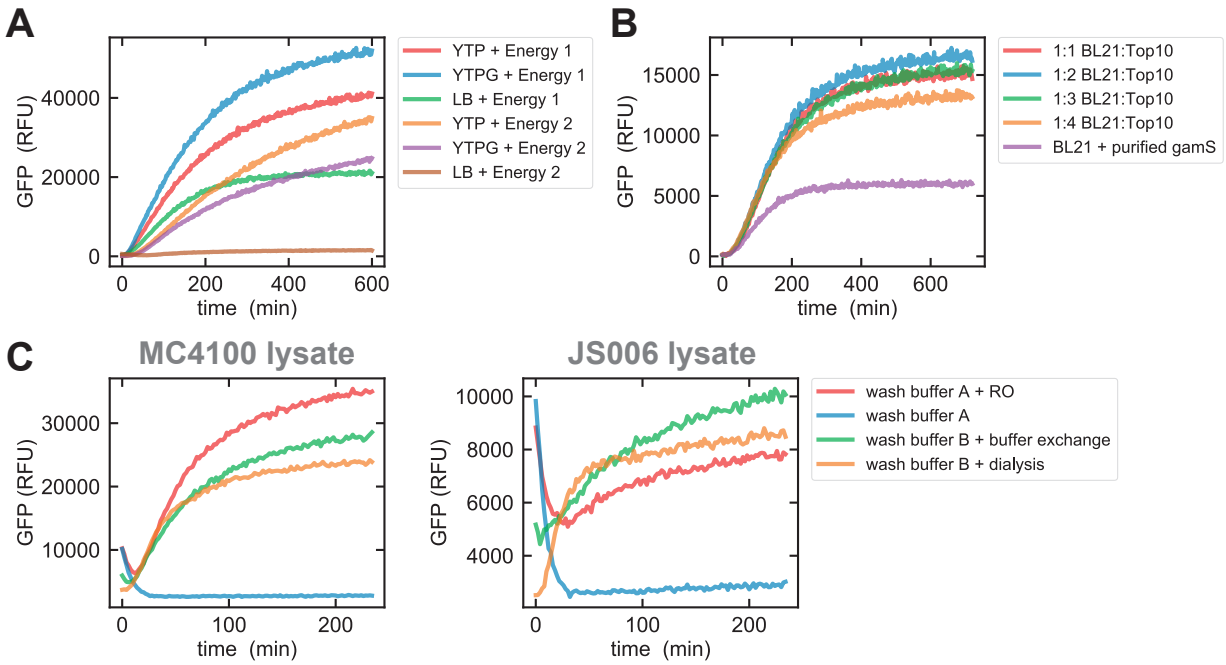

Figure 6.2: **Examples of different lysate TX-TL reactions.**

Caption on the next page.

Figure 6.2: **(A)** TX-TL reactions implemented with either the Sun *et al.* (1) or Cai *et al.* (2) energy solution with BL21 (DE3) lysates produced by growing cells with either YTP, YTPG or LB medium. **(B)** Combination of BL21 (DE3) and Top10 gamS lysates at different ratios compared with a reaction containing only BL21 (DE3) lysate and purified gamS protein. **(C)** TX-TL reactions using lysates prepared from two strains of *E. coli*: MC4100 and JS006 in four different ways: 1) with wash buffer A and a run-off reaction, 2) with wash buffer A and no run-off reaction, 3) with wash buffer B and a buffer exchange with Amicon filters, and 4) with wash buffer B and dialysis. All reactions were performed on a platereader with 10 μL total reaction volumes with 5 nM of a pTetO-sfGFP linear DNA template.

6.4 Supplementary tables

Table 6.3: Quantitative measures of cooperative interactions.

Design: PDZ	Sensitivity	Hill coefficient
BCB+ADD cooperative	0.592±0.007	1.3±0.2
BCB+ADD non-cooperative	0.312±0.003	1.0±0.2
BCB	0.165±0.001	1.1±0.4
ADD	0.183±0.001	1.1±0.4

Design: LZ	Sensitivity	Hill coefficient
BCB+ADD cooperative	0.627±0.009	1.3±0.2
BCB+ADD non-cooperative	0.422±0.002	1.1±0.3
BCB	0.166±0.001	1.2±0.4
ADD	0.182±0.001	1.3±0.5

Table 6.4: Inference of parameter values.

Dose response fits

Parameters: PDZ	Value	Units
A	$+5.76e+03^{+8.02e+02}_{-7.19e+02}$	RFU
C_0	$+6.62e-01^{+2.28e-01}_{-1.99e-01}$	
K_1	$+1.66e-01^{+7.12e-02}_{-5.09e-02}$	
K_2	$+8.24e-03^{+4.67e-03}_{-3.01e-03}$	
ε_{r1p}	$+1.43e+00^{+1.81e-01}_{-1.78e-01}$	k_BT
ε_{r2p}	$+1.32e+00^{+1.88e-01}_{-1.57e-01}$	k_BT
ε_{r12}	$-3.46e+00^{+4.36e-01}_{-4.66e-01}$	k_BT

Parameters: LZ	Value	Units
A	$+6.26e+03^{+7.54e+02}_{-6.95e+02}$	RFU
C_0	$+8.84e-01^{+2.18e-01}_{-1.95e-01}$	
K_1	$+6.86e-02^{+2.50e-02}_{-2.02e-02}$	
K_2	$+4.27e-02^{+1.92e-02}_{-1.45e-02}$	
ε_{r1p}	$+1.28e+00^{+1.86e-01}_{-1.74e-01}$	k_BT
ε_{r2p}	$+1.19e+00^{+1.77e-01}_{-1.54e-01}$	k_BT
ε_{r12}	$-3.05e+00^{+3.92e-01}_{-3.99e-01}$	k_BT

Parameters: AA-LZ	Value	Units
A	$+5.13e+03^{+8.87e+02}_{-8.27e+02}$	RFU
C_0	$+5.70e-01^{+2.77e-01}_{-2.48e-01}$	
K	$+8.42e-01^{+4.79e-01}_{-3.16e-01}$	
ε_{rp}	$+1.44e+00^{+1.98e-01}_{-1.35e-01}$	k_BT
ε_{r12}	$-9.48e+00^{+7.85e-01}_{-8.39e-01}$	k_BT

Parameters: Helical	Value	Units
$\ln(\lambda)$	$-3.41e+03^{+1.18e-01}_{-1.16e-01}$	
ϕ	$-1.92e+00^{+1.21e-01}_{-1.14e-01}$	
$\ln(R_0)$	$-2.24e+00^{+1.78e-01}_{-1.72e-01}$	

Binding site tuning fits

Parameters: AAA	Value	Units
C_0	$+1.55e-02^{+1.93e-03}_{-1.57e-03}$	
R	$+4.94e+02^{+5.04e+01}_{-5.09e+01}$	nM
ε_{rp}	$+1.13e+01^{+2.92e+00}_{-1.94e+00}$	k_BT

Parameters: BCB	Value	Units
C_0	$+1.35e-02^{+1.62e-03}_{-1.33e-03}$	
R	$+4.93e+02^{+5.03e+01}_{-5.05e+01}$	nM
ε_{rp}	$+1.20e+01^{+2.78e+00}_{-1.85e+00}$	k_BT

Parameters: AA-LZ	Value	Units
C_0	$+2.82e-03^{+1.64e-03}_{-1.15e-03}$	
R	$+9.78e+01^{+1.00e+01}_{-1.01e+01}$	nM
ε_{rp}	$+1.12e+01^{+7.33e-01}_{-6.70e-01}$	k_BT
ε_{r12}	$-4.12e+00^{+4.72e-01}_{-5.37e-01}$	k_BT

Parameters: BCB/ADD	Value	Units
C_0	$+1.64e-02^{+2.38e-02}_{-1.10e-02}$	
R_1	$+9.08e+01^{+9.06e+00}_{-8.80e+00}$	nM
R_2	$+5.00e+01^{+4.81e+00}_{-5.09e+00}$	nM
ε_{r1p}	$+1.04e+01^{+9.03e-01}_{-8.68e-01}$	k_BT
ε_{r2p}	$+1.06e+00^{+9.13e-01}_{-7.10e-01}$	k_BT
ε_{r12}	$-1.45e+00^{+5.34e-01}_{-5.94e-01}$	k_BT

Table 6.4: The posterior probability distribution of each parameter was quantified by reporting the value for the 50th percentile (large numbers) as well as uncertainty bounds given by the 16th and 84th percentiles (small numbers).

Table 6.5: ZF expression templates.

P_R-ZF	Cy5gacatggtgaagactatcgcaccatcagccagaaaaccgaattttgctgggtgggctaacgatatc cgcctgatgcgtgaacgtgacggacgtaaccaccgcgacatgtgtgtgctgttccgctgggcatgctgagc taacaccgtgcgtgttgacaattttacctctggcggtgataatggttgcagctagcaataattttgtttaac tttaagaaggagatataccATG----ZF----TAAtaagaatcaggggataacgcaggaaaga- BIOT
P_R-ZF + cognate ligand (VKESLV)	Cy5gacatggtgaagactatcgcaccatcagccagaaaaccgaattttgctgggtgggctaacgatatc cgcctgatgcgtgaacgtgacggacgtaaccaccgcgacatgtgtgtgctgttccgctgggcatgctgagc taacaccgtgcgtgttgacaattttacctctggcggtgataatggttgcagctagcaataattttgtttaac tttaagaaggagatataccATG----ZF---- GGCAGCGGCAGCGTGAAAGAAAGCCTGGTGTAATAAgaatcaggggataac gcaggaaaga-BIOT
P_R-ZF + non-cognate ligand (VKEAAA)	Cy5gacatggtgaagactatcgcaccatcagccagaaaaccgaattttgctgggtgggctaacgatatc cgcctgatgcgtgaacgtgacggacgtaaccaccgcgacatgtgtgtgctgttccgctgggcatgctgagc taacaccgtgcgtgttgacaattttacctctggcggtgataatggttgcagctagcaataattttgtttaac tttaagaaggagatataccATG----ZF---- GGCAGCGGCAGCGTGAAAGAAGCGGCGGCGTAATAAgaatcaggggataac gcaggaaaga-BIOT
P_R-ZF-PDZ	Cy5gacatggtgaagactatcgcaccatcagccagaaaaccgaattttgctgggtgggctaacgatatc cgcctgatgcgtgaacgtgacggacgtaaccaccgcgacatgtgtgtgctgttccgctgggcatgctgagc taacaccgtgcgtgttgacaattttacctctggcggtgataatggttgcagctagcaataattttgtttaac tttaagaaggagatataccATG----ZF---- AAAGACGGTGGCGGCGGTTCTCCAGCGCCAGCGCCACCGGAAGCGC TGCAGCGCCGCCGCGTGACCGTGCGCAAAGCGGATGCGGGCGGCCT GGGCATTAGCATTAAAGGCGGCCGCGAAAACAAAATGCCGATTCTGA TTAGCAAAATTTTTAAAGGCCTGGCGGCGGATCAGACCGAAGCGCTG TTTGTGGGCGATGCGATTCTGAGCGTGAACGGCGAAGATCTGAGCAG CGCGACCCATGATGAAGCGGTGCAGGCGCTGAAAAAAACCGGCAAA GAAGTGGTGCTGGAAGTGAAATATATGAAAGAATAAgcttgatatcgaattcct gcagcccgggggatcccatggtacgcgtgctagaggcatcaaataaaacgaaaggctcagtcgaaaga ctgggcctttcgttttatctgttgtttgtcggtgaacgctctcctgagtaggacaaatccgccgccctagacc taggcgttcggctgcggcgagcggtatcagctcactcaaaggcggtaatacggttatc-BIOT
P_R-ZF-GCN4	Cy5gacatggtgaagactatcgcaccatcagccagaaaaccgaattttgctgggtgggctaacgatatc cgcctgatgcgtgaacgtgacggacgtaaccaccgcgacatgtgtgtgctgttccgctgggcatgctgagc taacaccgtgcgtgttgacaattttacctctggcggtgataatggttgcagctagcaataattttgtttaac tttaagaaggagatataccATG----ZF---- AAAGACGGTGGCGGCGGTTCTCCAGCGCCAGCGCCACCGCATCGCG ATATTCAGCATATTCTGCCGATTCTGGAAGATAAAGTGGAAGAACTGC TGAGCAAAAACTATCATCTGGAAAACGAAGTGGCGCGCCTGAAAAAA CTGGTGGGCGAACGCTAATAAgcgaatcaggggataacgcaggaaaga-BIOT
P_R-ZF-GCN4mut (L67A-L68A-L74A-L81A)	Cy5gacatggtgaagactatcgcaccatcagccagaaaaccgaattttgctgggtgggctaacgatatc cgcctgatgcgtgaacgtgacggacgtaaccaccgcgacatgtgtgtgctgttccgctgggcatgctgagc taacaccgtgcgtgttgacaattttacctctggcggtgataatggttgcagctagcaataattttgtttaac tttaagaaggagatataccATG----ZF---- AAAGACGGTGGCGGCGGTTCTCCAGCGCCAGCGCCACCGCATCGCG ATATTCAGCATATTCTGCCGATTCTGGAAGATAAAGTGGAAGAAGCGG CGAGCAAAAACTATCATGCGGAAAACGAAGTGGCGCGCGCGAAAAAA CTGGTGGGCGAACGCTAATAAgcgaatcaggggataacgcaggaaaga-BIOT

Table 6.5: 3-finger ZFs were expressed from lambda PR promoters (blue, underlined) with conserved 5'UTR (grey, underlined), and could be modified to contain interaction domains and ligands (red).

Table 6.6: Three-finger ZF coding sequences.

ZF_{AAA}	ATGGAACGTCCGTACGCTTGCCCGGTTGAATCTTGCGACCGTCGTTTCTC TCGTTCTGACGAACTGACCCGTCATATTAGAATTCATACTGGACAAAAACC ATTCCAATGTAGAATTTGTATGAGAAATTTCTCTCGTTCTGACCACCTGAC CACCCACATCCGTACCCACACCGGTGAAAAACCGTTCGCTTGCGACATCT GCGGTCGTAAATTCGCTCGTTCTGACGAACGTAAACGTCACACCAAAATC CACCTGCGTCAGTAA
ZF_{BBB}	ATGGAACGTCCGTACGCTTGCCCGGTTGAATCTTGCGACCGTCGTTTCTC TCGTAACTTCATCCTGCAGCGTCATATTAGAATTCATACTGGACAAAAACC ATTCCAATGTAGAATTTGTATGAGAAATTTCTCTGACCGTGCTAACCTGCG TCGTCACATCCGTACCCACACCGGTGAAAAACCGTTCGCTTGCGACATCT GCGGTCGTAAATTCGCTGTCACGACCAGCTGACCCGTCACACCAAAATCC ACCTGCGTCAGTAA
ZF_{CCC}	ATGGAACGTCCGTACGCTTGCCCGGTTGAATCTTGCGACCGTCGTTTCTC TGACTCTCCGACCCTGCGTCGTCATATTAGAATTCATACTGGACAAAAACC ATTCCAATGTAGAATTTGTATGAGAAATTTCTCTCAGCGTTCTTCTCTGGT TCGTCACATCCGTACCCACACCGGTGAAAAACCGTTCGCTTGCGACATCT GCGGTCGTAAATTCGCTGAACGTGGTAACCTGACCCGTCACACCAAAATC CACCTGCGTCAGTAA
ZF_{DDD}	ATGGAACGTCCGTACGCTTGCCCGGTTGAATCTTGCGACCGTCGTTTCTC TGACAAAACCAAACTGCGTGTTCATATTAGAATTCATACTGGACAAAAACC ATTCCAATGTAGAATTTGTATGAGAAATTTCTCTGTTCGTCACAACCTGAC CCGTCACATCCGTACCCACACCGGTGAAAAACCGTTCGCTTGCGACATCT GCGGTCGTAAATTCGCTCAGTCTACCTCTCTGCAGCGTCACACCAAAATC CACCTGCGTCAGTAA
Example ZF_{ADD}	ATGGAACGTCCGTACGCTTGCCCGGTTGAATCTTGCGACCGTCGTTTCTC TGACAAAACCAAACTGCGTGTTCATATTAGAATTCATACTGGACAAAAACC ATTCCAATGTAGAATTTGTATGAGAAATTTCTCTGTTCGTCACAACCTGAC CCGTCACATCCGTACCCACACCGGTGAAAAACCGTTCGCTTGCGACATCT GCGGTCGTAAATTCGCTCGTTCTGACGAACGTAAACGTCACACCAAAATC CACCTGCGTCAGTAA

Table 6.6: Variable recognition helices for each finger (1-3) are highlighted. ZFs bind in the 3'-5' direction by convention, and thus to construct, for example, ZF_{ADD} the fingers must be arranged in reverse order F1(D)-F2(D)-F3(A).

Table 6.7: Two-finger ZF coding sequence.

ZF_{AA}	ATGAAACCGTTTCAGTGCCGCATTTGCATGCGCAACTTTAGCCGCAGCGAT CATCTGACCACCCATATTCGCACCCATACCGGCGAAAAACCGTTTGCGTGC GATATTTGCGGCCGCAAATTCGCCCGCAGCGATGAACGCAAACGC

Table 6.8: Reporter and target promoter design.

P_{PR} - deGFP	Cy3ccagccagaaaacgacctttctgtggtgaaaccggatgctgcaattcagagcggcagcaagtggggg acagcagaagacctgaccgccgcagagtggatgtttgacatggtgaagactatcgcaccatcagccagaaa accgaattttgctgggtgggctaacgatatccgcctgatgcgtgaacgtgacggacgtaaccaccgcgacat gtgtgtgctgttccgctgggcatgctgagctaacaccgtgcgtgttgacaattttacctctggcggtgataatg gttgcagctagcaataattttgtttaactttaagaaggagatataccATGGAGCTTTTCACTGG CGTTGTTCCCATCCTGGTCGAGCTGGACGGCGACGTAAACGGCCACAA GTTCAGCGTGTCCGGCGAGGGCGAGGGCGATGCCACCTACGGCAAGCT GACCCTGAAGTTCATCTGCACCACCGGCAAGCTGCCCGTGCCCTGGCC CACCCTCGTGACCACCCTGACCTACGGCGTGCAGTGCTTCAGCCGCTA CCCCGACCACATGAAGCAGCACGACTTCTTCAAGTCCGCCATGCCCGA AGGCTACGTCCAGGAGCGCACCATCTTCTTCAAGGACGACGGCAACTA CAAGACCCGCGCCGAGGTGAAGTTCGAGGGCGACACCCTGGTGAACCG CATCGAGCTGAAGGGCATCGACTTCAAGGAGGACGGCAACATCCTGGG GCACAAGCTGGAGTACAACTACAACAGCCACAACGTCTATATCATGGCC GACAAGCAGAAGAACGGCATCAAGGTGAACTTCAAGATCCGCCACAAC ATCGAGGACGGCAGCGTGCAGCTCGCCGACCACTACCAGCAGAACACC CCCATCGGCGACGGCCCCGTGCTGCTGCCCGACAACCACTACCTGAGC ACCCAGTCCGCCCTGAGCAAAGACCCCAACGAGAAGCGCGATCACATG GTCCTGCTGGAGTTCGTGACCGCCGCCGGGATCTAAactcgagcaaagcccgccg aaaggcgggcttttctgtgtcgaccgatgcccttgagagccttcaacccagtcagctccttccggtgggcgcgg ggcatgactatcgtcgccgcacttatgactgtcttctttatcatgcaactcgtaggacaggtgccggcagcgct cttccgcttcctcgctcactgactcgctgcgctcggtcgttcggctgcggcgagcggtatcagctcactcaaagg cggtaatacggttatccacagaatcaggggataacgcaggaaaga-BIOT
P_{ZF} - single site	Cy3ccagccagaaaacgacctttctgtggtgaaaccggatgctgcaattcagagcggcagcaagtggggg acagcagaagacctgaccgccgcagagtggatgtttgacatggtgaagactatcgcaccatcagccagaaa accgaattttgctgggtgggctaacgatatccgcctgatgcgtgaacgtgacggacgtaaccaccgcgacat gtgtgtgctgttccgctgggcatgctgagctaacaccgtgcgtgttgacaXNNNNNNNNNNXggcgg tgataat
P_{ZF} - two sites	Cy3ccagccagaaaacgacctttctgtggtgaaaccggatgctgcaattcagagcggcagcaagtggggg acagcagaagacctgaccgccgcagagtggatgtttgacatggtgaagactatcgcaccatcagccagaaa accgaattttgctgggtgggctaacgatatccgcctgatgcgtgaacgtgacggacgtaaccaccgcgacat gtgtgtgctgttccgctgggcatgctgagctaacXNNNNNNNNNNXttgacaXNNNNNNNNN NXggcggtgataat
P_{ZF} - cooperative	Cy3ccagccagaaaacgacctttctgtggtgaaaccggatgctgcaattcagagcggcagcaagtggggg acagcagaagacctgaccgccgcagagtggatgtttgacatggtgaagactatcgcaccatcagccagaaa accgaattttgctgggtgggctaacgatatccgcctgatgcgtgaacgtgacggacgtaaccaccgcgacat gtgtgtgctgttccgctgggcatgctgagctaacXNNNNNNNNNttgacaXNNNNNNNNN Xggcggtgataat
P_{ZF} - AA	Cy3ccagccagaaaacgacctttctgtggtgaaaccggatgctgcaattcagagcggcagcaagtggggg acagcagaagacctgaccgccgcagagtggatgtttgacatggtgaagactatcgcaccatcagccagaaa accgaattttgctgggtgggctaacgatatccgcctgatgcgtgaacgtgacggacgtaaccaccgcgacat gtgtgtgctgttccgctgggcatgctgagctaacaccgtgcgtgttgacaCGCCCACGCGTGGGC GTgataat

Table 6.8: deGFP was used as a reporter. The upstream regulatory region consisted of variations of the original lambda PR promoter containing 9-bp ZF binding sites (N) and their flanking bases (X).

Table 6.9: Three-finger ZF target sequences.

ZF	target
AAA	5' - tGCGTGGGCGt - 3'
ACA	5' - aGCGGTAGCGt - 3'
ADB	5' - aGCGGATGTGt - 3'
ADD	5' - aGCGGATGGAg - 3'
BAB	5' - tGAGTGGGTGt - 3'
BBB	5' - tGAGGACGTGt - 3'
BCB	5' - tGAGGTAGTGt - 3'
BCC	5' - tGAGGTAGCCt - 3'
BCD	5' - tGAGGTAGGAg - 3'
BDC	5' - tGAGGATGCCt - 3'
BDD	5' - tGAGGATGGAg - 3'
CBD	5' - aGATGACGGAg - 3'

Table 6.9: Each ZF binds a 9bp target; for each target we conserve single flanking bases on either side where possible.

Table 6.10: MITOMI PWM targets.

ZF	target
AAA	5'-GGCCAAAATGCGTGGGCGTGCGTTTCCGGCGGTATGAC-3'
ADD	5'-GGCCAAAAAGCGGATGGAGGCGTTTCCGGCGGTATGAC-3'
BCB	5'-GGCCAAAATGAGGTAGTGTGCGTTTCCGGCGGTATGAC-3'
AA	5'- GGCCAAATCCCACGCGTGGGAGTTTCCGGCGGTATGAC -3'

Table 6.10: The bases which were mutated are colored red and the underlined bases represent the core binding sequence.

Table 6.11: ZF plasmids.

ZF	Addgene #
AAA	127465
ACA	127466
ADB	127467
ADD	127468
BAB	127469
BBB	127470
BCB	127471
BCC	127484
BCD	127472
BDC	127473
BDD	127474
ADD-L	127477
BCB-PDZ	127478
ADD-GCN	127475
BCB-GCN	127476
AA-GCN	127479

Table 6.11: The following ZF coding sequences were cloned into a pET21a vector and are available on Addgene.

Bibliography

[1] A. S. Khalil and J. J. Collins, "Synthetic biology: applications come of age," *Nature Reviews Genetics*, vol. 11, no. 5, pp. 367–379, 2010.

[2] C. J. Bashor and J. J. Collins, "Understanding Biological Regulation Through Synthetic Biology," *Annual Review of Biophysics*, vol. 47, no. 1, 2018.

[3] J. Monod and F. Jacob, "Teleonomic mechanisms in cellular metabolism, growth, and differentiation," *Cold Spring Harbor Symposia on Quantitative Biology*, vol. 26, pp. 389–401, 1961.

[4] F. Jacob and J. Monod, "On the Regulation of Gene Activity," *Cold Spring Harbor Symposia on Quantitative Biology*, vol. 26, pp. 193–211, Jan. 1961.

[5] D. A. Jackson, R. H. Symons, and P. Berg, "Biochemical Method for Inserting New Genetic Information into DNA of Simian Virus 40: Circular SV40 DNA Molecules Containing Lambda Phage Genes and the Galactose Operon of Escherichia coli," *Proceedings of the National Academy of Sciences of the United States of America*, vol. 69, pp. 2904–2909, Oct. 1972.

[6] R. K. Saiki, S. Scharf, F. Faloona, K. B. Mullis, G. T. Horn, H. A. Erlich, and N. Arnheim, "Enzymatic amplification of beta-globin genomic sequences and restriction site analysis for diagnosis of sickle cell anemia," *Science*, vol. 230, pp. 1350–1354, Dec. 1985.

[7] R. K. Saiki, D. H. Gelfand, S. Stoffel, S. J. Scharf, R. Higuchi, G. T. Horn, K. B. Mullis, and H. A. Erlich, "Primer-directed enzymatic amplification of DNA with a thermostable DNA polymerase," *Science (New York, N.Y.)*, vol. 239, pp. 487–491, Jan. 1988.

[8] F. Sanger, G. M. Air, B. G. Barrell, N. L. Brown, A. R. Coulson, J. C. Fiddes, C. A. Hutchison, P. M. Slocombe, and M. Smith, "Nucleotide sequence of bacteriophage X174 DNA," *Nature*, vol. 265, pp. 687–695, Feb. 1977.

[9] J. C. Venter, S. Levy, T. Stockwell, K. Remington, and A. Halpern, "Massive parallelism, randomness and genomic advances," *Nature Genetics*, vol. 33, pp. 219–227, Mar. 2003.

[10] F. R. Blattner, G. Plunkett, C. A. Bloch, N. T. Perna, V. Burland, M. Riley, J. Collado-Vides, J. D. Glasner, C. K. Rode, G. F. Mayhew, J. Gregor, N. W. Davis, H. A. Kirkpatrick, M. A. Goeden, D. J. Rose, B. Mau, and Y. Shao, "The complete genome sequence of Escherichia coli K-12," *Science (New York, N.Y.)*, vol. 277, pp. 1453–1462, Sept. 1997.

[11] A. Goffeau, B. G. Barrell, H. Bussey, R. W. Davis, B. Dujon, H. Feldmann, F. Galibert, J. D. Hoheisel, C. Jacq, M. Johnston, E. J. Louis, H. W. Mewes, Y. Murakami, P. Philippsen, H. Tettelin, and S. G. Oliver, "Life with 6000 genes," *Science (New York, N.Y.)*, vol. 274, pp. 546, 563–567, Oct. 1996.

[12] J. L. DeRisi, V. R. Iyer, and P. O. Brown, "Exploring the Metabolic and Genetic Control of Gene Expression on a Genomic Scale," *Science*, vol. 278, pp. 680–686, Oct. 1997.

[13] V. E. Velculescu, L. Zhang, W. Zhou, J. Vogelstein, M. A. Basrai, D. E. Bassett, P. Hieter, B. Vogelstein, and K. W. Kinzler, "Characterization of the Yeast Transcriptome," *Cell*, vol. 88, pp. 243–251, Jan. 1997.

[14] E. A. Winzeler, D. D. Shoemaker, A. Astromoff, H. Liang, K. Anderson, B. Andre, R. Bangham, R. Benito, J. D. Boeke, H. Bussey, A. M. Chu, C. Connelly, K. Davis, F. Dietrich, S. W. Dow, M. E. Bakkoury, F. Foury, S. H. Friend, E. Gentalen, G. Giaever, J. H. Hegemann, T. Jones, M. Laub, H. Liao, N. Liebundguth, D. J. Lockhart, A. Lucau-Danila, M. Lussier, N. M'Rabet, P. Menard, M. Mittmann, C. Pai, C. Rebischung, J. L. Revuelta, L. Riles, C. J. Roberts, P. Ross-MacDonald, B. Scherens, M. Snyder, S. Sookhai-Mahadeo, R. K. Storms, S. Véronneau, M. Voet, G. Volckaert, T. R. Ward, R. Wysocki, G. S. Yen, K. Yu, K. Zimmermann, P. Philippsen, M. Johnston, and R. W. Davis, "Functional Characterization of the S. cerevisiae Genome by Gene Deletion and Parallel Analysis," *Science*, vol. 285, pp. 901–906, Aug. 1999.

[15] J. K. Joung, E. I. Ramm, and C. O. Pabo, "A bacterial two-hybrid selection system for studying protein–DNA and protein–protein interactions," *Proceedings of the National Academy of Sciences*, vol. 97, pp. 7382–7387, June 2000.

[16] K. H. Young, "Yeast Two-hybrid: So Many Interactions, (in) So Little Time...," *Biology of Reproduction*, vol. 58, pp. 302–311, Feb. 1998.

[17] G. MacBeath, "Protein microarrays and proteomics," *Nature Genetics*, vol. 32, pp. 526–532, Dec. 2002.

[18] G. Ramsay, "DNA chips: State-of-the art," *Nature Biotechnology*, vol. 16, pp. 40–44, Jan. 1998.

[19] D. S. Wilson and J. W. Szostak, "In Vitro Selection of Functional Nucleic Acids," *Annual Review of Biochemistry*, vol. 68, no. 1, pp. 611–647, 1999.

[20] D. E. Cameron, C. J. Bashor, and J. J. Collins, "A brief history of synthetic biology," *Nature Reviews Microbiology*, vol. 12, pp. 381–390, May 2014.

[21] L. H. Hartwell, J. J. Hopfield, S. Leibler, and A. W. Murray, "From molecular to modular cell biology," *Nature*, vol. 402, pp. C47–C52, Dec. 1999.

[22] D. Endy, "Foundations for engineering biology," *Nature*, vol. 438, pp. 449–453, Nov. 2005.

[23] E. Andrianantoandro, S. Basu, D. K. Karig, and R. Weiss, "Synthetic biology: new engineering rules for an emerging discipline," *Molecular Systems Biology*, vol. 2, p. 2006.0028, Jan. 2006.

[24] A. Arkin, "Setting the standard in synthetic biology," *Nature Biotechnology*, vol. 26, no. 7, pp. 771–774, 2008.

[25] B. Canton, A. Labno, and D. Endy, "Refinement and standardization of synthetic biological parts and devices," *Nature Biotechnology*, vol. 26, no. 7, pp. 787–793, 2008.

[26] R. Kwok, "Five hard truths for synthetic biology," *Nature*, vol. 463, pp. 288–290, Jan. 2010.

[27] T. S. Gardner, C. R. Cantor, and J. J. Collins, "Construction of a genetic toggle switch in Escherichia coli," *Nature*, vol. 403, no. 6767, pp. 339–342, 2000.

[28] M. B. Elowitz and S. Leibler, "A synthetic oscillatory network of transcriptional regulators," *Nature*, vol. 403, no. 6767, pp. 335–338, 2000.

[29] J. Hasty, D. McMillen, F. Isaacs, and J. J. Collins, "Computational studies of gene regulatory networks: in numero molecular biology," *Nature Reviews Genetics*, vol. 2, pp. 268–279, Apr. 2001.

[30] A. Becskei and L. Serrano, "Engineering stability in gene networks by autoregulation," *Nature*, vol. 405, pp. 590–593, June 2000.

[31] F. J. Isaacs, J. Hasty, C. R. Cantor, and J. J. Collins, "Prediction and measurement of an autoregulatory genetic module," *Proceedings of the National Academy of Sciences*, vol. 100, pp. 7714–7719, June 2003.

[32] C. C. Guet, M. B. Elowitz, W. Hsing, and S. Leibler, "Combinatorial Synthesis of Genetic Networks," *Science*, vol. 296, pp. 1466–1470, May 2002.

[33] E. M. Ozbudak, M. Thattai, I. Kurtser, A. D. Grossman, and A. v. Oudenaarden, "Regulation of noise in the expression of a single gene," *Nature Genetics*, vol. 31, pp. 69–73, May 2002.

[34] M. B. Elowitz, A. J. Levine, E. D. Siggia, and P. S. Swain, "Stochastic Gene Expression in a Single Cell," *Science*, vol. 297, pp. 1183–1186, Aug. 2002.

[35] C. A. Voigt, "Life from information," *Nature Methods*, vol. 5, pp. 27–28, Jan. 2008.

[36] C. Engler, R. Kandzia, and S. Marillonnet, "A one pot, one step, precision cloning method with high throughput capability," *PloS One*, vol. 3, no. 11, p. e3647, 2008.

[37] D. G. Gibson, L. Young, R.-Y. Chuang, J. C. Venter, C. A. Hutchison, and H. O. Smith, "Enzymatic assembly of DNA molecules up to several hundred kilobases," *Nature Methods*, vol. 6, pp. 343–345, May 2009.

[38] H. H. Wang, F. J. Isaacs, P. A. Carr, Z. Z. Sun, G. Xu, C. R. Forest, and G. M. Church, "Programming cells by multiplex genome engineering and accelerated evolution," *Nature*, vol. 460, pp. 894–898, Aug. 2009.

[39] A. E. Friedland, T. K. Lu, X. Wang, D. Shi, G. Church, and J. J. Collins, "Synthetic Gene Networks That Count," *Science*, vol. 324, pp. 1199–1202, May 2009.

[40] T. S. Moon, C. Lou, A. Tamsir, B. C. Stanton, and C. A. Voigt, "Genetic programs constructed from layered logic gates in single cells," *Nature*, vol. 491, pp. 249–253, Nov. 2012.

[41] P. E. M. Purnick and R. Weiss, "The second wave of synthetic biology: from modules to systems," *Nature Reviews Molecular Cell Biology*, vol. 10, pp. 410–422, June 2009.

[42] V. K. Mutalik, L. Qi, J. C. Guimaraes, J. B. Lucks, and A. P. Arkin, "Rationally designed families of orthogonal RNA regulators of translation," *Nature Chemical Biology*, vol. 8, pp. 447–454, May 2012.

[43] B. C. Stanton, A. A. K. Nielsen, A. Tamsir, K. Clancy, T. Peterson, and C. A. Voigt, "Genomic mining of prokaryotic repressors for orthogonal logic gates," *Nature Chemical Biology*, vol. 10, pp. 99–105, Feb. 2014.

[44] N. Hillson, M. Caddick, Y. Cai, J. A. Carrasco, M. W. Chang, N. C. Curach, D. J. Bell, R. L. Feuvre, D. C. Friedman, X. Fu, N. D. Gold, M. J. Herrgård, M. B. Holowko, J. R. Johnson, R. A. Johnson, J. D. Keasling, R. I. Kitney, A. Kondo, C. Liu, V. J. J. Martin, F. Menolascina, C. Ogino, N. J. Patron, M. Pavan, C. L. Poh, I. S. Pretorius, S. J. Rosser, N. S. Scrutton, M. Storch, H. Tekotte, E. Travnik, C. E. Vickers, W. S. Yew, Y. Yuan, H. Zhao, and P. S. Freemont, "Building a global alliance of biofoundries," *Nature Communications*, vol. 10, pp. 1–4, May 2019.

[45] P. A. Silver, J. C. Way, F. H. Arnold, and J. T. Meyerowitz, "Engineering explored," *Nature*, vol. 509, no. 7499, pp. 166–167, 2014.

[46] V. Hsiao, A. Swaminathan, and R. M. Murray, "Control Theory for Synthetic Biology: Recent Advances in System Characterization, Control Design, and Controller Implementation for Synthetic Biology," *IEEE Control Systems*, vol. 38, no. 3, pp. 32–62, 2018.

[47] M. Khammash, "An engineering viewpoint on biological robustness," *BMC Biology*, vol. 14, p. 22, dec 2016.

[48] D. D. Vecchio, A. J. Dy, and Y. Qian, "Control theory meets system biology," *Journal of the Royal Society Interfac*, vol. 13, p. 20160380, 2016.

[49] Y. Yokobayashi, R. Weiss, and F. H. Arnold, "Directed evolution of a genetic circuit," *Proceedings of the National Academy of Sciences of the United States of America*, vol. 99, pp. 16587–16591, Dec. 2002.

[50] M. J. Dougherty and F. H. Arnold, "Directed evolution: new parts and optimized function," *Current Opinion in Biotechnology*, vol. 20, pp. 486–491, Aug. 2009.

[51] J. J. Agresti, E. Antipov, A. R. Abate, K. Ahn, A. C. Rowat, J.-C. Baret, M. Marquez, A. M. Klibanov, A. D. Griffiths, and D. A. Weitz, "Ultrahigh-throughput screening in drop-based microfluidics for directed evolution," *PNAS*, vol. 107, pp. 4004–4009, Mar. 2010.

[52] A. Tinafar, K. Jaenes, and K. Pardee, "Synthetic Biology Goes Cell-Free," *BMC Biology*, vol. 17, p. 64, Aug. 2019.

[53] A. D. Silverman, A. S. Karim, and M. C. Jewett, "Cell-free gene expression: an expanded repertoire of applications," *Nature Reviews Genetics*, pp. 1–20, Nov. 2019.

[54] J. G. Perez, J. C. Stark, and M. C. Jewett, "Cell-Free Synthetic Biology: Engineering Beyond the Cell," *Cold Spring Harbor Perspectives in Biology*, vol. 8, p. a023853, Dec. 2016.

[55] Allen P. Liu, "The rise of bottom-up synthetic biology and cell-free biology," *Physical Biology*, 2019.

[56] P. Schwille, J. Spatz, K. Landfester, E. Bodenschatz, S. Herminghaus, V. Sourjik, T. Erb, P. Bastiaens, R. Lipowsky, A. Hyman, P. Dabrock, J.-C. Baret, T. Vidakovic-Koch, P. Bieling, R. Dimova, H. Mutschler, T. Robinson, D. Tang, S. Wegner, and K. Sundmacher, "MaxSynBio - Avenues towards creating cells from the bottom up," *Angewandte Chemie International Edition*, no. 10.1002/anie.201802288, 2018.

[57] F. Caschera and V. Noireaux, "Integration of biological parts toward the synthesis of a minimal cell," *Current opinion in chemical biology*, vol. 22, pp. 85–91, 2014.

[58] K. Göpfrich, I. Platzman, and J. P. Spatz, "Mastering Complexity: Towards Bottom-up Construction of Multifunctional Eukaryotic Synthetic Cells," *Trends in Biotechnology*, vol. 36, pp. 938–951, sep 2018.

[59] A. P. Liu and D. A. Fletcher, "Biology under construction: in vitro reconstitution of cellular function," *Nature Reviews Molecular Cell Biology*, vol. 10, pp. 644–650, sep 2009.

[60] K. A. Ganzinger and P. Schwille, "More from less – bottom-up reconstitution of cell biology," *J Cell Sci*, vol. 132, p. jcs227488, feb 2019.

[61] M. Elowitz and W. A. Lim, "Build life to understand it," *Nature*, vol. 468, pp. 889–890, 2010.

[62] D. Garenne and V. Noireaux, "Cell-free transcription–translation: engineering biology from the nanometer to the millimeter scale," *Current Opinion in Biotechnology*, vol. 58, pp. 19–27, 2019.

[63] M. R. Lamborg and P. C. Zamecnik, "Amino acid incorporation into protein by extracts of E. coli," *Biochimica et Biophysica Acta*, vol. 42, pp. 206–211, 1960.

[64] M. W. Nirenberg and J. H. Matthaei, "The dependence of cell-free protein synthesis in E. coli upon naturally occurring or synthetic polyribonucleotides.," *Proceedings of the National Academy of Sciences*, vol. 47, pp. 1588–602, oct 1961.

[65] W. B. Wood and P. Berg, "the Effect of Enzymatically Synthesized Ribonucleic Acid on Amino Acid Incorporation By a Soluble Protein-Ribosome System From Escherichia Coli," *Proceedings of the National Academy of Sciences*, vol. 48, no. 1, pp. 94–104, 1962.

[66] M. Lederman and G. Zubay, "DNA-directed peptide synthesis I. A comparison of T2 and Escherichia coli DNA-directed peptide synthesis in two cell-free systems," *Biochimica et Biophysica Acta*, vol. 149, pp. 253–258, 1967.

[67] J. K. DeVries and G. Zubay, "DNA-directed peptide synthesis II. The synthesis of the alpha-fragment of the enzyme beta-galactosidase," *Proceedings of the National Academy of Sciences*, 1967.

[68] M. W. Nirenberg, T. Caskey, R. Marshall, R. Brimacombe, D. Kellog, B. Doctor, D. Hatfield, J. Levin, F. Rottman, S. Pestka, M. Wilcox, and F. Anderson, "The RNA Code and Protein Synthesis," *Cold Spring Harbor Symposia on Quantitative Biology*, vol. 31, pp. 11–24, 1966.

[69] D. R. Mills, R. L. Peterson, and S. Spiegelman, "An extracellular Darwinian experiment with a self-duplicating nucleic acid molecule.," *Proceedings of the National Academy of Sciences of the United States of America*, vol. 58, pp. 217–224, July 1967.

[70] K. Kruger, P. J. Grabowski, A. J. Zaug, J. Sands, D. E. Gottschling, and T. R. Cech, "Self-splicing RNA: autoexcision and autocyclization of the ribosomal RNA intervening sequence of Tetrahymena," *Cell*, vol. 31, pp. 147–157, Nov. 1982.

[71] W. E. Balch, W. G. Dunphy, W. A. Braell, and J. E. Rothman, "Reconstitution of the transport of protein between successive compartments of the Golgi measured by the coupled incorporation of N-acetylglucosamine," *Cell*, vol. 39, pp. 405–416, Dec. 1984.

[72] L. Jermutus, L. A. Ryabova, and A. Plückthun, "Recent advances in producing and selecting functional proteins by using cell-free translation," *Current Opinion in Biotechnology*, vol. 9, pp. 534–548, oct 1998.

[73] V. Noireaux, R. Bar-Ziv, and A. Libchaber, "Principles of cell-free genetic circuit assembly," *Proceedings of the National Academy of Sciences*, vol. 100, pp. 12672–12677, Oct. 2003.

[74] L. Jermutus, L. A. Ryabova, and A. Plückthun, "Recent advances in producing and selecting functional proteins by using cell-free translation," *Current Opinion in Biotechnology*, vol. 9, pp. 534–548, Oct. 1998.

[75] N. E. Gregorio, M. Z. Levine, J. P. Oza, N. E. Gregorio, M. Z. Levine, and J. P. Oza, "A User's Guide to Cell-Free Protein Synthesis," *Methods and Protocols*, vol. 2, p. 24, mar 2019.

[76] R. Kelwick, A. J. Webb, J. T. MacDonald, and P. S. Freemont, "Development of a Bacillus subtilis cell-free transcription-translation system for prototyping regulatory elements," *Metabolic Engineering*, vol. 38, pp. 370–381, nov 2016.

[77] J. Failmezger, S. Scholz, B. Blombach, and M. Siemann-Herzberg, "Cell-Free Protein Synthesis From Fast-Growing Vibrio natriegens," *Frontiers in Microbiology*, vol. 9, p. 1146, jun 2018.

[78] S. Wang, S. Majumder, N. J. Emery, and A. P. Liu, "Simultaneous monitoring of transcription and translation in mammalian cell-free expression in bulk and in cell-sized droplets," *Synthetic Biology*, vol. 3, jan 2018.

[79] S. S. Yim, N. I. Johns, J. Park, A. L. Gomes, R. M. McBee, M. Richardson, C. Ronda, S. P. Chen, D. Garenne, V. Noireaux, and H. H. Wang, "Multiplex transcriptional characterizations

across diverse bacterial species using cell-free systems," *Molecular Systems Biology*, vol. 15, p. e8875, Aug. 2019.

[80] M. K. Takahashi, J. Chappell, C. A. Hayes, Z. Z. Sun, J. Kim, V. Singhal, K. J. Spring, S. Al-Khabouri, C. P. Fall, V. Noireaux, R. M. Murray, and J. B. Lucks, "Rapidly characterizing the fast dynamics of RNA genetic circuitry with cell-free transcription-translation (TX-TL) systems," *ACS Synthetic Biology*, vol. 4, pp. 503–515, 2015.

[81] S. D. Cole, K. Beabout, K. B. Turner, Z. K. Smith, V. L. Funk, S. V. Harbaugh, A. T. Liem, P. A. Roth, B. A. Geier, P. A. Emanuel, S. A. Walper, J. L. Chávez, and M. W. Lux, "Quantification of Interlaboratory Cell-Free Protein Synthesis Variability," *ACS Synthetic Biology*, vol. 8, pp. 2080–2091, Sept. 2019.

[82] A. D. Silverman, N. Kelley-Loughnane, J. B. Lucks, and M. C. Jewett, "Deconstructing Cell-Free Extract Preparation for in Vitro Activation of Transcriptional Genetic Circuitry," *ACS Synthetic Biology*, vol. 8, pp. 403–414, Feb. 2019.

[83] D. Foshag, E. Henrich, E. Hiller, M. Schäfer, C. Kerger, A. Burger-Kentischer, I. Diaz-Moreno, S. M. García-Mauriño, V. Dötsch, S. Rupp, and F. Bernhard, "The E. coli S30 lysate proteome: A prototype for cell-free protein production," *New Biotechnology*, vol. 40, pp. 245–260, Jan. 2018.

[84] J. Failmezger, M. Rauter, R. Nitschel, M. Kraml, and M. Siemann-Herzberg, "Cell-free protein synthesis from non-growing, stressed Escherichia coli," *Scientific Reports*, vol. 7, no. 1, pp. 1–10, 2017.

[85] G. B. Hurst, K. G. Asano, C. J. Doktycz, E. J. Consoli, W. L. Doktycz, C. M. Foster, J. L. Morrell-Falvey, R. F. Standaert, and M. J. Doktycz, "Proteomics-Based Tools for Evaluation of Cell-Free Protein Synthesis," *Analytical Chemistry*, vol. 89, pp. 11443–11451, Nov. 2017.

[86] Y. Shimizu, A. Inoue, Y. Tomari, T. Suzuki, T. Yokogawa, K. Nishikawa, and T. Ueda, "Cell-free translation reconstituted with purified components," *Nat Biotechnol*, vol. 19, pp. 751–755, Aug. 2001.

[87] A. Doerr, E. de Reus, P. van Nies, M. van der Haar, K. Wei, J. Kattan, A. Wahl, and C. Danelon, "Modelling cell-free RNA and protein synthesis with minimal systems," *Physical Biology*, vol. 16, p. 025001, jan 2019.

[88] Y. Shimizu and T. Ueda, "PURE Technology," *Methods in Molecular Biology*, vol. 607, pp. 247–248, 2010.

[89] B. Lavickova and S. J. Maerkl, "A Simple, Robust, and Low-Cost Method To Produce the PURE Cell-Free System," 2019.

[90] H. H. Wang, P.-Y. Huang, G. Xu, W. Haas, A. Marblestone, J. Li, S. P. Gygi, A. C. Forster, M. C. Jewett, and G. M. Church, "Multiplexed in Vivo His-Tagging of Enzyme Pathways for in Vitro Single-Pot Multienzyme Catalysis," *ACS Synthetic Biology*, vol. 1, pp. 43–52, Feb. 2012.

[91] J. Li, L. Gu, J. Aach, and G. M. Church, "Improved Cell-Free RNA and Protein Synthesis System," *PLOS ONE*, vol. 9, p. e106232, Sept. 2014.

[92] J. Li, C. Zhang, P. Huang, E. Kuru, E. T. C. Forster-Benson, T. Li, and G. M. Church, "Dissecting limiting factors of the Protein synthesis Using Recombinant Elements (PURE) system," *Translation*, vol. 5, p. e1327006, Jan. 2017.

[93] T. Matsuura, Y. Kazuta, T. Aita, J. Adachi, and T. Yomo, "Quantifying epistatic interactions among the components constituting the protein translation system," *Molecular Systems Biology*, vol. 5, no. 297, pp. 1–10, 2009.

[94] L. L. d. Maddalena, H. Niederholtmeyer, M. Turtola, Z. N. Swank, G. A. Belogurov, and S. J. Maerkl, "GreA and GreB Enhance Expression of Escherichia coli RNA Polymerase Promoters in a Reconstituted Transcription–Translation System," *ACS Synthetic Biology*, vol. 5, pp. 929–935, Sept. 2016.

[95] J. Shin and V. Noireaux, "An E. coli cell-free expression toolbox: application to synthetic gene circuits and artificial cells," *ACS Synthetic Biology*, vol. 1, no. 1, pp. 29–41, 2012.

[96] Z. Z. Sun, E. Yeung, C. A. Hayes, V. Noireaux, and R. M. Murray, "Linear DNA for Rapid Prototyping of Synthetic Biological Circuits in an Escherichia coli Based TX-TL Cell-Free System," *ACS Synthetic Biology*, vol. 3, no. 6, pp. 387–397, 2014.

[97] R. Marshall, C. S. Maxwell, S. P. Collins, C. L. Beisel, and V. Noireaux, "Short DNA containing sites enhances DNA stability and gene expression in E. coli cell-free transcription–translation systems," *Biotechnology and Bioengineering*, vol. 114, no. 9, pp. 2137–2141, 2017.

[98] D. Siegal-Gaskins, Z. A. Tuza, J. Kim, V. Noireaux, and R. M. Murray, "Gene Circuit Performance Characterization and Resource Usage in a Cell-Free 'Breadboard'," *ACS Synthetic Biology*, vol. 3, no. 6, pp. 416–425, 2014.

[99] A. Gyorgy and R. M. Murray, "Quantifying resource competition and its effects in the TX-TL system," *2016 IEEE 55th Conference on Decision and Control, CDC 2016*, vol. 1, no. Cdc, pp. 3363–3368, 2016.

[100] H. Niederholtmeyer, V. Stepanova, and S. J. Maerkl, "Implementation of cell-free biological networks at steady state," *Proceedings of the National Academy of Sciences*, vol. 110, no. 40, pp. 15985–15990, 2013.

[101] E. Karzbrun, A. M. Tayar, V. Noireaux, and R. H. Bar-Ziv, "Programmable on-chip DNA compartments as artificial cells," *Science*, vol. 345, no. 6198, pp. 829–832, 2014.

[102] N. Laohakunakorn, L. Grasemann, B. Lavickova, G. Michielin, A. Shahein, Z. Swank, and S. J. Maerkl, "Bottom-up construction of complex biological systems with cell-free synthetic biology," tech. rep., Zenodo, Dec. 2019.

[103] N. Ramachandran, E. Hainsworth, B. Bhullar, S. Eisenstein, B. Rosen, A. Y. Lau, J. C. Walter, and J. LaBaer, "Self-assembling protein microarrays," *Science (New York, N.Y.)*, vol. 305, pp. 86–90, July 2004.

[104] N. Ramachandran, J. V. Raphael, E. Hainsworth, G. Demirkan, M. G. Fuentes, A. Rolfs, Y. Hu, and J. LaBaer, "Next-generation high-density self-assembling functional protein arrays," *Nature Methods*, vol. 5, pp. 535–538, June 2008.

[105] D. Gerber, S. J. Maerkl, and S. R. Quake, "An in vitro microfluidic approach to generating protein-interaction networks," *Nature Methods*, vol. 6, pp. 71–74, Jan. 2009.

[106] S. J. Maerkl and S. R. Quake, "A systems approach to measuring the binding energy landscapes of transcription factors," *Science*, vol. 315, no. 5809, pp. 233–237, 2007.

[107] S. J. Maerkl and S. R. Quake, "Experimental determination of the evolvability of a transcription factor," *Proceedings of the National Academy of Sciences*, vol. 106, no. 44, pp. 18650–18655, 2009.

[108] L. Martin, M. Meier, S. M. Lyons, R. V. Sit, W. F. Marzluff, S. R. Quake, and H. Y. Chang, "Systematic reconstruction of RNA functional motifs with high-throughput microfluidics," *Nature Methods*, vol. 9, pp. 1192–1194, Dec. 2012.

[109] S. Rockel, M. Geertz, K. Hens, B. Deplancke, and S. J. Maerkl, "iSLIM: a comprehensive approach to mapping and characterizing gene regulatory networks," *Nucleic Acids Res*, vol. 41, pp. e52–e52, Feb. 2013.

[110] M. C. Blackburn, E. Petrova, B. E. Correia, and S. J. Maerkl, "Integrating gene synthesis and microfluidic protein analysis for rapid protein engineering," *Nucleic Acids Research*, vol. 44, no. 7, p. e68, 2015.

[111] S. J. Moore, J. T. MacDonald, S. Wienecke, A. Ishwarbhai, A. Tsipa, R. Aw, N. Kylilis, D. J. Bell, D. W. McClymont, K. Jensen, K. M. Polizzi, R. Biedendieck, and P. S. Freemont, "Rapid acquisition and model-based analysis of cell-free transcription-translation reactions from nonmodel bacteria," *Proceedings of the National Academy of Sciences*, vol. 115, no. 19, pp. E4340–E4349, 2018.

[112] A. Swaminathan, V. Hsiao, and R. M. Murray, "Quantitative modeling of integrase dynamics using a novel python toolbox for parameter inference in synthetic biology," *bioRxiv*, no. http://dx.doi.org/10.1101/121152, 2017.

[113] Y. Hori, C. Kantak, R. M. Murray, and A. R. Abate, "Cell-free extract based optimization of biomolecular circuits with droplet microfluidics," *Lab on a Chip*, vol. 17, pp. 3037–3042, Sept. 2017.

[114] J. Fan, F. Villarreal, B. Weyers, Y. Ding, K. H. Tseng, J. Li, B. Li, C. Tan, and T. Pan, "Multi-dimensional studies of synthetic genetic promoters enabled by microfluidic impact printing," *Lab on a Chip*, vol. 17, pp. 2198–2207, June 2017.

[115] V. Georgi, L. Georgi, M. Blechert, M. Bergmeister, M. Zwanzig, D. A. Wüstenhagen, F. F. Bier, E. Jung, and S. Kubick, "On-chip automation of cell-free protein synthesis: new opportunities due to a novel reaction mode," *Lab on a Chip*, vol. 16, pp. 269–281, Jan. 2016.

[116] Y. Elani, R. V. Law, and O. Ces, "Vesicle-based artificial cells as chemical microreactors with spatially segregated reaction pathways," *Nature Communications*, vol. 5, pp. 1–5, Oct. 2014.

[117] Y. Jiao, Y. Liu, D. Luo, W. T. S. Huck, and D. Yang, "Microfluidic-Assisted Fabrication of Clay Microgels for Cell-Free Protein Synthesis," *ACS Applied Materials & Interfaces*, vol. 10, pp. 29308–29313, Sept. 2018.

[118] K.-H. Lee, K.-Y. Lee, J.-Y. Byun, B.-G. Kim, and D.-M. Kim, "On-bead expression of recombinant proteins in an agarose gel matrix coated on a glass slide," *Lab on a Chip*, vol. 12, pp. 1605–1610, Apr. 2012.

[119] J.-Y. Byun, K.-H. Lee, K.-Y. Lee, M.-G. Kim, and D.-M. Kim, "In-gel expression and in situ immobilization of proteins for generation of three dimensional protein arrays in a hydrogel matrix," *Lab on a Chip*, vol. 13, pp. 886–891, Feb. 2013.

[120] A. S. Spirin, V. I. Baranov, L. A. Ryabova, S. Y. Ovodov, and Y. B. Alakhov, "A continuous cell-free translation system capable of producing polypeptides in high yield," *Science*, vol. 242, pp. 1162–1164, Nov. 1988.

[121] D.-M. Kim and C.-Y. Choi, "A Semicontinuous Prokaryotic Coupled Transcription/Translation System Using a Dialysis Membrane," *Biotechnology Progress*, vol. 12, pp. 645–649, Jan. 1996.

[122] K. Madin, T. Sawasaki, T. Ogasawara, and Y. Endo, "A Highly Efficient and Robust Cell-Free Protein Synthesis System Prepared from Wheat Embryos: Plants Apparently Contain a Suicide System Directed at Ribosomes," *Proceedings of the National Academy of Sciences of the United States of America*, vol. 97, no. 2, pp. 559–564, 2000.

[123] Q. Mei, C. K. Fredrickson, W. Lian, S. Jin, and Z. H. Fan, "Ricin Detection by Biological Signal Amplification in a Well-in-a-Well Device," *Analytical Chemistry*, vol. 78, pp. 7659–7664, Nov. 2006.

[124] Q. Mei, C. K. Fredrickson, A. Simon, R. Khnouf, and Z. H. Fan, "Cell-Free Protein Synthesis in Microfluidic Array Devices," *Biotechnology Progress*, vol. 23, no. 6, pp. 1305–1311, 2007.

[125] R. Khnouf, D. J. Beebe, and Z. H. Fan, "Cell-free protein expression in a microchannel array with passive pumping," *Lab on a Chip*, vol. 9, pp. 56–61, Jan. 2009.

[126] R. Khnouf, D. Olivero, S. Jin, and Z. H. Fan, "Miniaturized fluid array for high-throughput protein expression," *Biotechnology Progress*, vol. 26, no. 6, pp. 1590–1596, 2010.

[127] G.-H. Hahn, A. Asthana, D.-M. Kim, and D.-P. Kim, "A continuous-exchange cell-free protein synthesis system fabricated on a chip," *Analytical Biochemistry*, vol. 365, pp. 280–282, June 2007.

[128] P. Siuti, S. T. Retterer, and M. J. Doktycz, "Continuous protein production in nanoporous, picolitre volume containers," *Lab on a Chip*, vol. 11, pp. 3523–3529, Oct. 2011.

[129] M. Yelleswarapu, A. J. van der Linden, B. van Sluijs, P. A. Pieters, E. Dubuc, T. F. A. de Greef, and W. T. S. Huck, "Sigma Factor-Mediated Tuning of Bacterial Cell-Free Synthetic Genetic Oscillators, Supplementary Information," *ACS Synthetic Biology*, vol. 7, no. 12, p. 2879, 2018.

[130] Y. Efrat, A. M. Tayar, S. S. Daube, M. Levy, and R. H. Bar-Ziv, "Electric-Field Manipulation of a Compartmentalized Cell-Free Gene Expression Reaction," *ACS Synthetic Biology*, vol. 7, pp. 1829–1833, Aug. 2018.

[131] H. Niederholtmeyer, Z. Sun, Y. Hori, E. Yeung, A. Verpoorte, R. M. Murray, and S. J. Maerkl, "Rapid cell-free forward engineering of novel genetic ring oscillators," *eLife*, no. DOI: http://dx.doi.org/10.7554/eLife.09771, 2015.

[132] J. Chappell, K. Jensen, and P. S. Freemont, "Validation of an entirely in vitro approach for rapid prototyping of DNA regulatory elements for synthetic biology," *Nucleic Acids Research*, vol. 41, no. 5, pp. 3471–3481, 2013.

[133] A. C. Forster and G. M. Church, "Towards synthesis of a minimal cell," *Molecular Systems Biology*, vol. 2, no. 45, pp. 1–10, 2006.

[134] P. van Nies, I. Westerlaken, D. Blanken, M. Salas, M. Mencía, and C. Danelon, "Self-replication of DNA by its encoded proteins in liposome-based synthetic cells," *Nature Communications*, vol. 9, no. 1583, 2018.

[135] L. Otrin, N. Marušič, C. Bednarz, T. Vidakovic-Koch, I. Lieberwirth, K. Landfester, and K. Sundmacher, "Toward artificial mitochondrion: mimicking oxidative phosphorylation in polymer and hybrid membranes," *Nano Letters*, vol. 17, no. 11, pp. 6816–6821, 2017.

[136] M. C. Jewett, B. R. Fritz, L. E. Timmerman, and G. M. Church, "In vitro integration of ribosomal RNA synthesis, ribosome assembly, and translation," *Molecular Systems Biology*, vol. 9, no. 678, 2013.

[137] A. Bhattacharya, R. J. Brea, and N. K. Devaraj, "De novo vesicle formation and growth: an integrative approach to artificial cells," *Chemical Science*, vol. 8, no. 12, pp. 7912–7922, 2017.

[138] T. Furusato, F. Horie, H. T. Matsubayashi, K. Amikura, Y. Kuruma, and T. Ueda, "De novo synthesis of basal bacterial cell division proteins FtsZ, FtsA, and ZipA inside giant vesicles," *ACS Synthetic Biology*, vol. 7, no. 4, pp. 953–961, 2018.

[139] J. A. N. Brophy and C. A. Voigt, "Principles of genetic circuit design," *Nature Methods*, vol. 11, no. 5, pp. 508–520, 2014.

[140] A. A. K. Nielsen, B. S. Der, J. Shin, P. Vaidyanathan, V. Paralanov, E. A. Strychalski, D. Ross, D. Densmore, and C. A. Voigt, "Genetic circuit design automation," *Science*, vol. 352, no. 6281, p. aac7341, 2016.

[141] S. Basu, Y. Gerchman, C. H. Collins, F. H. Arnold, and R. Weiss, "A synthetic multicellular system for programmed pattern formation," *Nature*, vol. 434, no. 7037, pp. 1130–1134, 2005.

[142] B. C. Stanton, A. A. K. Nielsen, A. Tamsir, K. Clancy, T. Peterson, and C. A. Voigt, "Genomic mining of prokaryotic repressors for orthogonal logic gates," *Nature Chemical Biology*, vol. 10, no. 2, pp. 99–105, 2014.

[143] J. M. Vaquerizas, S. K. Kummerfeld, S. A. Teichmann, and N. M. Luscombe, "A census of human transcription factors: function, expression and evolution," *Nature Reviews Genetics*, vol. 10, no. 4, pp. 252–263, 2009.

[144] R. R. Beerli and C. F. Barbas III, "Engineering polydactyl zinc-finger transcription factors," *Nature Biotechnology*, vol. 20, no. 2, p. 135, 2002.

[145] P. Tebas, D. Stein, W. W. Tang, I. Frank, S. Q. Wang, G. Lee, S. K. Spratt, R. T. Surosky, M. A. Giedlin, G. Nichol, M. C. Holmes, and P. D. e. a. Gregory, "Gene editing of CCR5 in autologous CD4 T cells of persons infected with HIV," *The New England Journal of Medicine*, vol. 370, pp. 901–910, 2014.

[146] H. S. Najafabadi, S. Mnaimneh, F. W. Schmitges, M. Garton, K. N. Lam, A. Yang, M. Albu, M. T. Weirauch, E. Radovani, P. M. Kim, J. Greenblatt, B. J. Frey, and T. R. Hughes, "C2h2 zinc finger proteins greatly expand the human regulatory lexicon," *Nature Biotechnology*, vol. 33, no. 5, pp. 555–562, 2015.

[147] F. Fu and D. F. Voytas, "Zinc Finger Database (ZiFDB v2.0: a comprehensive database of c2h2 zinc fingers and engineered zinc finger arrays," *Nucleic Acids Research*, vol. 41, pp. D452–D455, 2013.

[148] R. Moore, A. Chandrahas, and L. Bleris, "Transcription activator-like effectors: a toolkit for synthetic biology," *ACS Synthetic Biology*, vol. 3, pp. 708–716, 2014.

[149] A. S. Khalil, T. K. Lu, C. J. Bashor, C. L. Ramirez, N. C. Pyenson, J. K. Joung, and J. J. Collins, "A Synthetic Biology Framework for Programming Eukaryotic Transcription Functions," *Cell*, vol. 150, no. 3, pp. 647–658, 2012.

[150] J. J. Lohmueller, T. Z. Armel, and P. A. Silver, "A tunable zinc finger-based framework for Boolean logic computation in mammalian cells," *Nucleic Acids Research*, vol. 40, no. 11, pp. 5180–5187, 2012.

[151] M. Ptashne, K. Backman, M. Z. Humayun, A. Jeffrey, R. Maurer, B. Meyer, and R. T. Sauer, "Autoregulation and function of a repressor in bacteriophage lambda," *Science*, vol. 194, no. 4261, pp. 156–161, 1976.

[152] R. S. Cox III, M. G. Surette, and M. B. Elowitz, "Programming gene expression with combinatorial promoters," *Molecular Systems Biology*, vol. 3, no. 145, pp. 1–11, 2007.

[153] R. Lutz and H. Bujard, "Independent and tight regulation of transcriptional units in Escherichia coli via the LacR/O, the TetR/O and AraC/I-I-I-2 regulatory elements," *Nucleic Acids Research*, vol. 25, pp. 1203–1210, 1997.

[154] M. Lanzer and H. Bujard, "Promoters largely determine the efficiency of repressor action," *Proceedings of the National Academy of Sciences*, vol. 85, pp. 8973–8977, 1988.

[155] E. Sharon, Y. Kalma, A. Sharp, T. Raveh-Sadka, M. Levo, D. Zeevi, L. Keren, Z. Yakhini, A. Weinberger, and E. Segal, "Inferring gene regulatory logic from high-throughput measurements of thousands of systematically designed promoters," *Nature Biotechnology*, vol. 30, no. 6, pp. 521–530, 2012.

[156] J. L. Garcia-Cordero and S. J. Maerkl, "Mechanically Induced Trapping of Molecular Interactions and its applications," *Journal of Laboratory Automation*, vol. 21, no. 3, pp. 356–367, 2016.

[157] J. B. Kinney, A. Murugan, C. G. J. Callan, and E. C. Cox, "Using deep sequencing to characterize the biophysical mechanism of a transcriptional regulatory sequence," *Proceedings of the National Academy of Sciences*, vol. 107, no. 20, pp. 9158–9163, 2010.

[158] T. Kamiuchi, E. Abe, M. Imanishi, T. Kaji, M. Nagaoka, and Y. Sugiura, "Artificial nine zinc-finger peptide with 30 base pair binding sites," *Biochemistry*, vol. 37, pp. 13827–13834, 1998.

[159] J.-S. Kim and C. O. Pabo, "Getting a handhold on DNA: design of poly-zinc finger proteins with femtomolar dissociation constants," *Proceedings of the National Academy of Sciences*, vol. 95, pp. 2812–2817, 1998.

[160] M. Moore, A. Klug, and Y. Choo, "Improved DNA binding specificity from polyzinc finger peptides by using strings of two-finger units," *Proceedings of the National Academy of Sciences*, vol. 98, no. 4, pp. 1437–1441, 2001.

[161] J. L. Pomerantz, S. A. Wolfe, and C. O. Pabo, "Structure-based design of a dimeric zinc finger protein," *Biochemistry*, vol. 37, no. 4, pp. 965–970, 1998.

[162] S. A. Wolfe, E. I. Ramm, and C. O. Pabo, "Combining structure-based design with phage display to create new Cys2His2 zinc finger dimers," *Structure*, vol. 8, pp. 739–750, 2000.

[163] S. A. Wolfe, R. A. Grant, and C. O. Pabo, "Structure of a designed dimeric zinc finger protein bound to DNA," *Biochemistry*, vol. 42, pp. 13401–13409, 2003.

[164] Z. Z. Sun, C. A. Hayes, J. Shin, F. Caschera, R. M. Murray, and V. Noireaux, "Protocols for Implementing an Eschrichia coli Based TX-TL Cell-Free Expression System for Synthetic Biology," *Journal of Visualized Experiments*, vol. 79, p. e50762, 2013.

[165] J. Shin and V. Noireaux, "Efficient cell free expression with the endogenous E. coli RNA polymerase and sigma factor 70," *J. Biol Eng*, vol. 4, no. 8, 2010.

[166] L. Bintu, N. E. Buchler, H. G. Garcia, U. Gerland, T. Hwa, J. Kondev, T. Kuhlman, and R. Phillips, "Transcriptional regulation by the numbers: applications," *Current Opinion in Genetics and Development*, vol. 15, pp. 125–135, 2005b.

[167] L. Bintu, N. E. Buchler, H. G. Garcia, U. Gerland, T. Hwa, J. Kondev, and R. Phillips, "Transcriptional regulation by the numbers: models," *Current Opinion in Genetics and Development*, vol. 15, pp. 116–124, 2005.

[168] D. Saro, T. Li, C. Rupasinghe, A. Paredes, N. Caspers, and M. R. Spaller, "A thermodynamic ligand binding study of the third PDZ domain (PDZ3) from the mammalian neuronal protein PSD-95," *Biochemistry*, vol. 46, pp. 6340–6352, 2007.

[169] N. K. Jana, S. Deb, B. Bhattacharyya, N. C. Mandal, and S. Roy, "A study of energetics of cooperative interaction using a mutant lambda-repressor," *Protein Engineering*, vol. 13, no. 9, pp. 629–633, 2000.

[170] X. Meng, M. H. Brodsky, and S. A. Wolfe, "A bacterial one-hybrid system for determining the DNA-binding specificity of transcription factors," *Nature Biotechnology*, vol. 23, no. 8, pp. 988–994, 2005.

[171] S. A. Wolfe, H. A. Greisman, E. I. Ramm, and C. O. Pabo, "Analysis of zinc fingers optimized via phage display: evaluating the utility of a recognition code," *Journal of Molecular Biology*, vol. 285, no. 5, pp. 1917–1934, 1999.

[172] A. S. Rajkumar, N. Dénervaud, and S. J. Maerkl, "Mapping the fine structure of a eukaryotic promoter input-output function," *Nature Genetics*, vol. 45, no. 10, pp. 1207–1215, 2013.

[173] S. L. Barnes, N. M. Belliveau, W. T. Ireland, J. B. Kinney, and R. Phillips, "Mapping DNA sequence to transcription factor binding energy in vivo," *bioRxiv*, no. doi:10.1101/331124, 2018.

[174] M. L. Bulyk, X. Huang, Y. Choo, and G. M. Church, "Exploring the DNA-binding specificites of zinc fingers with DNA microarrays," *Proceedings of the National Academy of Sciences*, vol. 98, no. 13, pp. 7158–7163, 2001.

[175] Y. Zhao, D. Granas, and G. D. Stormo, "Inferring binding energies from selected binding sites," *PLoS Computational Biology*, vol. 5, no. 12, p. e1000590, 2009.

[176] C. Jung, P. Bandilla, M. von Reutern, M. Schnepf, S. Rieder, U. Unnerstall, and U. Gaul, "True equilibrium measurement of transcription factor-DNA binding affinities using automated polarization microscopy," *Nature Communications*, vol. 9, no. 1, p. 1605, 2018.

[177] I. Mogno, J. C. Kwasnieski, and B. A. Cohen, "Massively parallel synthetic promoter assays reveal the in vivo effects of binding site variants," *Genome Research*, no. gr.157891.113, 2013.

[178] R. Amit, H. G. Garcia, R. Phillips, and S. E. Fraser, "Building enhancers from the ground up: a synthetic biology approach," *Cell*, vol. 146, no. 1, pp. 105–118, 2011.

[179] H. G. Garcia and R. Phillips, "Quantitative dissection of the simple repression input-output function," *Proceedings of the National Academy of Sciences*, vol. 108, no. 29, pp. 12173–12178, 2011.

[180] J. Boch, H. Scholze, S. Schornack, A. Landgraf, S. Hahn, S. Kay, T. Lahaye, A. Nickstadt, and U. Bonas, "Breaking the code of DNA binding specificty of TAL-type III effectors," *Science*, vol. 326, no. 5959, pp. 1509–1512, 2009.

[181] E. A. Boyle, J. O. L. Andreasson, L. M. Chircus, S. H. Sternberg, M. J. Wu, C. K. Guegler, J. A. Doudna, and W. J. Greenleaf, "High-throughput biochemical profiling reveals sequence determinants of dCas9 off-target binding and unbinding," *Proceedings of the National Academy of Sciences*, vol. 114, no. 21, pp. 5461–5466, 2017.

[182] L. Cuculis, Z. Abil, H. Zho, and C. M. Schroeder, "TALE proteins search DNA using a rotationally decoupled mechanism," *Nature Chemical Biology*, vol. 12, no. 10, pp. 831–837, 2016.

[183] M. Geertz, D. Shore, and S. J. Maerkl, "Massively parallel measurements of molecular interaction kinetics on a microfluidic platform," *PNAS*, vol. 109, no. 41, pp. 16540–16545, 2012.

[184] G. Cambray, J. C. Guimaraes, and A. P. Arkin, "Evaluation of 244,000 synthetic sequences reveals design principles to optimize translation in Escherichia coli," *Nature Biotechnology*, vol. 36, no. 10, pp. 1005–1015, 2018.

[185] K. Pardee, A. A. Green, M. K. Takahashi, D. Braff, G. Lambert, J. W. Lee, T. Ferrante, D. Ma, N. Donghia, M. Fan, N. M. Daringer, I. Bosch, D. M. Dudley, D. H. O'Connor, L. Gehrke, and J. J. Collins, "Rapid, low-cost detection of Zika virus using programmable biomolecular components," *Cell*, vol. 165, no. 5, pp. 1255–1266, 2016.

[186] K. Pardee, S. Slomovic, P. Q. Nguyen, J. W. Lee, N. Donghia, D. Burrill, T. Ferrante, F. R. McSorley, Y. Furuta, A. Vernet, M. Lewandowski, C. N. Boddy, N. S. Joshi, and J. J. Collins, "Portable, on-demand biomolecular manufacturing," *Cell*, vol. 167, no. 1, pp. 248–259.e12, 2016b.

[187] A. W. Goering, J. Li, R. A. McClure, R. J. Thomson, M. C. Jewett, and N. L. Kelleher, "In vitro reconstruction of nonribosomal peptide biosynthesis directly from DNA using cell-free protein synthesis," *ACS Synthetic Biology*, vol. 6, no. 1, pp. 39–44, 2016.

[188] J. C. Stark, A. Huang, P. Q. Nguyen, R. S. Dubner, K. J. Hsu, T. C. Ferrante, M. Anderson, A. Kanapskyte, Q. Mucha, J. S. Packett, P. Patel, R. Patel, D. Qaq, T. Zondor, J. Burke, T. Martinez, A. Miller-Berry, A. Puppala, K. Reichert, M. Schmid, L. Brand, L. R. Hill, J. F. Chellaswamy, N. Faheem, S. Fetherling, E. Gong, E. M. Gonzalzles, T. Granito, J. Koritsaris, B. Nguyen, S. Ottman, C. Palffy, A. Patel, S. Skweres, A. Slaton, T. Woods, N. Donghia, K. Pardee, J. J. Collins, and M. C. Jewett, "BioBits Bright: a fluorescent synthetic biology education kit," *Science Advances*, vol. 4, no. 8, p. eaat5107, 2018.

[189] R. S. Fuller and A. Kornberg, "Purified dnaA protein in initiation of replication at the Escherichia coli chromosomal origin of replication," *Proceedings of the National Academy of Sciences of the United States of America*, vol. 80, no. 19, pp. 5817–5821, 1983.

[190] D. Foreman-Mackey, D. W. Hogg, D. Lang, and J. Goodman, "emcee: The MCMC Hammer," no. arXiv:1202.3665v4, 2013.

[191] J. Goodman and J. Weare, "Ensemble samplers with affine invariance," *Comm. App. Math. and Comp. Sci.*, vol. 5, no. 1, pp. 65–80, 2010.

[192] D. Sprinzak and M. B. Elowitz, "Reconstruction of genetic circuits," *Nature*, vol. 438, pp. 443–448, 2005.

[193] Z. Swank, N. Laohakunakorn, and S. J. Maerkl, "Cell-free gene-regulatory network engineering with synthetic transcription factors," *Proceedings of the National Academy of Sciences*, vol. 116, no. 13, pp. 5892–5901, 2019.

[194] K. Woodruff and S. J. Maerkl, "Microfluidic Module for Real-Time Generation of Complex Multimolecule Temporal Concentration Profiles," *Anal. Chem.*, vol. 90, pp. 696–701, Jan. 2018.

[195] J.-C. Chang, Z. Swank, O. Keiser, S. J. Maerkl, and E. Amstad, "Microfluidic device for real-time formulation of reagents and their subsequent encapsulation into double emulsions," *Scientific Reports*, vol. 8, pp. 1–9, May 2018.

[196] Y. C. Kwon and M. C. Jewett, "High-throughput preparation methods of crude extract for robust cell-free protein synthesis," *Scientific Reports*, vol. 5, pp. 1–8, 2015.

[197] Y. Ding, J. Choo, and A. J. deMello, "From single-molecule detection to next-generation sequencing: microfluidic droplets for high-throughput nucleic acid analysis," *Microfluid Nanofluid*, vol. 21, p. 58, Mar. 2017.

[198] M. T. Guo, A. Rotem, J. A. Heyman, and D. A. Weitz, "Droplet microfluidics for high-throughput biological assays," *Lab Chip*, vol. 12, pp. 2146–2155, May 2012.

[199] H. N. Joensson and H. AnderssonSvahn, "Droplet Microfluidics—A Tool for Single-Cell Analysis," *Angewandte Chemie International Edition*, vol. 51, no. 49, pp. 12176–12192, 2012.

[200] S. L. Anna, N. Bontoux, and H. A. Stone, "Formation of dispersions using "flow focusing" in microchannels," *Appl. Phys. Lett.*, vol. 82, pp. 364–366, Jan. 2003.

[201] R. K. Shah, H. C. Shum, A. C. Rowat, D. Lee, J. J. Agresti, A. S. Utada, L.-Y. Chu, J.-W. Kim, A. Fernandez-Nieves, C. J. Martinez, and D. A. Weitz, "Designer emulsions using microfluidics," *Materials Today*, vol. 11, pp. 18–27, Apr. 2008.

[202] R. Dangla, S. C. Kayi, and C. N. Baroud, "Droplet microfluidics driven by gradients of confinement," *PNAS*, vol. 110, pp. 853–858, Jan. 2013.

[203] J. Q. Boedicker, L. Li, T. R. Kline, and R. F. Ismagilov, "Detecting bacteria and determining their susceptibility to antibiotics by stochastic confinement in nanoliter droplets using plug-based microfluidics," *Lab Chip*, vol. 8, pp. 1265–1272, July 2008.

[204] O. J. Miller, A. E. Harrak, T. Mangeat, J.-C. Baret, L. Frenz, B. E. Debs, E. Mayot, M. L. Samuels, E. K. Rooney, P. Dieu, M. Galvan, D. R. Link, and A. D. Griffiths, "High-resolution dose–response screening using droplet-based microfluidics," *Proc Natl Acad Sci U S A*, vol. 109, pp. 378–383, Jan. 2012.

[205] M. M. Kiss, L. Ortoleva-Donnelly, N. R. Beer, J. Warner, C. G. Bailey, B. W. Colston, J. M. Rothberg, D. R. Link, and J. H. Leamon, "High-Throughput Quantitative Polymerase Chain Reaction in Picoliter Droplets," *Anal. Chem.*, vol. 80, pp. 8975–8981, Dec. 2008.

[206] N. R. Beer, E. K. Wheeler, L. Lee-Houghton, N. Watkins, S. Nasarabadi, N. Hebert, P. Leung, D. W. Arnold, C. G. Bailey, and B. W. Colston, "On-Chip Single-Copy Real-Time Reverse-Transcription PCR in Isolated Picoliter Droplets," *Anal. Chem.*, vol. 80, pp. 1854–1858, Mar. 2008.

[207] Y. Zeng, R. Novak, J. Shuga, M. T. Smith, and R. A. Mathies, "High-Performance Single Cell Genetic Analysis Using Microfluidic Emulsion Generator Arrays," *Anal. Chem.*, vol. 82, pp. 3183–3190, Apr. 2010.

[208] C. L. Delley, L. Liu, M. F. Sarhan, and A. R. Abate, "Combined aptamer and transcriptome sequencing of single cells," *Sci Rep*, vol. 8, pp. 1–8, Feb. 2018.

[209] S. C. Kim, I. C. Clark, P. Shahi, and A. R. Abate, "Single-Cell RT-PCR in Microfluidic Droplets with Integrated Chemical Lysis," *Anal. Chem.*, vol. 90, pp. 1273–1279, Jan. 2018.

[210] F. Lan, B. Demaree, N. Ahmed, and A. R. Abate, "Single-cell genome sequencing at ultra-high-throughput with microfluidic droplet barcoding," *Nat Biotechnol*, vol. 35, pp. 640–646, July 2017.

[211] L. Mazutis, J. Gilbert, W. L. Ung, D. A. Weitz, A. D. Griffiths, and J. A. Heyman, "Single-cell analysis and sorting using droplet-based microfluidics," *Nat Protoc*, vol. 8, pp. 870–891, May 2013.

[212] J. Abatemarco, M. F. Sarhan, J. M. Wagner, J.-L. Lin, L. Liu, W. Hassouneh, S.-F. Yuan, H. S. Alper, and A. R. Abate, "RNA-aptamers-in-droplets (RAPID) high-throughput screening for secretory phenotypes," *Nat Commun*, vol. 8, pp. 1–9, Aug. 2017.

[213] B. L. Wang, A. Ghaderi, H. Zhou, J. Agresti, D. A. Weitz, G. R. Fink, and G. Stephanopoulos, "Microfluidic high-throughput culturing of single cells for selection based on extracellular metabolite production or consumption," *Nat Biotechnol*, vol. 32, pp. 473–478, May 2014.

[214] D. J. Eastburn, A. Sciambi, and A. R. Abate, "Picoinjection Enables Digital Detection of RNA with Droplet RT-PCR," *PLoS One*, vol. 8, Apr. 2013.

[215] M. Zagnoni, C. N. Baroud, and J. M. Cooper, "Electrically initiated upstream coalescence cascade of droplets in a microfluidic flow," *Phys. Rev. E*, vol. 80, p. 046303, Oct. 2009.

[216] H. Gu, M. H. G. Duits, and F. Mugele, "Droplets Formation and Merging in Two-Phase Flow Microfluidics," *International Journal of Molecular Sciences*, vol. 12, pp. 2572–2597, Apr. 2011.

[217] M. Chabert, K. D. Dorfman, and J.-L. Viovy, "Droplet fusion by alternating current (AC) field electrocoalescence in microchannels," *ELECTROPHORESIS*, vol. 26, no. 19, pp. 3706–3715, 2005.

[218] D. R. Link, E. Grasland-Mongrain, A. Duri, F. Sarrazin, Z. Cheng, G. Cristobal, M. Marquez, and D. A. Weitz, "Electric Control of Droplets in Microfluidic Devices," *Angewandte Chemie International Edition*, vol. 45, no. 16, pp. 2556–2560, 2006.

[219] A. R. Abate, T. Hung, P. Mary, J. J. Agresti, and D. A. Weitz, "High-throughput injection with microfluidics using picoinjectors," *PNAS*, vol. 107, pp. 19163–19166, Nov. 2010.

[220] I. Akartuna, D. M. Aubrecht, T. E. Kodger, and D. A. Weitz, "Chemically induced coalescence in droplet-based microfluidics," *Lab Chip*, vol. 15, pp. 1140–1144, Feb. 2015.

[221] A. M. Nightingale, T. W. Phillips, J. H. Bannock, and J. C. d. Mello, "Controlled multistep synthesis in a three-phase droplet reactor," *Nat Commun*, vol. 5, pp. 1–8, May 2014.

[222] H. Sugiura, M. Ito, T. Okuaki, Y. Mori, H. Kitahata, and M. Takinoue, "Pulse-density modulation control of chemical oscillation far from equilibrium in a droplet open-reactor system," *Nat Commun*, vol. 7, pp. 1–9, Jan. 2016.

[223] M. A. Holden, S. Kumar, E. T. Castellana, A. Beskok, and P. S. Cremer, "Generating fixed concentration arrays in a microfluidic device," *Sensors and Actuators B: Chemical*, vol. 92, pp. 199–207, July 2003.

[224] C. Neils, Z. Tyree, B. Finlayson, and A. Folch, "Combinatorial mixing of microfluidic streams," *Lab Chip*, vol. 4, pp. 342–350, July 2004.

[225] A. Baccouche, S. Okumura, R. Sieskind, E. Henry, N. Aubert-Kato, N. Bredeche, J.-F. Bartolo, V. Taly, Y. Rondelez, T. Fujii, and A. J. Genot, "Massively parallel and multiparameter titration of biochemical assays with droplet microfluidics," *Nat Protoc*, vol. 12, pp. 1912–1932, Sept. 2017.

[226] A. J. Genot, A. Baccouche, R. Sieskind, N. Aubert-Kato, N. Bredeche, J. F. Bartolo, V. Taly, T. Fujii, and Y. Rondelez, "High-resolution mapping of bifurcations in nonlinear biochemical circuits," *Nature Chem*, vol. 8, pp. 760–767, Aug. 2016.

[227] J. Marschewski, S. Jung, P. Ruch, N. Prasad, S. Mazzotti, B. Michel, and D. Poulikakos, "Mixing with herringbone-inspired microstructures: overcoming the diffusion limit in co-laminar microfluidic devices," *Lab Chip*, vol. 15, pp. 1923–1933, Mar. 2015.

[228] A. D. Stroock, S. K. W. Dertinger, A. Ajdari, I. Mezić, H. A. Stone, and G. M. Whitesides, "Chaotic Mixer for Microchannels," *Science*, vol. 295, pp. 647–651, Jan. 2002.

[229] N.-T. Nguyen and Z. Wu, "Micromixers—a review," *J. Micromech. Microeng.*, vol. 15, pp. R1–R16, Dec. 2004.

[230] M. A. Unger, H.-P. Chou, T. Thorsen, A. Scherer, and S. R. Quake, "Monolithic Microfabricated Valves and Pumps by Multilayer Soft Lithography," *Science*, vol. 288, pp. 113–116, Apr. 2000.

[231] T. Thorsen, S. J. Maerkl, and S. R. Quake, "Microfluidic Large-Scale Integration," *Science*, vol. 298, pp. 580–584, Oct. 2002.

[232] Y. Xia and G. M. Whitesides, "Soft lithography," *Annu. Rev. Mater. Sci.*, vol. 28, pp. 153–184, Aug. 1998.

[233] J.-B. Nobs and S. J. Maerkl, "Long-Term Single Cell Analysis of S. pombe on a Microfluidic Microchemostat Array," *PLOS ONE*, vol. 9, p. e93466, Apr. 2014.

[234] S. Einav, D. Gerber, P. D. Bryson, E. H. Sklan, M. Elazar, S. J. Maerkl, J. S. Glenn, and S. R. Quake, "Discovery of a hepatitis C target and its pharmacological inhibitors by microfluidic affinity analysis," *Nat Biotechnol*, vol. 26, pp. 1019–1027, Sept. 2008.

[235] N. Dénervaud, J. Becker, R. Delgado-Gonzalo, P. Damay, A. S. Rajkumar, M. Unser, D. Shore, F. Naef, and S. J. Maerkl, "A chemostat array enables the spatio-temporal analysis of the yeast proteome," *PNAS*, vol. 110, pp. 15842–15847, Sept. 2013.

[236] F. Piraino, F. Volpetti, C. Watson, and S. J. Maerkl, "A Digital–Analog Microfluidic Platform for Patient-Centric Multiplexed Biomarker Diagnostics of Ultralow Volume Samples," *ACS Nano*, vol. 10, pp. 1699–1710, Jan. 2016.

[237] A. Ainla, I. Gözen, O. Orwar, and A. Jesorka, "A Microfluidic Diluter Based on Pulse Width Flow Modulation," *Anal. Chem.*, vol. 81, pp. 5549–5556, July 2009.

[238] D. Irimia, D. A. Geba, and M. Toner, "Universal Microfluidic Gradient Generator," *Anal. Chem.*, vol. 78, pp. 3472–3477, May 2006.

[239] X. Zhang, A. Grimley, R. Bertram, and M. G. Roper, "Microfluidic System for Generation of Sinusoidal Glucose Waveforms for Entrainment of Islets of Langerhans," *Anal. Chem.*, vol. 82, pp. 6704–6711, Aug. 2010.

[240] C. L. Hansen, S. Classen, J. M. Berger, and S. R. Quake, "A Microfluidic Device for Kinetic Optimization of Protein Crystallization and In Situ Structure Determination," *J. Am. Chem. Soc.*, vol. 128, pp. 3142–3143, Mar. 2006.

[241] K. R. King, S. Wang, A. Jayaraman, M. L. Yarmush, and M. Toner, "Microfluidic flow-encoded switching for parallel control of dynamic cellular microenvironments," *Lab Chip*, vol. 8, pp. 107–116, Dec. 2007.

[242] B. Krishnaswamy, C. M. Austin, J. P. Bardill, D. Russakow, G. L. Holst, B. K. Hammer, C. R. Forest, and R. Sivakumar, "Time-Elapse Communication: Bacterial Communication on a Microfluidic Chip," *IEEE Transactions on Communications*, vol. 61, pp. 5139–5151, Dec. 2013.

[243] Y. Kim, B. Kuczenski, P. R. LeDuc, and W. C. Messner, "Modulation of fluidic resistance and capacitance for long-term, high-speed feedback control of a microfluidic interface," *Lab Chip*, vol. 9, pp. 2603–2609, Sept. 2009.

[244] C. L. Hansen, M. O. A. Sommer, and S. R. Quake, "Systematic investigation of protein phase behavior with a microfluidic formulator," *PNAS*, vol. 101, pp. 14431–14436, Oct. 2004.

[245] K. Brower, R. R. Puccinelli, C. J. Markin, T. C. Shimko, S. A. Longwell, B. Cruz, R. Gomez-Sjoberg, and P. M. Fordyce, "An open-source, programmable pneumatic setup for operation and automated control of single- and multi-layer microfluidic devices," *HardwareX*, vol. 3, pp. 117–134, Apr. 2018.

[246] J. A. White and A. M. Streets, "Controller for microfluidic large-scale integration," *HardwareX*, vol. 3, pp. 135–145, Apr. 2018.

[247] A. Vian, V. Favrod, and E. Amstad, "Reducing the shell thickness of double emulsions using microfluidics," *Microfluid Nanofluid*, vol. 20, p. 159, Nov. 2016.

[248] D. Pekin, Y. Skhiri, J.-C. Baret, D. L. Corre, L. Mazutis, C. B. Salem, F. Millot, A. E. Harrak, J. B. Hutchison, J. W. Larson, D. R. Link, P. Laurent-Puig, A. D. Griffiths, and V. Taly, "Quantitative and sensitive detection of rare mutations using droplet-based microfluidics," *Lab Chip*, vol. 11, pp. 2156–2166, June 2011.

[249] C. Holtze, A. C. Rowat, J. J. Agresti, J. B. Hutchison, F. E. Angilè, C. H. J. Schmitz, S. Köster, H. Duan, K. J. Humphry, R. A. Scanga, J. S. Johnson, D. Pisignano, and D. A. Weitz, "Biocompatible surfactants for water-in-fluorocarbon emulsions," *Lab Chip*, vol. 8, pp. 1632–1639, Sept. 2008.

[250] G. Etienne, M. Kessler, and E. Amstad, "Influence of Fluorinated Surfactant Composition on the Stability of Emulsion Drops," *Macromolecular Chemistry and Physics*, vol. 218, no. 2, p. 1600365, 2017.

[251] P. Gruner, B. Riechers, B. Semin, J. Lim, A. Johnston, K. Short, and J.-C. Baret, "Controlling molecular transport in minimal emulsions," *Nat Commun*, vol. 7, pp. 1–9, Jan. 2016.

[252] A. Rotem, A. R. Abate, A. S. Utada, V. V. Steijn, and D. A. Weitz, "Drop formation in non-planar microfluidic devices," *Lab Chip*, vol. 12, pp. 4263–4268, Oct. 2012.

[253] H. Niederholtmeyer, L. Xu, and S. J. Maerkl, "Real-Time mRNA Measurement during an in Vitro Transcription and Translation Reaction using Binary Probes," *ACS Synthetic Biology*, vol. 2, no. 8, pp. 411–417, 2012.

[254] D. Imburgio, M. Rong, K. Ma, and W. T. McAllister, "Studies of Promoter Recognition and Start Site Selection by T7 RNA Polymerase Using a Comprehensive Collection of Promoter Variants," *Biochemistry*, vol. 39, pp. 10419–10430, Aug. 2000.

[255] Q. Cai, J. A. Hanson, A. R. Steiner, C. Tran, M. R. Masikat, R. Chen, J. F. Zawada, A. K. Sato, T. J. Hallam, and G. Yin, "A simplified and robust protocol for immunoglobulin expression in E scherichia coli cell-free protein synthesis systems," *Biotechnology Progress*, vol. 31, no. 3, pp. 823–831, 2015.

Zoe Swank

+41 78 672 02 85
zoswank@gmail.com

Education

2015-2020 **PhD in Bioengineering and Biotechnology**
École Polytechnique Fédérale de Lausanne (EPFL)

2013-2014 **M.S. in Biophysics**
Universität Basel

2008-2012 **B.S. in Biochemistry, Department of Chemistry**
B.S. in Evolutionary Biology, Department of Molecular Biology
University of California, Santa Barbara

Research Experience

2015-2020 **PhD Thesis: Microfluidic platforms for synthetic biology**
Laboratory of Biological Network Characterization, Prof. Sebastian Maerkl
Institute for Bioengineering, Dept. of Engineering, EPFL

- Microfluidic devices were developed to screen a library of genetic parts in order to engineer functional transcriptional regulatory networks *de novo*
- Thermodynamic modeling paired with quantitative measurements led to an increased understanding of the underlying biophysics
- Collaboration with a group in the Materials Science Department enabled the design of a microfluidic device for encapsulating cell-free reagents in double emulsion droplets

2013-2014 **M.S. Thesis: Physical dynamics of actin polymers**
Laboratory for Soft Matter Biophysics, Prof. Thomas Pfohl
Dept. of Physical Chemistry, University of Basel

- Using a microfluidic platform, the hydrodynamic interactions of actin filaments were studied in varying geometrical confinements
- Other side projects included the design of a microfluidic device for investigating eukaryotic cell elasticity with optical trapping and in situ imaging of nuclear oscillations in yeast cells with small-angle X-ray scattering (Microfocus Beamline, European Synchrotron, Grenoble)

2011-2012 **Research Internships in Science and Engineering**
Laboratory of Prof. Kevin Plaxco, Dept. of Chemistry, UCSB

- Electrochemical DNA biosensors for detecting small biomolecules *in vivo*

2009-2011 **Early Undergraduate Research and Knowledge Acquisition Fellowship**
Laboratory of Prof. Luc Jaeger, Dept. of Chemistry, UCSB

- Computational design and in vitro testing of programmable RNA nano-particles
- Writer for the UCSB undergraduate research blog

2008 **Summer Institute for Math and Science**
Laboratory of Prof. Umesh Mishra, Dept. of Electrical and Computer Engineering

- Characterization of gallium nitride epitaxy on silicon

Technical Skills

- **Microfluidics**: device design, mask writing and multilayer mold fabrication using photolithography techniques in the clean room, one and two-layer PDMS device fabrication
- **High-throughput screening of DNA variants**: optimization of an experimental setup that coupled the use of microarray liquid handling robots and microfluidic devices for *in vitro* gene expression reactions and DNA-protein binding assays
- **Experimental automation**: control of microscope, camera and microfluidic chip with LabView
- **Biochemistry and molecular biology**: PCR, gel electrophoresis, protein purification, molecular cloning, *E. coli* lysate preparation for cell-free TX-TL, mammalian cell culture
- **Optical and analytical techniques**: fluorescence microscopy, optical tweezers, SAXS, AFM
- **Image/data analysis and biophysical modeling**: Python and Matlab

Conference Proceedings

- SEED (Synthetic Evolution, Engineering and Design), New York, 2019 - oral presentation
- 1st European Congress for Cell-free Synthetic Biology, Ascona, 2017 - poster presentation
- Deutsche Physikalische Gesellschaft Spring Meeting, Dresden, 2014 - poster presentation

Publications

N. Laohakunakorn, L. Grasemann, B. Lavickova, G. Michielin, A. Shahein, **Z. Swank** and S. J. Maerkl. Bottom-up construction of complex biological systems with cell-free synthetic biology. *Frontiers in Biotechnology and Bioengineering*. 2020

N. Laohakunakorn, B. Lavickova, **Z. Swank**, J. Laurent and S. J. Maerkl. Steady-state cell-free gene expression with microfluidic chemostats. *protocols.io*. 2019

A. J. van der Linden, M. Yelleswarapu, P. A. Peters, **Z. Swank**, W. T. S. Huck, S. J. Maerkl and T. F. A. de Greef. A multilayer microfluidic platform for the conduction of prolonged cell-free gene expression. *Jove*. 2019

Z. Swank, N. Laohakunakorn and S. J. Maerkl. Cell-free gene regulatory network engineering with synthetic transcription factors. *PNAS*. 2019

J. Chang, **Z. Swank**, O. Keiser, S. J. Maerkl, and E. Amstad. Microfluidic device for on-chip mixing and encapsulation of lysates. *Scientific Reports*. 2018

L. L. Maddalena, H. Niederholtmeyer, M. Turtola, **Z. Swank**, G. A. Belogurov, S. J. Maerkl. GreA and GreB enhance Escherichia coli RNA polymerase transcription rate in a reconstituted transcription-translation system. *ACS Synth. Bio.* 2016

Z. Swank, S. Deshpande, T. Pfohl. Trapping, entrainment and synchronization of semiflexible polymers in narrow, asymmetric confinements. *Soft Matter*. 2016

W. Grabow, Z. Zhuang, **Z. Swank**, J. Shea, L. Jaeger. The right angle (RA) motif: a prevalent structural pattern found in group I introns. *Journal of Molecular Biology*. 2012